UNIVERSITÀ DEGLI STUDI DI PARMA

Dottorato di Ricerca in Ingegneria Geotecnica

Ciclo XXVII

The SLIP model: A major step towards the application in real time civil protection integrated platforms for landslide prevention.

Head of the Ph.D. program in Geotechnical Engineering:

Chiar.mo Prof. Lorella Montrasio

Tutor:

Chiar.mo Prof. Lorella Montrasio

Author

Andrea Terrone

Index

Chapter 1

Introduction and Problem Assessment

1.1 Introduction

Landslides can be triggered by natural, meteorological, geophysical, and anthropogenic causes. Landslides triggered by meteorological events occur every year and cause significant social and economic damage, including loss of human lives (Guzzetti *et al.,* 2007, Guzzetti *et al.,* 2008). For instance, according to a study by Petley (2012), between 2004 and 2010 2,620 nonseismically triggered landslides were recorded worldwide, causing a total of 32'322 fatalities. In the same period, the total economic losses associated with only this type of events, was estimated in the order of $ 1.5 billion (source: EM-DAT – The OFDA/CRED International Disaster database). This amount, along with the high number of casualties, underlines how great the impact of these phenomena is on society. Shallow landslides in steep soil covered landscapes can evolve in debris flows that pose a significant hazard, and if human development areas have encroached on debris flow source and run-out areas hazard results in high risk (Borga *et al.,* 2002). Failures are triggered during rainstorms or rapid snowmelt where an increase in pore-water pressure often results in a reduction of shear strength due to apparent cohesion. The increase in pore-water pressure may be directly related to rainfall infiltration (saturation from above) or may be the result of a build up of a groundwater table (saturation from below). In these conditions, a slope failure can occur within the soil mantle, where portions of soil generally detach from the lower thickened layers, or at the contact with the impermeable underlying bedrock boundary. When the detached mass moves downslope it may increase in water content and form a debris flow further downslope (Iverson *et al.,* 1997). Rainfall induced landslides may occur in groups or individually, can be deep or superficial and may develop into periods of time ranging from a few minutes to several days. These movements of land assume a special interest for the areal distribution and their unpredictability. Within this category of natural disasters, shallow landslides (in particular debris-flows) pose a serious threat to life or property, in particular due to their high velocity, impact forces and long runout, combined with poor temporal predictability (Jacob & Hungr, 2005). These phenomena are rapid, gravity-induced mass movements that generally occur on slopes covered by unconsolidated rocks and soil, where a water supply that saturates the debris and an adequate slope inclination (Hungr et al., 2001; 2014) trigger a flow that rapidly moves downslope eroding the soil cover and increasing its original volume (Iovine et al., 2003). Due to their high destructiveness, these events frequently cause significant damage to infrastructures and constructions, as well as human

casualties. For this reason, the study of these processes is an important research topic that can provide useful information for urban planning.

One type of these landslides is called soil slip, characterized by the sliding surface of the debris layer, whose thickness is approximately 1-1.5m. The soil slip phenomena are instabilities that arise both for rainfalls of short duration and high intensity, and as a result of precipitation of medium intensity but prolonged in time. In most cases these events leave ephemeral traces on the ground, that are cleared within a few months or years from natural processes or by human intervention. Often, these landslides, cause damages that create a general public interest threatening cultivated areas (Figure 1.1), vineyards, private houses, roads (Figure 1.2), causing all together, significant economic damage.

Figure 1.1 Soil slips occurred in a cultivated area (Tizzano Val Parma, April 2013)

Figure 1.2 A road damaged by a superficial landslide (Tizzano Val Parma, April 2013)

Sometimes these landslides may be responsible for the origin of very dangerous debris flow situations (Figure 1.3), unsafe human life itself.

Phenomena of this sort have been recorded in Italy, for example, in the Langhe (Piedmont) in 1994, Alta Versilia in 1996, Sarno (Campania) in 1998, Ceriana (Liguria) in 2000, Casamicciola Terme (Campania), Giampilieri (Sicily) in 2009, Uscio (Liguria) and San Fratello (Sicily) in 2010, Liguria in 2011, Parma Apennines (Emilia-Romagna) in 2013 and most recently in many regions of North Italy (October-November 2014) and along with floods, have caused considerable damage and casualties.

Figure 1.3 Image of a debris flow that hit Giampilieri and Scaletta Zanclea on October 1st 2009. This event caused 37 deaths and destroyed many habitations (http://www.meteoweb.eu/2014/10/1-ottobre-2009-5-anni-fa-lalluvione-giampilieri-scaletta-per-non-dimenticare/329339/)

The particular danger of these natural events is related to the difficulty of identifying the location before the slip occurs, to the rapid development and exhaustion of the phenomenon and to the high density of landslides over a limited area.

The main element that makes soil slips dangerous is not the volume of material involved, but the development speed. In fact, shallow landslides are classified as instantaneous events because they run out within a few seconds, at speeds between 2 and 10 m/s (Govi et al., 1985).

The evolution of a landslide can be affected by different factors that contribute to the impairment of the stability of a slope, but in the case of soil slips a direct connection between rainfall and triggering of the landslide can be detected.

In recent years numerous studies have been activated, nationally and internationally, to determine, with different approaches, various models able to describe the initiation of these landslides. The main goal of these models is to implement a real time early warning system that correlates directly the rainfall amount to the safety factor of a slope. A brief description of these models is presented in Chapter 2.

In this thesis the results of a research activity whose aim is to validate a physically-based model are presented. The research activity focalized mainly on two events:

- the landslide event of Giampilieri (Messina – Sicily) occurred the 1st October of 2009. On that day, a heavy rainstorm triggered several hundreds of shallow landslides, causing 37 fatalities and severe damage to buildings and infrastructures.

- the landslide events of the Parma Apennines occurred in April 2013. In this month, continuous intense rainfalls triggered hundreds of shallow landslides in the hilly and mountainous municipalities of the Parma province causing heavy damage to infrastructures and structures, fortunately causing no fatalities.

Given the nature and the number of landslides triggered over a small area during these two events, they can be considered particularly representative of the studied phenomenon and, thus, suitable for testing the reliability of the physically-based model;

The results of this research are a consequence of many complementary activities including:

- In situ survey of occurred shallow landslides;
- Data mapping the surveyed landslides in GIS environment;
- Small scale landslide modeling in a laboratory flume test;
- Geotechnical laboratory characterization of the soil;
- Mathematical modeling with physically-based models;
- Comparison of results with other well established physically based models.
- Evaluation of the predictive capacity of the models

1.2 Thesis outline

Chapter 2: A brief presentation of the shallow landslide phenomena and modeling;

Chapter 3: The SLIP model, a physically based model for shallow landslide instability prediction;

Chapter 4: The Parma Apennine landslide event of April 2013 – study area;

Chapter 5: The Parma Apennine landslide event of April 2013 – modeling;

Chapter 6: The landslide event of Giampilieri (ME) occurred on October 1st 2009 ;

Chapter 7: Laboratory flume tests on Giampilieri soil;

Chapter 8: Application and comparison of two physically based models (SLIP and TRIGRS) to the Giampilieri event;

Chapter 9: Conclusions.

Chapter 2

A brief presentation of the shallow landslide phenomena and modeling

2.1 Shallow landslides: general aspects

Landslides triggered by rainfall are the cause of thousands of deaths worldwide every year (Jakob & Weatherly, 2003). The term “shallow landslide” is used to describe material movement (generally colluvium or weathered soil) displaced over a discrete slip surface close to the land surface. This type of landslide typically involves a small volume of material but usually has a high impact energy due to its high velocity and erosion capability. In fact, after the triggering phase, this phenomenon can be characterized by a global translational movement of a few centimeters (“incipient translational slide” (Varnes, 1978), Figure 2.1a) to several meters, evolving to other landslide types like debris slide (Figure 2.1b) or, if the sliding movement becomes flow-like, debris-flow (Figure 2.1c).

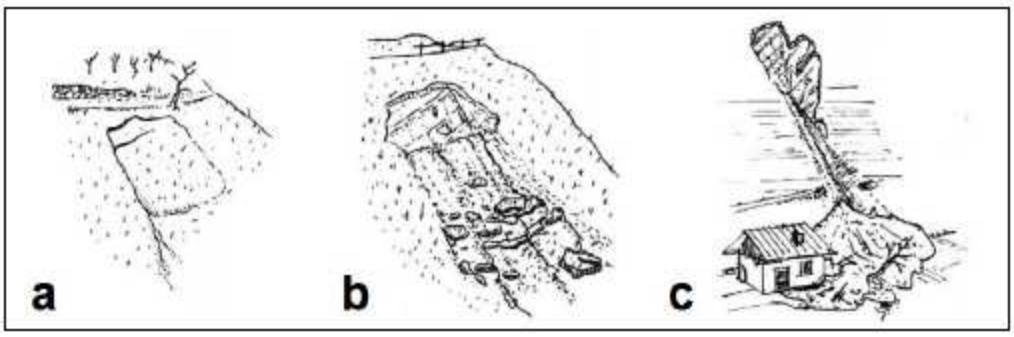

Figure 2.1 Illustration of different types of shallow landslides: a) incipient translational slide; b) debris slide; c) debris-flow

A typical debris-flow is a torrential flow of a mixture of water, mud and debris that suddenly pushes ahead with a vanguard of huge, jostling and roaring boulders (Takahashi, 2007). For this purpose, a classical distinction is generally made between a debris flood, corresponding to a rapid, surging flow of water, heavily charged with debris in a steep channel, and a debris avalanche, corresponding to a rapid or extremely rapid shallow flow of partially or fully saturated debris on a steep slope without confinement in an established channel (Hungr et al., 2008). As they travel through a drainage network, debris-flows can dramatically increase their volume by entraining sediment (McCoy et al., 2012) due to the destabilization and erosion of the stream bed and banks. As a consequence, debris-flow magnitude (i.e. the total volume of material moved to the deposition area

during an event) is rarely determined by the volume of the initiating landslide (Hungr et al., 2005). Another important feature of these phenomena is the high velocity of movement, typically between 2-10 m/s ("extremely rapid" according to the velocity classification proposed by Cruden & Varnes, 1996). However, several authors have reported velocities even higher than 15-20 m/s (Wieczorek et al., 2000; Revellino et al., 2003; Prochaska et al., 2008). Considering the mobilized volumes and the reached velocities, it is clear that debris-flows are generally extremely destructive. This type of events may be triggered by different factors, like rapid snow melt (Cardinali et al., 2000) or unexpected outburst of glacial lakes (Breien et al., 2008), but a debris-flow is typically initiated by intense, rapid precipitation capable of mobilizing soil, colluvium and even ancient clayey or pyroclastic deposits (Guadagno et al., 2003; Zanchetta et al., 2004). Due to the usual large extension of the rainfall events, many shallow landslides frequently initiate almost simultaneously over large areas (up to tens of square kilometers) involving shallow soil deposit of different grading and origin (Cascini et. al., 2010; Giannecchini et al., 2012). For this reason, these phenomena are found in a wide variety of environments worldwide such as glacial (Lionel & Jackson, 1979; Clague et al., 1985; Narama et al., 2010; Mergili et al., 2011), volcanic (Pierson, 1985; Pierson et al., 1990; Scott et al., 1995; Vallance & Scott, 1997; Mothes et al., 1998), and alpine settings (Berti et al., 1999; Marchi et al., 2002; Hürlimann et al., 2003; Chiarle et al., 2007; Carrara et al., 2008; Bardou et al., 2011). Among the most extreme events, one example that can be cited is the December 16th, 1999 event occurred in Venezuela, when heavy rainstorms induced thousands of landslides and debris flows, causing about 15,000 casualties and extensive damage in the urban development located along the central coast of the country (Pérez, 2001; García-Martínez & López, 2005). Heavy debris-flow events frequently occur in Japan, for instance in 1999 (Wang et al., 2003) and 2003 (Sidle & Chigira, 2004; Wang et al., 2006), but also in the United States (Wieczorek et al., 2004; Baum & Godt, 2010) and in different countries of the Caucasian (Petrakov & Krylenko, 2007; Gavardashvili & Ayyub, 2011), Latin American (Fernandes et al., 2004; Kanji et al., 2008) and Central Asian regions. Referring to this last region, two particularly devastating events must be cited. The first one occurred in the Gansu Province (northwestern China) on August 7th, 2010, when two giant debris-flows (total estimated volume: about 2.2 million m^3) killed 1,765 people living on the existing alluvial fan (Tang et al., 2011). The second one took place just six days later in the Qingping area (southwestern China), where an abundance of loose co-seismic landslide debris (present on the slopes after the May 12th, 2008 Wenchuan earthquake) served as source material for numerous rainfall-induced landslides, included a giant debris-flow that transported a total volume of about 3 million m^3 of sediment to the Mianyuan river. It generated a temporary debris-dam that entirely blocked the river, causing the subsequent flooding of the newly constructed houses and streets in

Qingping town (Tang et al., 2012). In Italy, as well as the October 1st, 2009 Giampilieri event one example that can be cited is the event occurred in May 1998 in the Sarno area (Campania Region), where tens of debris flows and debris avalanches were triggered by intense and prolonged rainfall, causing 148 fatalities (Guadagno et al., 2005; Cascini et al., 2011).

2.2 Shallow landslides susceptibility assessment and modeling

Currently, the research methods for shallow-landslide studies are generally based on field observations coupled with the development of empirical, rheological and numerical models. However these models, in particular numerical ones, are exceptionally demanding in terms of parameterization, and the required information often exceed available data (Merritt et al., 2003). Many research studies have been developed in the fields of geomorphology and applied geomorphology to identify correlations between rainfall affecting a particular area and mass movements that occur consequently. The triggering of some types of landslides, including soil slips, appears to be closely related to the rainfalls that hit an area in a specified period of time prior to the landslide. Usually soil slips trigger after very intense short precipitations or, less frequently, after rainfalls of moderate intensity but prolonged in time (Campbell 1975; Moser & Hohensinn 1983; Cancelli & Nova 1985; Cannon & Ellen 1985, and Wieczorek 1987; Crosta et. al. 1990; Buchanan and Savigny 1990). These rains have markedly localized characteristics, their evolutionary dynamics is strongly influenced by orography, slope exposure, altitude, wind and thermal gradient. Rainfall distribution may have markedly different characteristics in neighboring basins (left and right of watershed or top and toe of a valley).

In literature, a great variety of approaches and methods are proposed for landslide initiation susceptibility assessment, resulting in the production of susceptibility maps. A landslide susceptibility map contains a subdivision of the study area in zones that have a different likelihood of occurrence of landslides of a specific type (e.g. shallow landslides). The likelihood may be indicated either qualitatively (as high, moderate low, and not susceptible) or quantitatively (e.g. as Safety Factor or Probability of Failure). The researches that have studied the correlation between rainfall and gravitational movements can be classified in two main categories:

- Studies aimed at identifying rainfall thresholds for the triggering of landslides, valid at local or regional scale, determined on statistical surveys based on past event data in the studied area. To carry out this type of analysis a large database, relating to both rainfalls and occurred landslides, is required. The spatial effectiveness of the threshold must be specified.

- Studies using physically based models of a slope where slope stability is evaluated through a physical approach that takes into account many factors including geotechnical characteristics, topography, and hydrology (infiltration and runoff). Analysis of this type are usually carried out on a limited portion of the slope or, at most, at the catchment area scale, often with the aid of GIS technologies: in fact these models require numerous parameters that are subject to high spatial variability;

2.2.1 Statistical models for the definition of rainfall thresholds for landslide triggering

Rainfall thresholds for the possible occurrence of landslides are defined through the statistical analysis of past rainfall events that have resulted in slope failures, and can be classified based on the geographical extent for which they are determined (i.e., global, national, regional, or local thresholds), and the type of rainfall information used to establish the threshold (Guzzetti et al., 2007, 2008).

The numerous studies related to rainfall thresholds differ mainly on the basis of:

- types of instability examined;
- rainfall parameters (intensity, duration, average annual precipitation, precipitation accumulated prior to the event, etc.).
- size and location of the study area.

Since this is fundamentally a statistical approach, the reliability of the results is linked to the availability of data, relating both to rainfalls and the landslide events. Furthermore, the triggering of gravitational movements, in particular of soil slips, depends on many physical, geological, morphological and climatic parameters, therefore the spatial validity of the results obtained from each study is determined by the distribution of the analyzed events. Each operation of spatial extension of rainfall thresholds must carefully consider the spatial variation of many factors that influence the triggering of the considered phenomena.

In the following paragraphs some of the main studies based on the empirical approach are briefly presented.

Caine (1980), a pioneering work, proposes a global threshold after studying 73 cases of shallow landslides *"less than 2 or 3 meters deep"* that occurred in different parts of the world with different climatic, geologic and topographic environments. All of the studied landslides occurred in natural slopes, not modified by anthropologic activities or stream erosion. The proposed threshold is reported in equation 1.1 and 1.2 respectively in terms of intensity/duration and depth/duration.

$$I = 14.82D^{-0.39} \quad (2.1)$$

$$d = 14.82D^{0.61} \quad (2.2)$$

In which I is the rainfall intensity (mm/h), D the duration of the rainfall (h) and d the rainfall depth (mm). These relations are valid for durations between 10 minutes and 10 days. The average rainfall intensity needed to trigger debris flows was found to be much higher for short duration rains when compared to long duration rains extending for several days.

In *Govi et al.,* (1985) the researchers examine the relation between rainfall depth and landslide triggering, particularly regarding the landslides in which soil fluidization occurred. 22 meteoric events were analyzed taking into account the cumulated rainfall regarding the event and the rainfall depth of a period between 30 and 60 days prior the event, expressed as a percentage of the Mean Annual Precipitation (MAP). The following results were observed:

- in the initial stage (where 3 to 15 landslides per km^2 develop) the critical heights of precipitation vary in rather large values, as a function of average hourly rainfall intensity and of seasonal conditions;
- once the critical threshold is exceeded the following stages (intermediate with 15 to 30 landslides per km^2 develop, or catastrophic if there are more than 30 landslides per km^2) are quickly reached, during heavy rainfalls, even with light increments of the percentage of MAP;
- high hourly intensities compensate insufficient critical values of prior cumulated rain depth and vice versa. The hourly intensity of rainfalls influences the time in which landslides occur: during summer or autumn events, where there are high intensities, the landslide event evolves and runs out within 2-4 hours. During winter or spring events, characterized by low intensities, the time span is higher, between 10 and 24 hours.

The relation between the initial landslide stage and the hydrologic parameters is defined by two threshold curves for which higher rainfalls trigger the first landslides in the considered area. The two thresholds are seasonally valid (winter-spring events or summer-autumn events). It has also been found that both the storm rainfall totals and rainfall intensities necessary to trigger debris flows are expected to vary with the MAP.

Wieczorek (1987) analyzed the characteristics of rainfall intensity and duration of 22 storms, between 1975 and 1984, leading to debris-flow initiation in a 10 km^2 area near La Honda, CA. He found that some antecedent rain was necessary for triggering debris flows, and no landslides had occurred before 28 mm had accumulated in the season. He also found that moderate intensity

storms of long duration triggered complex soil slumps and debris flows in thick soils whereas high-intensity storms of short duration caused soil slides and debris flows in thinner soils.

However, the role of the antecedent rain in triggering debris flows in tropical regions and other parts in the world where soil permeabilities are very high has been questioned by *Brand* (1995) who considers that only short term rainfall intensity is the dominant landslide-controlling parameter

The purpose of *Corominas & Moya,* (1999) was to present a methodology to reconstruct a history of landslide events and their triggering causes in regions that lack historical information. In this study a chronology of landslides occurred between 1958 and 1996 in the upper basin of the Llobregat River, Eastern Pyrenees, was reconstructed from technical reports, field surveys and dendrogeomorphological analysis. The precipitation conditions were recorded by two rain gauges located in the area. Two different rainfall/landslide patterns were found:

- without antecedent rainfall, high intensity and short duration rains trigger mostly debris flows and shallow slides developed in colluvium and weathered rocks. A rainfall threshold of around 190 mm in 24 h initiates failures whereas more than 300 mm in 24–48 h are needed to cause widespread shallow landsliding;
- with antecedent rain, moderate intensity precipitation of at least, 40 mm in 24 h reactivates mudslides and both rotational and translational slides affecting clayey and silty–clayey formations. In this case, several weeks and 200 mm of precipitation are needed to cause landslide reactivation.

Many unnoticed reactivations of the landslides were identified by dendrogeomorphology analyses, proven to be very useful in reconstructing the history of antecedent landslides. In this work *Corominas & Moya (1999)* also present, on the base of 106 events, a threshold line that roughly divides the rain events that are associated with landslide reactivations from those that are not. This line has the following equation:

$$Ac = 32D + 133 \qquad (2.3)$$

Where *Ac*, is the accumulated rain in mm and, *D* is the duration of the rain event in weeks. Here, *Ac* includes both the 24 hour precipitation of the rainfall event and the weekly antecedent rain. An important conclusion of this work is that very pervious soils on steep slopes will only build-up high pore water pressures under very intense and short-rains while clayey soil slopes will require only moderate but long lasting rainfall.

In *Jakob & Weatherly*, (2003) the authors propose a method that incorporates antecedent rainfall and stream flow data to develop a landslide initiation threshold for the North Shore Mountains of

Vancouver, British Columbia. Hydroclimatic data were gathered for 36 storms 18 of which triggered landslides. Discriminant function analysis separated the landslide-triggering storms from those storms that did not trigger landslides and selected the most meaningful variables that allow this separation. The variables identified that optimize the separation of the two storm groups are 4-week rainfall prior to a significant storm, 6-h rainfall during a storm, and the number of hours 1 m3/s discharge was exceeded at a creek nearby the study area during a storm. Three thresholds were identified. The Landslide Warning Threshold (LWT), The Conditional Landslide Initiation Threshold (CTLI) and it implies that landslides are likely if 4 mm/h rainfall intensity is exceeded at which point the Imminent Landslide Initiation Threshold (ITLI) is reached. The LWT allows time for the issuance of a landslide advisory and to move personnel out of hazardous areas. The methodology proposed in this work can be transferred to other regions worldwide where type and quality of data are appropriate for this type of analysis.

In *Guzzetti et al.* (2008) the authors purpose is to update the global threshold proposed by Caine in 1980 through analyses of a global database of 2,626 rainfall events that have resulted in shallow landslides and debris flows compiled through a literature search. The rainfall intensity–duration (ID) values were plotted in logarithmic coordinates, and it was established that with increased rainfall duration, the minimum average intensity likely to trigger shallow slope failures decreases linearly, in the range of durations from 10 min to 35 days. The minimum ID for the possible initiation of shallow landslides and debris flows was determined. The most generic threshold, valid for durations between 0.1 and 1000h is described in equation 2.4 and was obtained from rainfall data of every event gathered in the database:

$$I = 2.20 \times D^{-0.44} \qquad (2.4)$$

The obtained global ID threshold is significantly lower than the one proposed by Caine, (1980), and lower than other global thresholds proposed in literature. This new global ID threshold can be used in a worldwide operational landslide warning system based on global precipitation measurements where local and regional thresholds are not available.

In *Brunetti et al.,* (2010), the authors used a catalogue listing 753 rainfall events that have resulted in landslides in Italy to define new thresholds for the possible occurrence of rainfall-induced landslides, in Italy and in the Abruzzo Region, central Italy. The authors describe and propose two statistical methods for the definition of objective rainfall thresholds, including a Bayesian inference method and a new method based on a Frequentist probabilistic approach. These methods are applied to the catalogue to determine new intensity-duration (ID) thresholds for possible landslide occurrence in Italy and in the Abruzzo Region, central Italy.

The equations of these thresholds are:

$$I = 7.17 \times D^{-0.55} \quad (2.5)$$

$$I = 5.54 \times D^{-0.59} \quad (2.6)$$

$$I = 7.74 \times D^{-0.64} \quad (2.7)$$

$$I = 4.23 \times D^{-0.55} \quad (2.8)$$

Equations 2.5 and 2.6 are the thresholds found using the Bayesian method respectively for Italy and Abruzzo, while equations 2.7 and 2.8 are the Frequentist probabilistic thresholds, considering 1% of events triggering landslides below the threshold, respectively for Italy and Abruzzo. The output of this study reveals that the new regional thresholds for the Abruzzo Region are lower than the new national thresholds for Italy, and lower than regional thresholds proposed for Piedmont (Aleotti, 2004), Lombardy (Ceriani et al., 1994), and the Campania Region (Calcaterra et al., 2000). This unexpected result is relevant because it shows that landslides in Italy can be triggered by less severe rainfall conditions that previously recognized. It is an important information to forecast landslide occurrence and to ascertain landslide hazards.

With the aim of defining the critical rainfall thresholds for the Middle Serchio River Valley, a detailed analysis of the main rainstorm events was carried out in Giannecchini et al., (2012). The hourly rainfall recorded by three rain gauges in the 1935–2010 interval was analyzed and compared with the occurrence of shallow landslides. The rainfall thresholds were defined in terms of mean intensity I , rainfall duration D, and normalized using the mean annual precipitation. Some attempts were also carried out to analyze the role of rainfall prior to the damaging events. Finally, the rainfall threshold curves obtained for the study area were compared with the local, regional and global curves proposed by various authors. The results of this analysis suggest that in the study area landslide activity initiation requires a higher amount of rainfall and greater intensity than elsewhere.

A complete list of studies and publications regarding rainfall thresholds can be found on the IRPI (Istituto di Ricerca per la Protezione Idrogeologica) website**:**

http://rainfallthresholds.irpi.cnr.it/references.htm.

2.3 Physically based models for slope stability analyses.

Physically based models rely upon the understanding of the physical laws controlling slope instability, and attempt to extend spatially the simplified stability models widely adopted in geotechnical engineering. Stability conditions are evaluated through a static stability model where the local equilibrium along a potential slip surface is considered. Most commonly, the slip surface is

assumed planar, of fixed depth, and parallel to the topographic surface. Values for the pore fluid pressure are assumed, or obtained by adopting more or less complex rainfall infiltration models. (Brunetti et al. 2010). Limit equilibrium theory is often used to analyze the stability of natural slopes. A number of methods and procedures based on limit equilibrium principles have been developed for this purpose. Regardless of the specific procedures, the following principles (Morgenstern and Sangrey, 1978) are common to all methods of limit equilibrium analysis.

- A failure surface or mechanism is postulated.
- The shearing resistance required to equilibrate the failure mass is calculated by means of statics. The potential failure mass is assumed to be in a state of 'limit equilibrium', and the shear strength of the soil or rock in the failure mass is mobilized everywhere along the slip surface.
- The calculated shearing resistance required for equilibrium is compared with the available shear strength. This comparison is made in terms of the factor of safety, which is defined as the factor by which the shear strength parameter must be reduced in order to bring the slope into a state of limiting equilibrium along a given slip surface.
- The mechanism or slip surface with the lowest factor of safety is generally found by iteration.

Planar infinite slope analysis have been widely applied to the determination of natural slope stability, particularly where the thickness of the soil mantle is small compared with the slope length and where landslides are due to the failure of a soil mantle that overlies a sloping drainage barrier. The drainage barrier may be bedrock or a denser soil mass**.** In this case, soil depth is obviously the depth to the drainage barrier. However, a translational failure plane may develop at any hydraulic conductivity contrast where positive pore water pressure can develop. Therefore, the depth to the failure plane may be much less than the depth to competent bedrock (Borga et al., 2002). The role played by vegetation in improving slope stability is well recognized, and comprehensive reviews may be found in the literature (Morgan and Rickson, 1995; Gray and Sotir, 1996). The most obvious way in which woody vegetation enhances slope stability is via root reinforcement.

In the following paragraphs a brief report of some physically based models used in slope stability analyses is presented.

In Montgomery & Dietrich (1994) an algorithm for a stability model (consequently named SHALSTAB) is presented. The model for the topographic influence on shallow landslide initiation is developed by coupling digital terrain data with near-surface flow and slope stability models. The degree of saturation of the soil is predicted by the hydrologic model TOPOG (O'Loughlin, 1986) in

response to a steady state rainfall. This saturation value is used by slope stability components to analyze the stability of each topographic element for the case of soils of spatially constant thickness and saturated conductivity. The steady state rainfall predicted to cause instability in each topographic element provides an index of the potential for shallow landsliding. SHALSTAB calculation scheme can be applied to all the events regarding superficial shifting of the top shallow soil, less than one and a half meters thick, whose dynamics is due to the convergence of the subsurface flow. The model consists in a stability calculation of an infinitely extended slope, understood as the balance of destabilizing components due to gravity with the stabilizing components due to cohesion. The slope consists of a cohesive soil with the following characteristics:

ρs (saturated volume weight);

n (porosity);

k (lateral saturated hydraulic conductivity);

C (cohesion);

φ (angle of friction).

It is subject to its own weight and that of a uniform flow of depth "h" that interacts with the soil mass flowing over the contact surface between soil and substrate. Through elementary observations of static equilibrium, not taking into account the cohesion parameter, it is possible to determine the equation of limit equilibrium as follows:

$$\frac{h}{z} = \frac{\rho_s}{\rho_w} \cdot \left(1 - \frac{\tan\theta}{\tan\varphi}\right) \tag{2.9}$$

Where θ is the slope angle, ρ_s is soil density (kg/m^3), ρ_w is water density (kg/m^3), z is the soil thickness above the substrate (m), h is the thickness of saturated soil where water flows above the substrate (m), and φ is the internal friction angle. When the value of hydraulic saturated conductivity k (m/h) is assumed to be constant along the vertical, the flow rate q_0 of the filtration parallel to the slope can be obtained in the following way:

$$q_0 = k \cdot h \cdot \cos\theta \cdot \sin\theta \tag{2.10}$$

Assuming conditions of permanent motion, the value of q_0 can be determined for each cell of the regular mesh used to discretize the slope by imposing the respect of the continuity equation written in the following way:

$$i_e \cdot A = q_0 \cdot b \tag{2.11}$$

Where i_e represents the effective inflow to the aquifer (m/h), A is the drained area (m^2) from the concerned cell and b is the cell width (m) in the direction of the filtration motion. The substitution of equations 2.10 and 2.11 leads to the following expression:

$$k \cdot h \cdot \cos\theta = \frac{i_e \cdot A}{\sin\theta \cdot b} \tag{2.12}$$

Which can be rewritten introducing transmissivity T (m^2/h):

$$T = k \cdot z \cdot \cos\theta \tag{2.13}$$

$$\frac{h}{z} = \frac{i_e \cdot A}{\sin\theta \cdot b \cdot T} \tag{2.14}$$

The final expression adopted for the model, based on the geomechanical component (equation 2.9) and the hydrological component (equation 2.14), adding the cohesion parameter (C), is written as:

$$i_{e,cr} = T \cdot \sin\theta \cdot \frac{b}{A} \cdot \left[\frac{\rho_s}{\rho_w} \cdot \left(1 - \left(1 - \frac{C}{\sin\theta \cdot \cos\theta} \right) \cdot \frac{\tan\theta}{\tan\varphi} \right) \right] \tag{2.15}$$

$$C = \frac{C_r + C_s}{\rho_s \cdot g \cdot z} \tag{2.16}$$

Where Cr is root cohesion (N/m^2), Cs is soil cohesion (N/m^2), and g (m/s^2) is gravitational acceleration. A, the contributing area, is calculated with the *"Multiple Flow"* calculating scheme. Assuming that the inflow due to rain isn't affected by losses during its transformation into effective aquifer influx, i_{cr} represents the prediction variable of the model, called critical rainfall, understood as the amount of rainfall required to trigger a shallow landslide.

In Pack et al.(1998), the authours present a stability model based on the same assumptions of infinite slope of SHALSTAB named SINMAP (Stability Index MAPping) with some differences regarding mainly the procedure to calculate the drained area and the predictive index, not expressed as a critical rainfall but as a probability of occurrence within a given range of input parameters. The method for the determination of the flow directions refers to the algorithm D∞ (Tarboton, 1997). The hydrological component that triggers the destabilization of soil is defined by the concept of relative saturation designed according to the assumptions of TOPMODEL (Beven & Kirkby, 1979). The SINMAP methodology is based on the infinite slope stability model, which consists in calculating the balance between the gravitational force parallel to the slope and the forces of cohesion and friction that oppose mass movements along a shearing plane parallel to the slope

itself. Pore water pressure reduces the normal component of the gravitational force that is related to shear strength through the internal friction angle of the material. The pressure in the porous matrix is calculated assuming that the state of saturation of the soil depends on the ratio between the hydraulic transmissivity of a certain portion of the soil and its Specific Catchment Area, i.e. its supply area. The method is planned to perform a better calibration of the mechanical characteristics of the slope by drawing information from multiple levels of information: in this way it is possible to obtain a more detailed calibration of the region, that includes in the stability analyses the contribution of various factors such as the land cover, soil type, vegetation, etc. The stability index equation is presented:

$$SI = \frac{C_r + C_s + \cos^2\theta[\rho_s \cdot g(D - D_w) + (\rho_s \cdot g - \rho_w \cdot g)D_w]\tan\varphi}{D \cdot \rho_s \cdot g \cdot \sin\theta \cdot \cos\theta} \quad (2.17)$$

Where Cr is root cohesion, Cs (Pa) is soil cohesion, ρ_s (kg/m^3) is wet soil density, ρ_w (kg/m^3) is water density, g (m/s^2) is gravitational acceleration, D (m) the vertical soil depth, D_w (m) is the vertical height of the water table within the soil layer, ϑ (°) is the slope angle and φ (°) is the internal friction angle of the soil.

The SI expresses the probability that in a certain region a landslide may occur. Areas where SI> 1.5 are considered stable, while those close to 0 are considered extremely unstable. The method requires that some calibration parameters, such as the internal friction angle, the cohesion and the ratio between Transmissivity and rainfall recharge (T / R), are defined within each region.

In Borga et al., (2002), a model for the triggering of shallow landslides by heavy rainstorms was presented. The model was applied in two mountainous catchments in the Dolomites where field surveys provided a description of hydraulic and geotechnical properties of soils and an inventory of landslide scars was available. The stability mapping procedure combines steady-state hydrologic concepts with the infinite slope stability model. The model provides a spatial mapping of the minimum steady-state rainfall (critical rainfall) predicted to cause instability. Different equations for the calculation of the safety factor were used according to differences in topography, saturation and presence of vegetation that contributes to stability through root cohesion.

The equation for the calculation of the safety factor in the most general case, where there is presence of slope-parallel seepage and presence of root cohesion is the following:

$$FS = \frac{C_r + C_s + \left[\rho_s \cdot g(D - D_w)\cos^2\theta + (\rho_s \cdot g - \rho_w \cdot g)D_w \cdot \cos^2\theta + W \cdot \cos\theta\right]\tan\varphi}{D \cdot \rho_s \cdot g \cdot \sin\theta \cdot \cos\theta + W \cdot \sin\theta} \quad (2.18)$$

Where Cr is root cohesion, Cs (Pa) is soil cohesion, ρ_s (kg/m^3) is wet soil density, ρ_w (kg/m^3) is water density, g (m/s^2) is gravitational acceleration, D (m) the vertical soil depth, D_w (m) is the vertical height of the water table within the soil layer, ϑ (°) is the slope angle, W (Pa) is vegetation surcharge and φ (°) is the internal friction angle of the soil. Being referred to an infinite slope model the equation proposed by Borga et al. (2002) is very similar to the SINMAP equation, with the only difference that vegetation surcharge is computed.

TRIGRS (Baum et al. 2002) (Transient Rainfall Infiltration and Grid-based Regional Slope Model) is a Fortran program for the spatiotemporal modeling of rainfall induced shallow landslides (Baum et al. 2008). Hereby only a brief description of the model is given as many authors have already explained it in detail in recent years (Baum et al., 2008, Salciarini et al., 2008, Kim et al., 2010). The model is based on the method proposed by Iverson (2000), that considers the complex history of rainfall, a waterproof substrate at a finite depth, and a simple surface runoff. The program computes the changes in pore water pressure, and consequent changes of the safety factor, due to rain infiltration. Rain infiltration modeling, that takes into account precipitations that vary in duration from few hours to a few days, is made through the analytical resolution of differential equations representing one dimensional vertical flow in homogeneous materials (saturated or unsaturated). The use of incremental series allows the program to represent the changes in the rainfall data, and a simple modeling of surface runoff may exclude the excessive water. TRIGRS uses an infinite slope model for the evaluation of the safety factor in each cell of the mesh. The safety factor, Fs, is calculated for transient pressures at different depths Z according to the following equation:

$$FS(Z,t) = \frac{\tan\varphi'}{\tan\delta} + \frac{c' - \psi(Z,t)\cdot\gamma_w\cdot\tan\varphi'}{\gamma_s\cdot Z\cdot sen\delta\cdot\cos\delta} \qquad (2.19)$$

Where c’ is the effective cohesion, ψ is the pore water pressure at depth Z and time t, φ’ is the internal friction angle of the material, γ_w is water unit volume weight, γ_s is soil unit volume weight and β is the slope angle. The depth Z where the safety factor drops below the unit is identified as the sliding depth. Its value depends on the properties of the soil, by time and by the variation of pore pressure, which, in turn, depends on the history of precipitation. The horizontal heterogeneity is taken into account by the properties of materials that are variable from cell to cell. A more detailed description of this model is given in chapter 8.2.

2.4 Examples of model application – The Round Robin Test (Naples – October 2013)

For a further description and comparison of different approaches used for landslide modeling for mitigation and prevention, the results of the Round Robin Test, a special session held during the Third Italian Workshop on Landslides in Naples (October 2013), are briefly presented. A Round Robin is an interlaboratory comparison test performed independently, centered around a competition among modelers with the ultimate aim to discuss and improve modeling concepts for better prediction of landslide occurrence In particular, the test dealt about how to put together information taken at different observation scales (laboratory, flume or field) to effectively model the hydrological initiation of a landslide, and about the differences of different models. To such aim, all the participants were provided with identical information used for the calibration of their models. Two information packages were delivered to participants: the first package included results of laboratory tests, the second one describes the performance of two small scale experiments of slopes subjected to simulated rainfall in a flume. After model calibration, the participants were asked to provide blind predictions of the following experiments: controlled infiltration in a physical model of a slope reconstituted in a laboratory flume, lasting until the failure of the slope; measured rainfall infiltrating in a monitored field site. The results obtained by the participants using very different models show that complex coupled physically-based models, requiring large sets of data for their calibration, allow to shed light upon the hydrological processes leading to landslide triggering, while simpler models, easier to calibrate, may be preferred when only the major macroscopic aspects of the phenomena, such as approximate time and location of the failure, are needed. (Bogaard et al., 2014).

The analyzed soil is a typical granular volcanic soil of the mountains surrounding Naples. This soil is known for its' disruptive flow-like sudden shallow landslides such as the events occurred near Cervinara in December 1999. The soil cover consists of an alternation of loose volcanic ashes and pumices lying upon a fractured limestone bedrock. The principal physical properties of the ashes are:

- specific weight, γ_s=25-26 [kN/m^3]
- unit volume weight, γ=21-14 [kN/m^3]
- porosity, n = 67-75 % [-]
- saturated hydraulic conductivity, $k_{sat} = 1{,}5 \cdot 10^{-7} - 5{,}7 \cdot 10^{-6}$ [m/s]
- effective friction angl, $\varphi' = 38°$ [-]
- cohesion, c' = 0 [kPa]

2.4.1 Group 1 – Middle East Technical University - **Prediction of seepage and slope stability in a flume test and an experimental field case.** (Mohammed Ahmadi-Adli, N. Kartal Toker, Nejan Huvaj)

Middle East Technical University (METU) team defined separate numerical models for simulation of the flume infiltration test and for the field experiment. Estimation of suction distribution and stability change in slopes due to rainfall and evaporation were done using calibrated models. Both infiltration flume test and field experiment were simulated numerically by SEEP/W and SLOPE/W softwares (Geo Slope 2007). Hydraulic properties of Cervinara soil were found accurately using provided laboratory test data and calibration in back analysis due to suction response. The calculated suction values are very sensitive to the small changes in SWCC (soil water characteristic curve) and HCF (hydraulic conductivity curve) curves. An observation is that HCF primarily affects the time axis (in suction-time plots) while SWCC primarily affects the suction axis, although their effects are interrelated. In slope stability analyses of the flume, failure time was found to be very sensitive to the shear strength criterion.

2.4.2 Group 2 – Università degli Studi di Palermo – **Modeling Round Robin test: an uncoupled approach.** (Camillo Airò Farulla, Marco Rosone)

The solution of the modeling test presented in the paper is based on an uncoupled hydro-mechanical approach. Firstly, the controlled infiltration process is modeled by a finite element transient groundwater seepage software. Afterwards, calculated pore water pressures at successive instants are used for the slope stability analysis. Time evolution of the slope stability is analyzed by using the infinite slope model, according to the classical limit equilibrium method. The safety factor of the slope is calculated according to equation (18) where the cohesive component is due to partial saturation being the effective cohesion null (c'=0), according to a modified Mohr-Coulomb shear resistance criterion:

$$FS = \frac{c}{\gamma \cdot z \cdot sen\alpha \cdot \cos\alpha} + \frac{\tan\varphi'}{\tan\alpha} \tag{2.20}$$

$$c = c' + \frac{s}{\cot\varphi' + \frac{s}{c^*}} \tag{2.21}$$

Where γ is the unit volume weight, z is the soil depth, c is the cohesive component α is the slope angle; s is suction; c* is a fitting parameter determined by the least square method.
The results presented by this group reveal that uncoupled hydro-mechanical approaches are not able to grasp significant aspect of the soil behavior when it depends on the coupling between retention and mechanical properties, and when significant volumetric deformations develop before soil failure, due to the rigid-perfectly plastic behavior assumed by the limit equilibrium method. However, referring to the pore water pressure and failure time evolutions, the presented results are similar to the experimental data relative to the flume tests and the prediction of failure (38.5 minutes) is near the real failure time (nearly after 35 minutes). In this respect, the utility of the proposed approach should be considered due to its' simplicity. It can be used to perform systematic analyses of conditions triggering slope failure, in order to evaluate possible critical climatic or environmental conditions.

2.4.3 Group 3 – Universitat Politècnica de Catalunya - **Small scale slope failure benchmark test. Modelling and prediction** (C. Hoffmann, N. Meler, N.M. Pinyol E.E. Alonso)

The UPC group used the finite element code "Code_Bright" (2010) , which solves coupled THM problems in deformable saturated-unsaturated porous media, and the Barcelona Basic Model (Alonso 1990) as the constitutive model for the unsaturated soils for their modeling. The modeling approach followed a "rational" set of stages: selection of the elastoplastic model to represent the soil mechanical behavior, finding constitutive parameters from delivered data, predicting/back analyzing the two prototype flume tests, identifying failure and applying the model to the blind experiment. The determination of hydraulic conductivity, water retention curves and displacement calculations are difficult if based only on samples and sample derived parameters. The marked drying-wetting hysteresis makes very unreliable predictions based on drying branches if the real problem involves soil wetting. Despite the difficulties mentioned, the final prediction of the failure time of the blind flume test experiment (34-39 minutes) was similar to the real failure time (nearly after 35 minutes).

2.4.4 Group 4- Università degli Studi di Parma – **Application of the SLIP Model** (Lorella Montrasio, Roberto Valentino, Andrea Terrone)
The modeling of the flume tests and field data was made using SLIP, a mathematical model used by the research team of the University of Parma. Since SLIP is the model that was used for other works in this thesis a complete description of the model is presented in chapter 3. In this section only the

main conclusions of the application for the Round Robin test are reported. After a calibration of the model parameters for the two prototype flume tests in which same input data were used (except rainfall intensity and porosity which were different in the two tests), the same parameters were used also in the blind prediction test. The failure, corresponding to FS=1, was predicted to occur at 22 minutes, a much shorter time than the rail failure. This result can be attributed to the following causes: (1) the real initial water content was unknown, and it was difficult to match the real value of ϑ_0 by considering only one point on the SWCC; and (2) the soil porosity in the blind test was much lower than the soil porosity in the prototype tests. This difference implies a reduction of β* (the amount of rainfall that effectively infiltrates into the soil) compared to the other tests, but we assumed β*=1 as in the prototype tests, because the amount of runoff was unknown. This caused the SLIP model to predict an earlier failure than actually occurred. A successive analysis was made changing the infiltration ratio to 70% of the rainfall, a standard value used in other previous works (Montrasio, 2000, Montrasio & Valentino 2007, 2008, Montrasio et al. 2009, 2011, 2012, 2013, 2014), and the failure prediction time varied significantly (32 minutes) thus predicting similar time to the real failure (35 minutes).

The second task required by the Round Robin committee was the simulation of field conditions consequently to rapid changing climatic conditions (rainfall – evaporation cycles). The SLIP model was used to assess the evolution of the safety factor of the slope over time for the following periods:

- 1 Oct. 2011 - 12 Feb. 2012 (observation period; Figure 2.2a): in this case, Fs > 1 for the entire time span, which indicates slope stability; no failure was observed during this period;
- 1 Oct. 1999 - 30 Dec. 1999 (Figure 2.2b): in this case, the measured daily rainfall depths (Fiorillo et al., 2001) were used as input data. Unstable conditions (Fs = 1) are reached on 16 Dec. 1999, which is when the shallow landslide actually occurred.

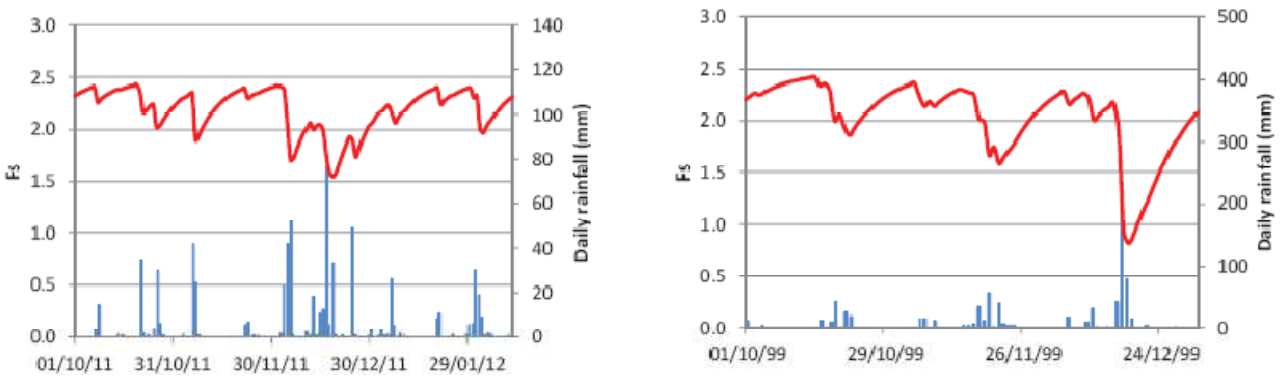

Figure 2.2. Daily rainfall and results of the SLIP model for field conditions a)2011-2012 b)October-December 1999

The input parameters used are reported in table 2.1:

β	H	Gs	φ'	c'	A	λ	α	β*	Sr	kt	Rain
°	m	-	°	kPa	-	-	-	-	-	s^{-1}	mm/h
40	1.2	2.63	38	0	45	1.2	3.4	0.7	0.37	$3 \cdot 10^{-7}$	Observed

Table 2.1 Input parameters used to simulate field conditions

The output of the SLIP model is represented with time varying safety factor maps, which gives the daily value of the safety factor in each cell (5x5 m). The different colors on the map correspond to different factors of safety. Fig. 2 shows four Fs maps that correspond to the three days before the event and to the day of the event (which occurred during the night between 15 and 16 Dec. 1999) and shows the evolution of the stability conditions before and during the rainfall. Fig. 2d compares the results of the SLIP analysis and the locations of the sites where shallow landslides occurred; the black lines correspond to the surveyed landslide scars. The red areas, where the model indicates unstable conditions (FS < 1), generally correspond to the mapped source areas of the shallow landslides, though the model overestimates the unstable areas.

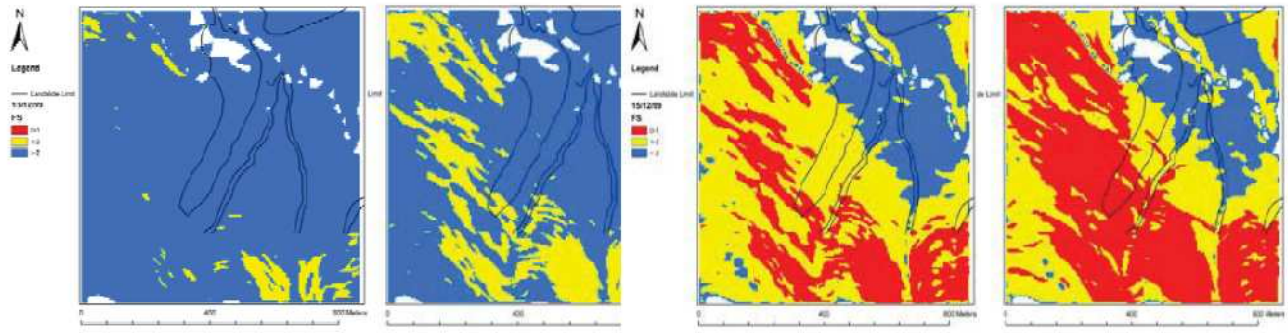

Figure 2.3 SLIP analysis at large scale: time varying safety factor maps between Dec. 13 and Dec. 16 - 1999

The SLIP model was also used to assess the mean water content under field conditions. To do this, the mean water content (ϑeq) was evaluated using SLIP as an inverse model. The equivalent degree of saturation (Sr_{eq}) value is obtained by considering all the water present in the soil as equally distributed through the whole depth. Figure 2.3 shows the steps involved in the inverse modeling and simply calculating $\vartheta eq = Sr_{eq} \cdot n$. The results for the soil profile obtained using this procedure by assuming that the soil porosity (n) remains constant and using the physical and geometrical parameters reported in Table 1 and the observed daily rainfall depths are represented by the black curve in Fig. 4. Despite a slight overestimation, the calculated assessed mean equivalent water contents are consistent with the field measurements.

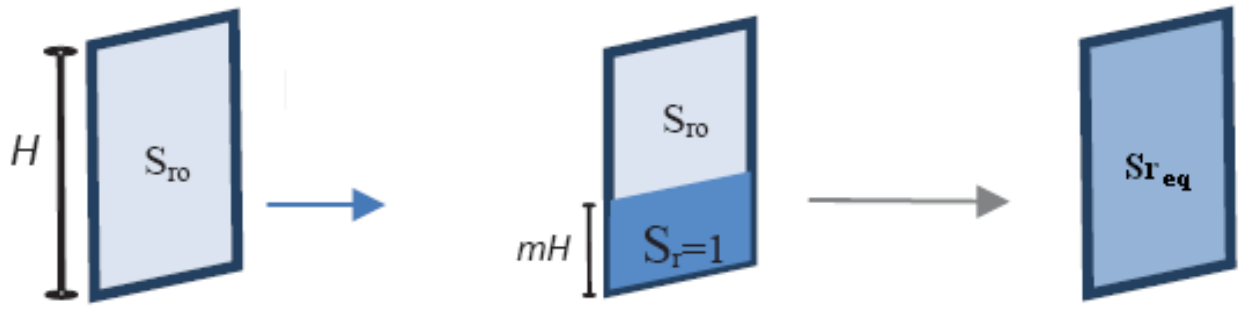

Figure 2.4 Steps used to evaluate the mean equivalent water content

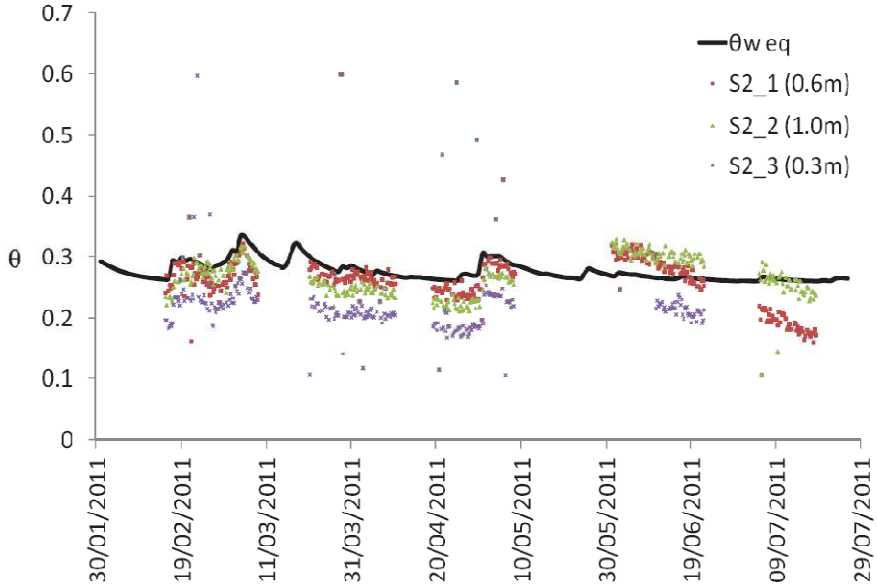

Figure 2.5 Modeling the mean water content versus time.

2.4.5 Group 5 – *University of Naples Federico II & Italian Aerospace Research Center* - **Prediction of suction evolution of silty pyroclastic covers in flume tests and field monitoring** (Alfredo Reder, Guido Rianna, Luca Pagano)

Calibrations, validations and blind predictions for both the flume tests and the field study, have been carried out by using a simplified approach, modeling seepage in an unsaturated and rigid medium under isothermal conditions. For the field case neglecting thermal effects and related evaporation phenomena can lead to overestimation of predicted pore water pressures during the dry periods while it should represent a reliable hypothesis for the wet periods. For flume tests the isothermal assumption is realistic since evaporation phenomena are negligible during the simulated rainfall event. The possible effects of changes in soil porosity due to soil collapse in the wetting phase are neglected since a rigid-soil skeleton hypothesis is adopted. The prediction of pore water

pressure development over time has been carried out by solving Richards' equation numerically through SEEP/W FEM code. The prediction of stability conditions has been carried out by referring to an infinite slope geometry. Under unsaturated conditions the safety factor FS may be expressed as:

$$FS = \frac{\tan\varphi'}{\tan\alpha} + \frac{s\tan\varphi_b}{\gamma \cdot z \cdot sen\alpha \cdot \cos\alpha} \qquad (2.22)$$

where φ' is the soil friction angle, α is the slope inclination, γ is the soil unit weight, *z* is the vertical height, *s* is the soil suction, φ_b is the friction angle due to suction.

Once determined soil parameters experimentally fitting the provided data, equation (2.22) has been used to quantify the slope safety factor over time corresponding to suction provided by numerical analyses. For the modeling of the flume tests the discretized geometry has been refined near the slope surface in order to accommodate the high gradients here assumed by hydraulic variables due to the presence of boundary flows. The top surface normal to the slope development and lowermost surface parallel to the slope development have been modeled as impervious; the down-slope surface (normal to slope development)has been modeled as a seepage surface, in order to simulate the capillary barrier effects induced by the geosynthetic material. The blind prediction for failure in the flume test is 36-37 minutes, a good prediction being the real triggering instant around 35 minutes.

2.4.6 Group 6 – Universitat Politècnica de Catalunya - **Modelling landslides induced by rainfall: a coupled approach** (Claudia Villarraga, Daniel Ruiz, Jean Vaunat, Francesca Casini)

The numerical analyses of the hydro-mechanical response of the two case studies in pyroclastic soils has been implemented at two different scales using a thermo-hydro-mechanical Finite Element code, (CODE_BRIGHT, 2010) that includes a special boundary condition to simulate the ground-atmosphere interactions. The suction dependent mechanical model is based on an adaptation of CASM (Yu, 1988) model for unsaturated soils developed by Gonzalez (2011). The model well predicts the evolution of suction at different depths, surface settlement and time of failure of a mock-up test that simulate the failure of a 40º slope under rainfall. The soil-atmosphere formulation is based on a consistent thermo-hydro-mechanical framework based upon fundamental physics. The model proves to provide good predictions of suction and water content variations in a real slope under meteorological actions.

Chapter 3

The SLIP model, a physically based model for shallow landslide instability prediction

3.1. Introduction and main hypothesis

As mentioned in the previous chapters soil slips usually develop in pre-alpine environment or in hilly areas, involving mostly limited portions of the soil surface. The relative hazard is related to the triggering speed, to the lack of warning signals on the territory where soil slips occur, and to the high intensity and distribution of single events. Thus, during certain weather conditions, portions of the top soil are detached from the underlying denser layers (or from the underlying bedrock), moving on a generally sub-planar surface, translating towards valley evolving at times in mudflows. These phenomena are rapid, gravity-induced mass movements that generally occur on slopes covered by unconsolidated rock and soil, where a water supply sufficient to saturate the debris and an adequate slope inclination (Hungr et al., 2001; 2014) triggers a flow that rapidly moves downslope eroding the soil cover and increasing its original volume (Iovine et al., 2003). Compared to an obvious hazard, especially for infrastructures, crops and even for populated areas, it is remarkable that this type of landslide has been rarely associated with a historical memory and only in the last decades researchers have focused on this type of instability. From the experience of past events, it is certain that the triggering of soil slips is strictly correlated to rapid climatic changes, principally rainfall and snowmelt. Thus, to predict their occurrence, the assessment of rainfall depths, soil geotechnical characteristics, slope geometry and land use is essential. Therefore, to predict the triggering of soil slips, a physically based model that allows a direct correlation between soil properties and precipitation trends and at the same time, sufficiently simple to be implemented in a real time monitoring device, is necessary. To achieve this goal a simplified model, named SLIP (Shallow Landslide Instability Prediction), capable to evaluate the time-varying safety factor of potentially unstable slopes directly correlated with the rainfall patterns was developed. SLIP is a simple physically based model that was developed by the research group of the University of Parma after the Piedmont flood, which injured hundreds of people and caused considerable damage in the northern Italian Apennines (Langhe) in November 1994 (Montrasio, 2000). The model has had a continuous improvement since it was developed through many case studies (Montrasio & Valentino, 2007, 2008; Montrasio et al., 2009, 2011, 2012, 2013, 2014). The following paragraphs

describe the main hypotheses that form the basis of the SLIP model and its mathematical formulations.

The determination of the soil conditions and processes that cause instability during climatic events have been based on hundreds of field observations and include:

1. Soil slips occur in thin superficial covers (maximum soil depth of 1-1.5 m) that are different from commonly intended geotechnical engineering soils in many aspects, mainly in their hydraulic characteristics. This type of soil, which is commonly removed during civil constructions, contains numerous pores, macro-channels and fissures that are created by several processes, including soil fauna, vegetation and wetting-drying cycles. This pore scheme forms two rain-infiltration directions: through the pores in the soil matrix and through the macro-porosity. The latter is considered to be prevalent in the soil cover, where slips occur, thus in the SLIP model infiltration through the pore matrix is neglected. These infiltration characteristics are considered to be similar for all kinds of top-soils.

2. Cohesion due to partial saturation contributes to the slopes shear strength.

3. The rain infiltrates through the macro-pores faster than through the micro-pores creating randomly distributed saturated zones. The dimensions of the saturated volumes increase during rain infiltration. The presence of the saturated zones results in a decrease in shear strength and a consequent loss of slope stability. Given sufficient rainfall depth the expansion of the saturated zones continues until slope failure.

4. The infinite slope model is considered to be appropriate for shallow slope stability analysis, based on field observations, in recent years (Montrasio & Valentino, 2008; Montrasio et al., 2009, 2011, 2012), of the geometric characteristics of hundreds of unstable slopes.

3.2 The SLIP model

SLIP was developed to model processes that have been confirmed by recent studies (Flury et. al 1994, Zhan et al. 2007, Krzeminska et al. 2013, Springman et al., 2013). The aim was to predict slope failure through a simplified formulation by modeling the main characteristics of the instability triggering without including too many elements of the complex mechanism. This choice was made because excessive parameters would limit the application of the model at the large scale. The model defines the safety factor Fs by applying the limit equilibrium method to an equivalent infinite slope

that is composed of two homogeneous soil portions: a partially saturated portion and a fully saturated portion representing the saturated zones around the macro channels. Homogenization is used to obtain, with respect to the original conditions, the loss of shear strength of an equivalent soil that is stable in the presence of both saturated and partially saturated zones; this is consistent with both the principles of soil mechanics and the application of the limit equilibrium method. For simplicity, the saturated zones are represented in the model by a saturated sub-layer of thickness *m*H (0 < m < 1) where H represents the potentially unstable top soil layer (first 1-1.5m). This sub-layer (*m*H) could be put in a random position inside the potentially unstable layer (H) but, for simplicity and because this choice does not change the consistency of the approach, it is positioned at the base of the layer, growing upwards during rain infiltration from the underlying bedrock or denser soil. This choice avoids adding an insignificant parameter, i.e., the location of the saturated sub-layer. This assumption does not affect the solidity of the approach as the saturated sub-layer *m*H co-exists with an unsaturated sub-layer of thickness (1-m)H (Figure 3.1). The parameter *m*H is related to the total amount of rainwater, *h*, as follows:

$$m \cdot H = \frac{\beta^* \cdot h}{n \cdot (1 - S_r)} \tag{3.1}$$

Where *h* is the time-varying rainfall depth, H is the thickness of the potentially unstable superficial soil, β* is the percentage of rain that infiltrates into the soil (being [1 - β*] the surface and subsurface runoff), *n* is soil porosity, and Sr is the degree of saturation.

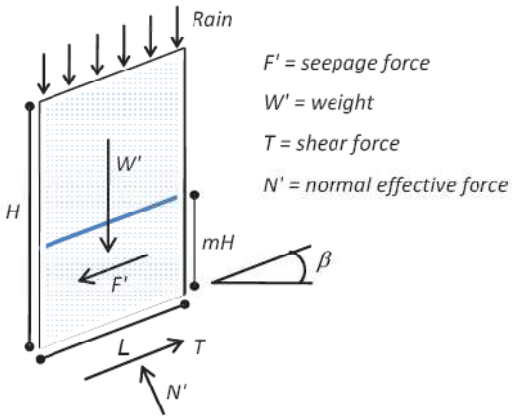

Figure 3.1 Infinite model geometry, homogenized soil portions and forces involved in the calculation of Fs

The shear strength of the saturated sub-layer (mH) is described by the Mohr-Coulomb criterion:

$$\tau = c' + \sigma' \cdot \tan\varphi' \tag{3.2}$$

The shear strength of the unsaturated soil is described by the simplified extended Mohr-Coulomb criterion for unsaturated soils (Fredlund & Rahardjo, 1993)

$$\tau_{ff} = c' + (\sigma_f - u)_f \cdot \tan\varphi' + (u_a - u_w)\tan\varphi^n \quad (3.3)$$

where $\sigma' = (\sigma_f - u)_f$ is the effective normal stress on the failure plane at failure, $(u_a - u_w)$ is the matric suction, c' is the effective cohesion, φ' is the internal friction angle, and φ^n is the friction angle associated with the matric suction. The quantity $(u_a - u_w)\cdot\tan\varphi^n$ is independent of σ', and in Equation (3.3) it represents an "apparent cohesion", which is named c_ψ (Fredlund & Rahardjo, 1993). Thus, the final shear strength criterion can be expressed as:

$$\tau = c' + c_\psi + \sigma' \cdot \tan\varphi' \quad (3.4)$$

The apparent cohesion c_ψ is a function of the matric suction; however, in SLIP, it is directly correlated to the degree of saturation Sr. This allows better control of the uncertainties in the evaluation of the soil state parameters because Sr varies over a smaller range than the matric suction. The link between c_ψ and the degree of saturation Sr is obtained from the results of experiments on different kinds of soils (Fredlund et al., 1996, Bogaard et al., 2014), such as medium and fine grained sands (Figure 3.2). By neglecting isteresis that occurs during the wetting/drying cycles, $c_{\psi*}$ can be expressed as a function of Sr as:

$$c_\psi^* = A \cdot S_r \cdot (1 - S_r)^\lambda \quad (3.5)$$

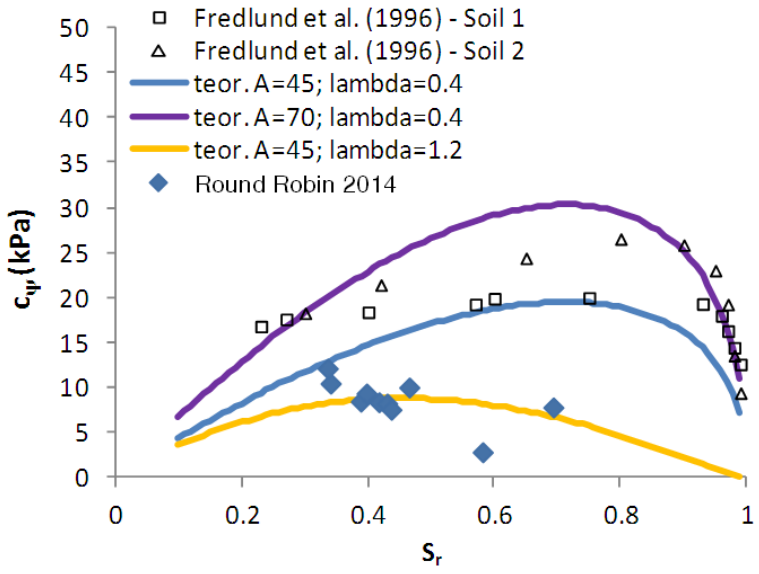

Figure 3.2 Apparent Cohesion vs degree of Saturation for 3 soil samples (Fredlund et al., 1996, Bogaard et al., 2014)

where A and λ are model parameters that depends on the type of soil.

The values of the parameters λ and A have been identified by experimental tests (Mari, 2000; Montrasio and Valentino, 2003 and 2007) for the most common types of soil of the Italian territory and are shown in Table 2.1.

Types of soil	***λ***	***A(kPa)***
Clay OCR = 1	0.4	100
Clay 1 < OCR < 2	0.4	100
Clay OCR > 2	0.4	100
Silty Clay	0.4	80
Silt	0.4	80
Silty Sand	0.4	80
Loose sand	0.4	40
Sand	0.4	40
Packed Sand	0.4	40

Table. 3.1 Parameters *λ* e *A* for different kinds of soil.

Finally, the apparent cohesion of the homogenized equivalent slope, c_ψ, depends on both c_ψ and the thickness $m \cdot H$ of the saturated sub-layer. The expression for c_ψ was obtained by performing a series of experiments on stratified soils in a flume (Montrasio & Valentino, 2007; Silva 2000) and is given by:

$$c_{\psi} = c_{\psi}^{*}(1-m)^{\alpha} \tag{3.6}$$

The safety factor is time-dependant through water variations in the top soil. Saturation ratio increases in time due to rain infiltration and decreases by evapo-transpiration, down flow and percolation. The decrease of water content is modeled in a simplified way represented by the decrease of *m* with time, which is obtained using a negative exponential function of time:

$$m_{(t)} = m_0 \cdot \exp(-k_t \cdot t) \tag{3.7}$$

where k_t represents the global drainage capability of the slope, which takes into account evapo-transpiration, down flow and percolation. The value of k_t is derived from the back-analysis of shallow landslides that occur on different kinds of soils. Finally, the formulation of the safety factor (Fs), according to the limit equilibrium method is the following:

$$F_S = \frac{\cot\beta \cdot \tan\varphi' \cdot [\Gamma + m \cdot (n_w - 1)] + C' \cdot \Omega}{\Gamma + m \cdot n_W} \tag{3.8}$$

Where:

$$\Gamma = G_S \cdot (1-n) + n \cdot S_r \tag{3.9}$$

$$n_w = n \cdot (1 - S_r) \tag{3.10}$$

$$\Omega = \frac{2}{\sin 2\beta \cdot H \cdot \gamma_w} \tag{3.11}$$

$$C' = [c' + c_\psi] \cdot L = [c' + A \cdot S_r \cdot (1 - S_r)^\lambda \cdot (1 - m)^\alpha] \tag{3.12}$$

$$m(t) = \frac{\beta^*}{n \cdot H \cdot (1 - S_r)} \sum_{i=1}^{\omega} \exp[-k_t (t - t_i)] \tag{3.13}$$

- β is the slope angle of the potentially unstable slope;
- φ' is the shear resistance angle of the soil;
- γ_w is the weight per unit volume of water;
- H is the thickness of the potentially unstable layer;
- L is the length of the soil layer;
- n is the porosity of the soil;
- G_S is the ratio between the specific unit weight of the soil and water unit weight;
- S_r is the degree of saturation of the soil;
- c' is the effective cohesion of the soil;
- c_ψ is the apparent cohesion given by the partial saturation of the soil;
- kt is the global permeability of the soil;
- A, λ are shear strength parameters under unsaturated conditions;
- α is a model parameter that is related to the homogenization.
- β^* is the amount of rain water that infiltrates into soil
- ξ is the amount of rain water that runs off (1- β^*)

Slope instability is reached when Fs < 1

Fs is a function of slope geometry (β, H), soil state (Gs, n, Sr), the shear strength parameters of the soil under saturated conditions (φ', c'), the shear strength under unsaturated conditions (A, λ), a model parameter that is related to the homogenization modeling (α), the drainage capability of the slope (k_t), the water's unit weight (γ_w) and the rainfall depth (h).

The model has been previously applied at several scales, including the *field scale* (single slope, territorial, regional, national) and the *laboratory scale* (flume tests). At the *field scale*, the approach used to evaluate the model parameters and to calculate Fs differs depending on the size of the studied area. At the scale of a single slope, the model parameters are obtained by a geotechnical

characterization of the soil (lab and in situ tests), and Fs is a deterministic value that unequivocally defines the moment of failure when its value reaches 1. At the larger scale, the parameters must be linked to geological, lithological, land use, vegetation cover and geometry (DEM - Digital Elevation Model) information, and the safety factor is defined in areas of fixed dimensions, called cells through a $n_x n$ grid (the same as the DEM). At the larger scale, the meaning of the approach is different and is linked to the susceptibility of a certain area to the occurrence of hydro-geological instability. A complete forecast of instability requires additional methods. In this case, the output of the model can be represented both as time varying safety factor maps, which give a value of Fs for each elementary cell with the same resolution as the DEM (non-aggregated results), and "instability index" maps (aggregated results). Thus, for operational purposes, the safety factors obtained on the elementary cells can be aggregated by considering larger reference areas. The "instability index" is defined as the ratio between the number of elementary cells in which Fs < 1 (instability condition) and the total number of cells in each reference area. Laboratory scale investigations such as flume tests can be used to determine the influence of the model parameters and to calibrate them. As described above, the model assumes double porosity in the soil, which strongly influences the infiltration; in lab tests, if some arrangements aren't made, the soil (even if it has the same matrix as the in situ soil) doesn't reproduce the macro-porosity which implies a process that is different from that in the field.

In chapter 7 the results of some laboratory flume tests on a silty sand, with and without these arrangements are presented. The arrangements consisted of inserting in the homogeneous soil matric some preferential infiltration channels made by gravel inclusions. The double porosity of the soil can be well seen in these tests.

Chapter 4

The Parma Apennine landslide event of April 2013 – study area

4.1 Introduction

In April 2013 a severe precipitation event hit the northern part of the Italian Apennines triggering thousands of landslides, which caused heavy damages to structures and infrastructures with consequent economic losses. The municipalities involved by the landslide events are located in the southern part of the Parma province (Figure 4.1); the mountainous territories occupy a thin Apenninic ridge between the Enza and Baganza rivers (elevation range 600 – 1800 m. a.s.l.). The geology of this area comprises complex units: the Monte Caio formation, which is a succession of calcareous marls, fine grained sandstones and thin shale layers and the Tizzano marls, which occasionally outcrop (Cerrina et al., 2002). The quaternary deposits are mainly dormant and active landslides, eluvial and colluvial deposits and talus.

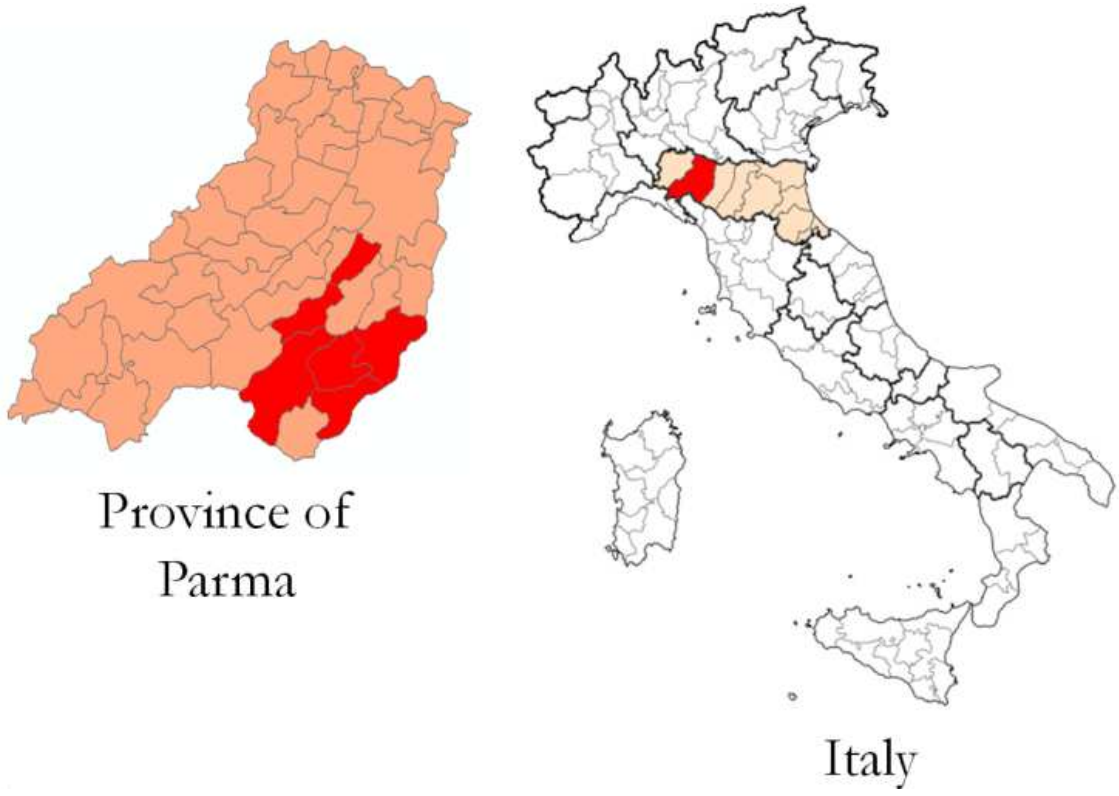

Figure 4.1 Province of Parma. In red the municipalities in which landslides were surveyed

Mean temperatures and precipitations

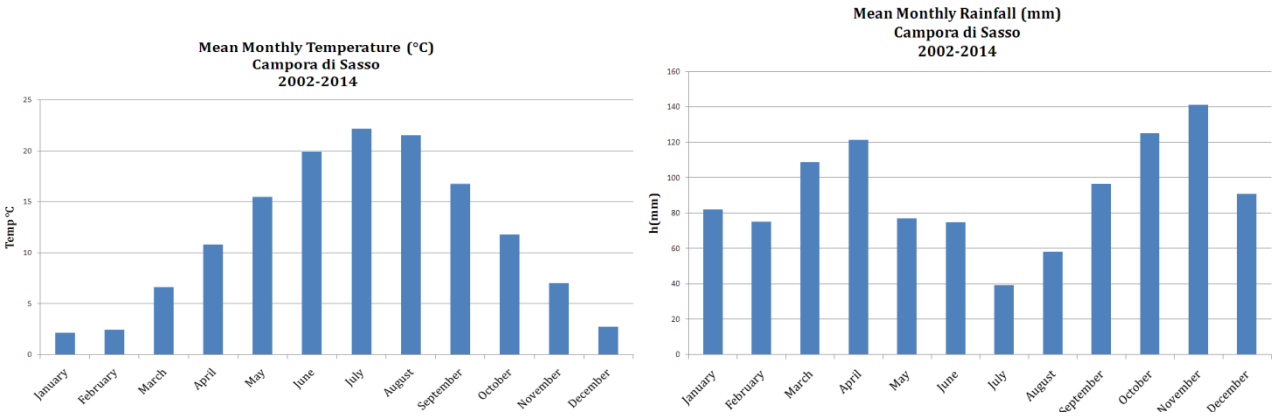

Figure 4.2 Mean monthly a) temperatures and b) precipitations at the Campora di Sasso Station (2002-2014)

The study area is characterized by a mean annual precipitation, ranging from about 1000 mm in mountain areas and about 800 mm in the hills. The trend in annual rainfall has two peaks, one in fall (October-November) and the other in spring (March-April), interspersed with two minima, a more pronounced in summer (July) and the other in winter (February). These observations are evident from analyses of daily rain averages for the period 2002-2014 detected from the thermo-pluviometric station of Campora di Sasso (649 m a.s.l, longitude 10.5212, latitude 44.2755) (Figure 4.2b), which can be considered representative of the study area. From the same station the average daily temperatures were found, the trend of which is shown in figure 4.2a which shows a maximum (20-25 °C) in July and a minimum (0-5 °C) in January. The area analyzed according to the classification of Köppen, falls in the sub-continental climate (Rossetti, 1988).

The period from March 1st to April 7th was characterized by a significant share of cumulative precipitation, especially along the Emilia-Romagna Apennines and, more generally, in the central-western part of the region. Figure 4.4 shows the cumulative precipitation between March 1, 2013 and April 7, 2013 and the precipitation anomalies for the same period compared to rainfalls between 1991-2010. What characterized this period was in fact the persistence in rainfall, which led to positive anomalies for more than half of the area with values ranging from 200% to 350% of the average rainfall for the period. These anomalies have been also preceded by an extremely rainy autumn and winter and by abundant snowfalls in February, which have contributed significantly to the activation of landslides in the following period (ARPA-SIMC 2013).

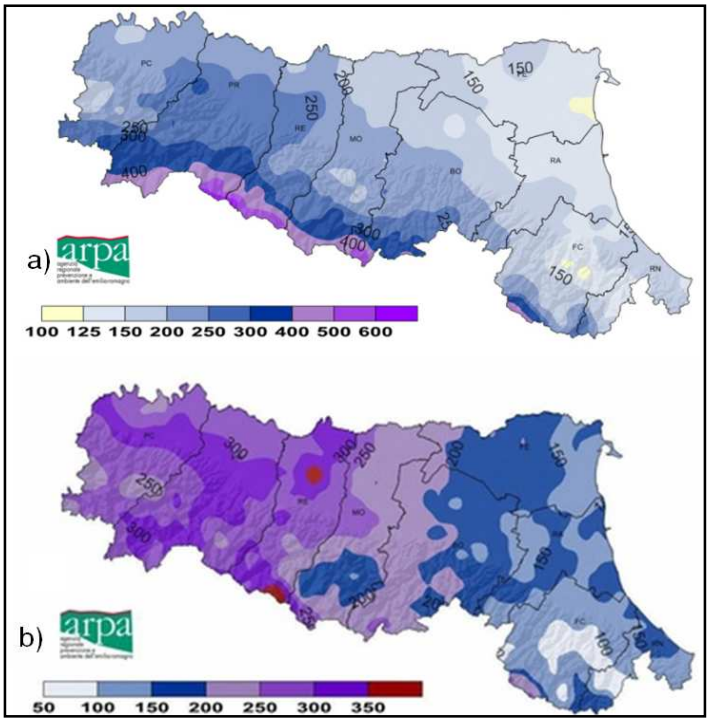

Figure 4.3 a) Precipitation map for the period: 1/03/2013-7/04/2013 and b) precipitation anomaly for the same period compared to rainfall maps between 1991-2010

4.2 Surveyed landslides

In the past years, the Apennines gained increasing interest in the scientific community and recent events underlined the need of a tool to study and prevent this fragile territory from rainfall-induced instability phenomena. Weather conditions that triggered shallow landslides in April 2013 were significantly different from previous years. In fact, analyzing the data collected by the Campora di Sasso station, only in the night between April 4th and 5th approximately 60 mm of rain fell in less than 12 hours (Figure 4.3).

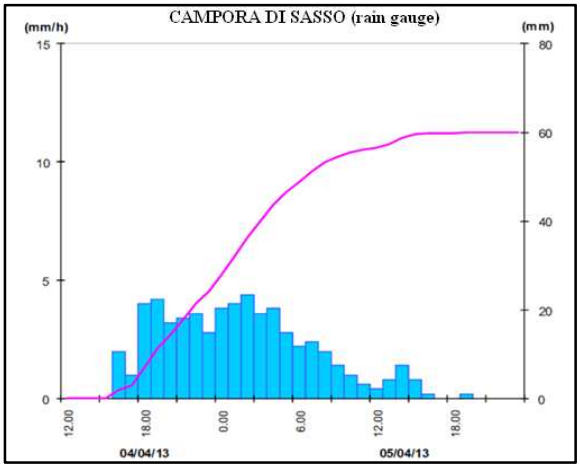

Figure 4.4 Cumulated and hourly rainfall registered at the Campora di Sasso rainfall station, situated in the Neviano degli Arduini municipality, between April 4th and April 5th 2013.

The Parma province and its municipalities have been deeply affected by the severe rainfall precipitation occurred in April 2013: in less than a month several landslides triggered in the Apennine municipalities of Calestano, Corniglio, Felino, Neviano degli Arduini, Palanzano, and Tizzano Val Parma, causing damage to crops, settlements and disruption of many road sections. The occurred landslides were located through indications provided by the Civil Protection. On the basis of this information in situ measurements of GPS coordinates locating the source area of landslides were reported. For each landslide several pictures were taken to document the event (Figures 4.6-4.11).

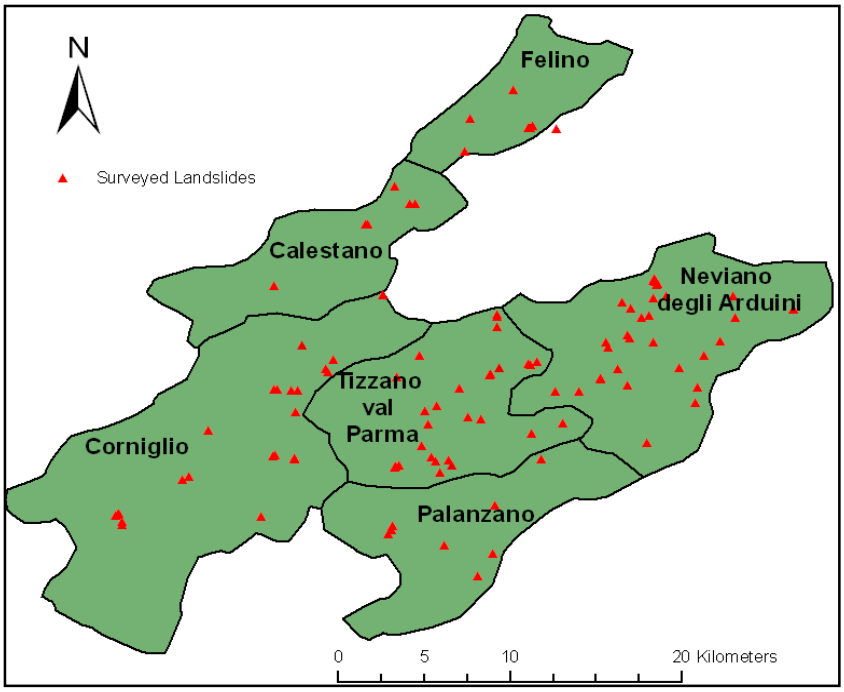

Figure 4.5 Study area: localization of surveyed landslides

A total of 97 landslides in the municipalities of Corniglio, Neviano degli Arduini, Tizzano Val Parma and Palanzano were surveyed. Subsequently a catalog reporting the type of damage (whether or not involving civil structures or infrastructures) was prepared. The municipalities that have been mostly affected were Corniglio, Neviano degli Arduini Palanzano and Tizzano Val Parma. Tables 4.1-4.6 show the location (divided by municipalities) surveyed with a brief description of the type of damage that the landslide caused. The mapped soil slips involve only the upper most part of the colluvium, composed of clayey silt, whose thickness ranges from 1 to 2 m (Montrasio and Valentino, 2008) except for the three landslides of Boschetto, Capriglio and Sauna which mobilized much greater volumes. This data was mapped in a GIS (geographical information system) environment (Figure 4.5) and used to validate the SLIP model by a comparison with its output (i.e. safety factor maps) which will be presented in the following chapter.

Landslides occurred in Calestano

Municipality	Location	Latitude	Longitude	Brief description
Calestano	Marzolara	44.6299	10.1738	Shallow slip, upstream of the road embankment, involving the roadway.
	Ramiano-ponte	44.6092	10.1598	Shallow slip , involving the roadway.
	Ramiano-2	44.6093	10.1588	Shallow slip, downstream of the road embankment, involving the roadway.
	Vallerano-capannone	44.6205	10.1848	Shallow slip on agricultural land. No road involved.
	Vallerano-strada	44.6206	10.1818	Shallow slip, downstream of the road embankment, involving the roadway.
	Vigolone	44.5755	10.1107	Shallow slip, downstream of the road embankment, involving the roadway.

Table 4.1 Location and brief description of landslides surveyed in Calestano

Figure 4.6 Photographs of some landslides surveyed in Calestano.

Landslides occurred in Corniglio

Municipality	Location	Latitude	Longitude	Brief description
Corniglio	AGNA TUFI	44.4802	10.1216	Shallow slip, downstream of the road embankment, involving the roadway.
	BELLASOLA MONTEBELLO	44.4486	10.1042	Instability, downstream of the road embankment, partially involving the roadway.
	COSTA VENTURINA	44.5348	10.1418	Instability, downstream of the road embankment, involving the roadway.
	CURIATICO SAN ROCCO 1	44.5281	10.1391	Shallow slip, downstream of the road embankment, involving the roadway.
	CURIATICO SAN ROCCO 2	44.5297	10.1381	Shallow slip, upstream of the road embankment, involving the roadway.
	LA BREA	44.4445	10.0316	Shallow slip, downstream of the road embankment, involving the roadway.
	LA BREA 2	44.4458	10.0317	Shallow slip, downstream of the road embankment, involving the roadway.
	LA MORETTA	44.5063	10.1221	Shallow slip, downstream of the road embankment, involving the roadway.
	MARTANO SESIOLO	44.5706	10.1677	Shallow slip, downstream of the road embankment, involving the roadway.
	SAUNA	44.5184	10.1108	Complex landslide that caused damage to homes and prefabricated buildings for agricultural use
	SAUNA 2	44.5186	10.1126	Complex landslide that caused damage to homes and prefabricated for agricultural use
	SAUNA (BOSCO)	44.5179	10.1201	Shallow slip on agricultural land. No road involved.
	SAUNA (Road to)	44.5178	10.1233	Instability, downstream of the road embankment, partially involving the roadway.
	SIGNATICO	44.5429	10.1255	Reactivation of a historical landslide
	SP 40 TO BOSCO	44.4706	10.0663	Instability, downstream of the road embankment, partially involving the roadway.
	SP 40 TO BOSCO	44.4691	10.0629	Instability, downstream of the road embankment, partially involving the roadway.
	STAIOLA	44.4496	10.0278	Translational landslide, upstream of the road embankment, involving the roadway.
	STAIOLA 2	44.4499	10.0291	Translational landslide, upstream of the road embankment, involving the roadway.
	STAIOLA 3	44.4505	10.0295	Translational landslide, upstream of the road embankment, involving the roadway.
	VILLULA AGNA	44.4819	10.1105	Shallow slip, downstream of the road embankment, involving the roadway.
	VILLULA AGNA 2	44.4824	10.1112	Shallow slip, upstream of the road embankment, involving the roadway.
	VESTANA	44.4959	10.0765	Shallow slip, downstream of the road embankment, involving the roadway.
	VILLULA TUFI	44.4807	10.1216	Shallow slip, downstream of the road embankment, involving the roadway.

Table 4.2 Location and brief description of landslides surveyed in Corniglio

Figure 4.7 Photographs of some landslides surveyed in Corniglio

Landslides occurred in Felino

Municipality	Location	Latitude	Longitude	Brief description
Felino	Babbiano 1 nicchia	44.6622	10.2442	Shallow slip on agricultural land. No road involved.
	Babbiano 2 nicchia	44.6619	10.2434	Shallow slip on agricultural land. No road involved.
	Babbiano 3	44.6619	10.2449	Shallow slip, downstream of the road embankment, involving the roadway.
	Babbiano 4	44.6632	10.2459	Shallow slip, downstream of the road embankment, involving the roadway.
	Tiorre	44.6619	10.2581	Shallow slip on agricultural land. No road involved.
	Felino 1 (cevola)	44.6673	10.2134	Shallow slip on agricultural land. No road involved.
	Felino 2 (castello)	44.6832	10.2360	Shallow slip, upstream of the road embankment, involving the roadway.
	Sant'Ilario B.	44.6493	10.2102	Shallow slip, upstream of the road embankment, involving the roadway.

Table 4.3 Location and brief description of landslides surveyed in Felino

Figure 4.8 Photographs of some landslides surveyed in Felino

Landslides occurred in Neviano degli Arduini

Municipality	Location	Latitude	Longitude	Brief description
Neviano degli Arduini	La Ripa1	44.5777	10.3099	Instability, downstream of the road embankment, partially involving the roadway.
	La Ripa2	44.5761	10.3105	Instability, downstream of the road embankment, partially involving the roadway.
	La Ripa3	44.5764	10.3113	Instability, downstream of the road embankment, partially involving the roadway.
	Monte Mozzano	44.5414	10.2856	Shallow slip on agricultural land. No road involved.
	Bazzano 1	44.5448	10.3441	Shallow slip, downstream of the road embankment, involving the roadway.
	Bazzano-Monterosso	44.5581	10.3521	Shallow slip involving the roadway.
	Bazzano-Monticello	44.5627	10.3821	Complex landslide involving civilian buildings.
	Bazzano-Pezzalunga	44.5614	10.3711	Shallow slip, downstream of the road embankment, involving the roadway.
	Bazzano-Prussia	44.5700	10.3508	Shallow slip, downstream of the road embankment, involving the roadway.
	Campora-Barchetto	44.5175	10.2699	Shallow slip, downstream of the road embankment, involving the roadway.
	Ca' Notari	44.5248	10.2814	Shallow landslide
	Campora-Strada	44.5240	10.2814	Shallow slip, downstream of the road embankment, involving the roadway.
	Case Barbieri	44.5698	10.3156	Shallow slip involving the roadway.
	Cedogno	44.5371	10.3356	Shallow slip, upstream of the road embankment, involving the roadway.
	Ceretolo	44.5112	10.3309	Shallow slip, downstream of the road embankment, involving the roadway.
	Ceretolo Frana 2	44.5196	10.3319	Shallow slip, downstream of the road embankment, involving the roadway.
	I Boschi	44.5467	10.2966	Shallow slip on agricultural land. No road involved.
	I Boschi 2	44.5483	10.2957	Shallow slip on agricultural land. No road involved.
	I Boschi 3	44.5443	10.3089	Shallow slip on agricultural land. No road involved.
	La Ripa 4	44.5781	10.3095	Shallow slip involving the roadway.
	La Ripa 5	44.5783	10.3092	Shallow slip, downstream of the road embankment, involving the roadway.
	La Ripa 6	44.5793	10.3098	Shallow slip, downstream of the road embankment, involving the roadway.
	Lupazzano Altavilla	44.5591	10.3068	Shallow slip on agricultural land. No road involved.
	Lupazzano Altavilla	44.5582	10.3028	Shallow slip on agricultural land. No road involved.
	Molinetto	44.5687	10.3088	Complex Landslide near agricultural buildings.
	Monte di Mozzano	44.5443	10.2842	Shallow slip on agricultural land. No road involved.
	Ripa Pavone	44.5302	10.3224	Shallow slip, downstream of the road embankment, involving the roadway.
	Scurano	44.5210	10.2955	Shallow slip, downstream of the road embankment, involving the roadway.
	Scurano_2	44.4894	10.3056	Shallow slip, downstream of the road embankment, involving the roadway.
	Sella di Lodignano	44.5301	10.2904	Shallow slip, downstream of the road embankment, involving the roadway.
	Urzano Mozzano	44.5628	10.2974	Shallow slip on agricultural land. No road involved.
	Urzano-Mozzano2	44.5662167	10.2926	Shallow slip on agricultural land. No road involved.

Table 4.4 Location and brief description of landslides surveyed in Neviano degli Arduini

Figure 4.9 Photographs of some landslides surveyed in Neviano degli Arduini.

Landslides occurred in Palanzano

Municipality	Location	Latitude	Longitude	Brief description
Palanzano	Isola di Palanzano	44.4331	10.1724	Shallow slip, upstream of the road embankment, involving the roadway.
	Lalatta	44.4625	10.2149	Instability, downstream of the road embankment, partially involving the roadway.
	Selvanizza	44.4353	10.2227	Shallow slip, upstream of the road embankment, involving the roadway.
	SP 665 Km 42	44.4802	10.2506	Shallow slip, downstream of the road embankment, involving the roadway.
	SP102	44.4328	10.1998	Instability, downstream of the road embankment, partially involving the roadway.
	Strada per la Grotta	44.4284	10.2250	Shallow slip on agricultural land. No road involved.
	Trevignano	44.4389	10.1705	Shallow slip, downstream of the road embankment, involving the roadway.
	Trevignano 2	44.4414	10.1722	Shallow slip on agricultural land. No road involved.
	Trevignano 3	44.4440	10.1725	Instability, downstream of the road embankment, partially involving the roadway.
	Vaestano	44.4163	10.2173	Shallow slip on agricultural land. No road involved.
	Vezzano	44.5174	10.2580	Shallow slip involving the roadway.

Table 4.5 Location and brief description of landslides surveyed in Palanzano.

Figure 4.10 Photographs of some landslides surveyed in Palanzano.

Landslides occurred in Tizzano Val Parma

Municipality	Location	Latitude	Longitude	Brief description
Tizzano	Antognola	44.5021	10.2190	Shallow slip on agricultural land. No road involved.
	Boschetto_body	44.5316	10.2289	Complex landslide with great damage to road.
	Boschetto_detachment area	44.5306	10.2286	Complex landslide with great damage to road.
	Capoponte1	44.5600	10.2273	Shallow slip on agricultural land. No road involved.
	Capoponte2	44.5587	10.2276	Shallow slip on agricultural land. No road involved.
	Capoponte3	44.5532	10.2272	Shallow slip on agricultural land. No road involved.
	Capriglio	44.4768	10.2036	Complex Landslide on agricultural land.
	Capriglio 2	44.4800	10.2018	Instability partially involving the roadway.
	Capriglio 3	44.4792	10.1950	Instability partially involving the roadway.
	Carpaneto	44.5194	10.2076	Shallow slip, upstream of the road embankment, involving the roadway.
	Casa Galvana	44.4728	10.1978	Instability partially involving the roadway.
	Cisole Strada 1	44.5271	10.2241	Instability partially involving the roadway.
	Cisole Strada 2	44.5265	10.2233	Instability partially involving the roadway.
	Fontanafredda Groppo	44.5033	10.2122	Shallow slip on agricultural land. No road involved.
	Groppizioso	44.4876	10.1881	Shallow slip, downstream of the road embankment, involving the roadway.
	Groppo - Lagrimone	44.4996	10.1913	Shallow slip, upstream of the road embankment, involving the roadway.
	Moragnano	44.4941	10.2454	Shallow slip, downstream of the road embankment, involving the roadway.
	Musiara	44.5069	10.1895	Shallow slip, downstream of the road embankment, involving the roadway.
	Pietta_1	44.5327	10.2436	Shallow slip on agricultural land. No road involved.
	Pietta_2	44.5323	10.2446	Shallow slip on agricultural land. No road involved.
	Pietta_3	44.5339	10.2482	Shallow slip on agricultural land. No road involved.
	Pratopiano	44.4551	10.2263	Shallow slip, downstream of the road embankment, involving the roadway.
	Reno	44.5374	10.1869	Shallow slip on agricultural land. No road involved.
	Rusino	44.4998	10.2616	Shallow slip on agricultural land. No road involved.
	Schia	44.4757	10.1740	Shallow slip, downstream of the road embankment, involving the roadway.
	Schia 2	44.4768	10.1761	Shallow slip, downstream of the road embankment, involving the roadway.
	Schia 3	44.4761	10.1743	Shallow slip, downstream of the road embankment, involving the roadway.
	Strada Casola Reno	44.5254	10.1749	Shallow slip, downstream of the road embankment, involving the roadway.
	Strada Font-Groppo	44.5096	10.1957	Shallow slip, downstream of the road embankment, involving the roadway.
	Strada per Schia	44.4813	10.1928	Shallow slip, downstream of the road embankment, involving the roadway.

Table 4.6 Location and brief description of landslides surveyed in Tizzano Val Parma

Figure 4.11 Photographs of some landslides surveyed in Tizzano Val Parma.

4.3 Geotechnical characterization

Geotechnical tests have been made on the superficial portion of the soil involved in Emilian Apennine soil slips in previous works of our research team (Montrasio & Valentino 2008, Losi 2012) on different sites in the provinces of Parma, Reggio Emilia and Modena. The proximity and similarities in geological formations, topography and climatic conditions of these study areas justifies the extension of this data to our study area. In the future, further geotechnical analysis can be made on soils involved in landslides triggered in the Parma province in 2013 to confirm these assumptions. The data provided by Losi (2012) is the following:

Index properties

The soil samples of the triggered landslides were taken at a depth of 0.30 m, 0.60 m and 1.00 m and were subjected to laboratory tests which have allowed to obtain the following index properties:
water content (w), unit volume weight of the dry soil (γ_d), void ratio (e), porosity (n), and saturation ratio (Sr). The results of these tests are plotted in Figures 4.12-4.16. The investigated properties are different for the various samples at changing depths but this variability is included in a range of values plotted by the dashed red lines and summarized in Table 4.7.
The natural water content is the ratio between the mass of water (W_w) and the mass of the solid particles of the soil (W_s):

$$w = \frac{Ww}{Ws} \cdot 100(\%) \tag{4.1}$$

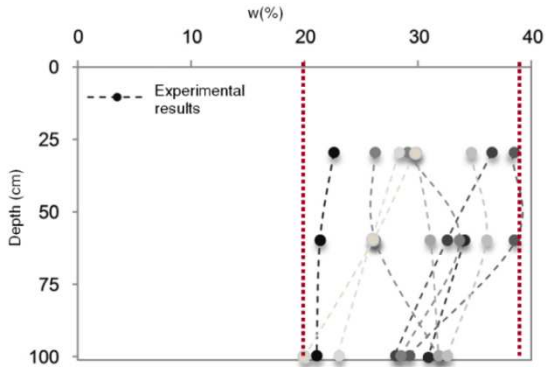

Figure 4.12 Water content vs. depth for 8 sites involved in shallow landsliding in the Emilian Apennines

The dry unit volume weight γ_d of the soil can be determined by drying an undisturbed specimen of known volume V in a heated oven (105 °C) until it reaches a constant weight W_d

$$\gamma_d = \frac{W_d}{V}\left[\frac{kN}{m^3}\right] \tag{4.2}$$

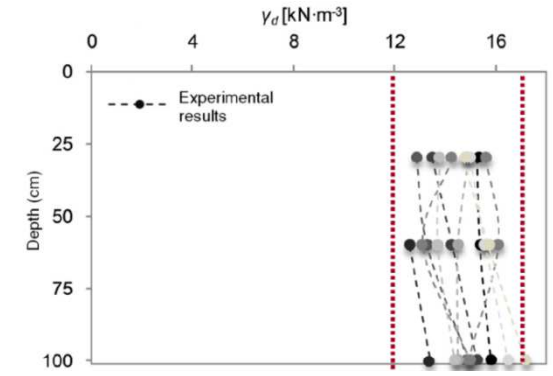

Figure 4.13 Dry unit volume weight vs. depth for 8 sites involved in shallow landsliding in the Emilian Apennines

The void ratio (e) is expressed by the ratio between the void volume (Vv) and the solid volume (Vs) of a specimen while porosity (n) is the ratio between the void volume (Vv) and the total volume of the specimen (*V*).

$$e = \frac{Vv}{Vs} = \frac{n}{1-n} \tag{4.3}$$

$$n = \frac{Vv}{V} = \frac{e}{1+e} \tag{4.4}$$

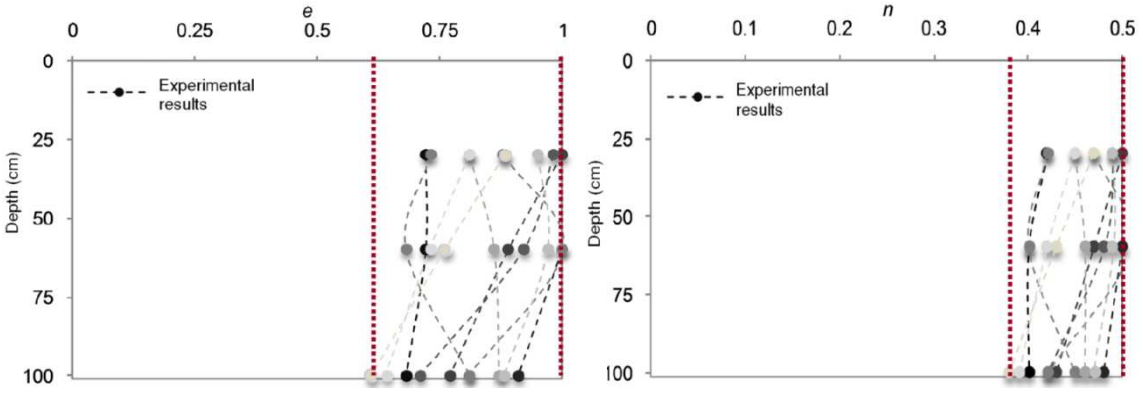

Figure 4.14 a) Void ratio and b) porosity vs. depth for 8 sites involved in shallow landsliding in the Emilian Apennines

The saturation ratio (*Sr*) expresses the percentage of water volume (Vw) that fills the voids (Vv) and ranges from 0 (dry soil) to 1 (saturated soil):

$$Sr = \frac{Vw}{Vv} \cdot 100(\%) \tag{4.5}$$

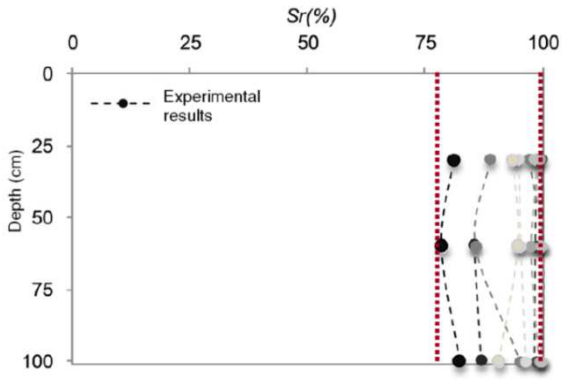

Figure 4.15 Saturation ratio vs. depth for 8 sites involved in shallow landsliding in the Emilian Apennines

Property	Range of values
w % [-]	20-40
γ_d [kN/m^3]	12-16
e [-]	0.65-1.00
n % [-]	38-50
Sr % [-]	78-100

Table 4.7 Range of values of index properties of the superficial soil involved in shallow landsliding in the Emilian Apennines.

Grain size distribution

The tests were carried out first by sieving the whole amount of soil and then by sedimentation tests on the fine grained portion of the superficial soil.

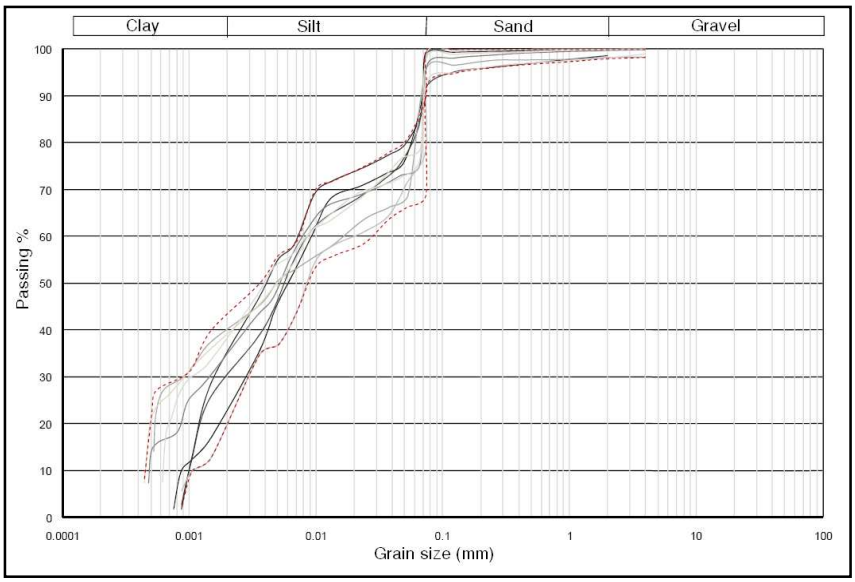

Figure 4.16 Grain size distribution of the superficial soil involved in shallow landsliding in the Emilian Apennines.

The mean percentages of soil are 0,5% of gravel, 2,9 % of sand, 65,4 % of silt and 31,2 % of clay. The soil is predominantly a clayey silt.

Atterberg Limits

The behavior of sands and gravels is greatly influenced by the size and shape of the particles that compose them while that of fine-grained soils depends on the mineralogical composition, the water content and structure. Therefore, for clays and silts, a completely different set of parameters must be considered. In fact, clay materials acquire different plasticity characteristics with the varying of the water content. A clay specimen can present a liquid, plastic, semi-solid and solid state (Figure 4.17).

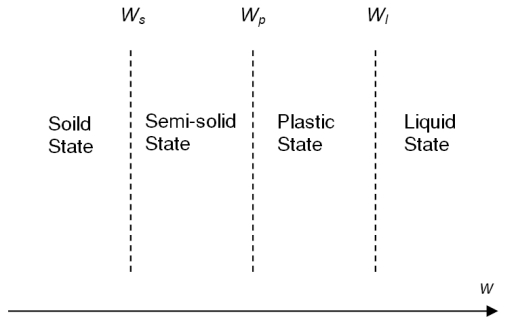

Figure 4.17 States of consistency of clay (Lancellotta, 2004).

The limits of water content, which define the field of plastic behavior of a material, are defined as liquid limit W_L and plastic limit W_P and are indicated in the literature as Atterberg limits, from the name of the researcher who in 1900 introduced them, although their potential in soil mechanics was explained only by Terzaghi in 1926. For the determination of the liquid limit the Casagrande spoon is used. For this test, a soil specimen sieved through the 40 ASTM sieve (mesh opening 0.425 mm) is used. The plastic limit is evaluated through the realization of sticks of soil of diameter 3.2 mm, which are molded on a glass plate. The plastic limit is reached in correspondence with the appearance of the first cracks on the sticks where the water content is evaluated.

The interval within which the material has a plastic behavior is defined by the index of plasticity PI.

$$PI = w_L - w_P \tag{4.6}$$

Once the plasticity index is determined, the fine-grained soils can be classified using the Casagrande plasticity chart adapted to the unified system (Unified Soil Classification System). The chart is divided into four regions by line A (Equation 4.7) and a vertical line in correspondence of w_L = 50%. The results of the tests are plotted in Figure 4.18

$$A: PI = 0.73(w_L - 20) \tag{4.7}$$

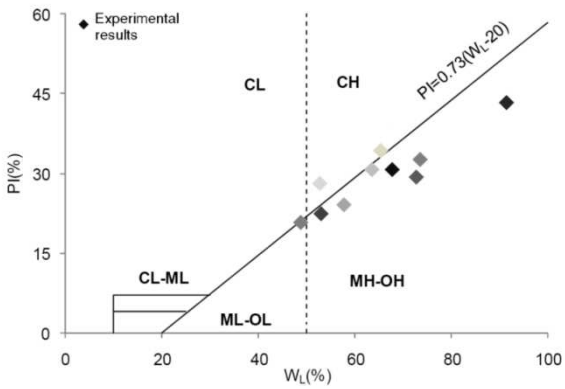

Figure 4.18 Results of Atterberg limit tests plotted in the plasticity chart of Casagrande

The results of these tests indicate that the soil is predominantly MH-OH indicating a highly compressible silt. The mechanical properties of this soil were found through consolidated drained triaxial tests ran in the geotechnical laboratory of Parma. The results of these tests show how the majority of the specimens are normally consolidated, with the typical hardening deviatoric stress-axial strain path and decreasing volumetric strain (shearing at constant volume). Referring to the Mohr-Coulomb criterion the internal friction angle (φ') ranges from 23-26° and the effective cohesion (c') is considered null. Table 4.8 summarizes the range of values found by laboratory tests.

Input parameter	Description	Value
H	Soil depth	1.5 m
n	Porosity	48 (%)
Gs	Solid weight ratio	2.6
c'	Effective cohesion	0 (kPa)
φ'	Internal friction angle	35 (°)

Table 4.8 Values of input parameters of the SLIP model for Apennine soil

Chapter 5

The Parma Apennine landslide event of April 2013 – modeling

In this chapter the results of the application of the SLIP model to the study area described in chapter 4 are shown. SLIP was applied to the four municipalities of Corniglio, Neviano degli Arduini, Palanzano and Tizzano being the most affected by the landslide events. Two different sets of parameters were applied to this area, the first based only on laboratory tests and previous works, the latter taking information also from a new innovative technique based on a spatial differentiation of land use classes from flight photo-interpretation.

5.1 Rainfall Maps

A fundamental data input of the SLIP model are time varying rainfall maps. 12 hour cumulated rain depths collected from 8 rain stations situated inside the studied municipalities (Figure 5.1) were used to create rainfall maps using the invert distance weighted (IDW) method. The IDW method is a straightforward and non-computationally intensive method (Lu & Wong, 2008). It has been regarded as one of the standard spatial interpolation procedures in geographic information science (Burrough & McDonnell, 1998; Longley et al., 2001). The IDW method used consists of superimposing a grid of square mesh with equally spaced lines with generic orientation to the study area. In each node of the grid the rainfall depth is calculated by considering the values of the 4 nearest rain gauges. The depth h_i, referring to the i-th node, is given by the following formula:

$$h_i = \sum_{j=1}^{4} h_j \cdot P_{ij} \qquad (5.1)$$

Where h_j is the rain depth of the j-th station and P_{ij} is the weight of that station proportional to the square of the distance (d_{ij}) between the node and the station.

$$P_{ij} = \frac{1}{d_{ij}^2} \cdot \frac{1}{\sum_{j=1}^{4} \left(\frac{1}{d_{ij}} \right)^2} \qquad (5.2)$$

$$\sum P_{ij} = 1$$

Each node is assigned to an area of influence where the rain depth is assumed homogeneous. The areas of influence in our analysis are square cells of 5 m side according to the resolution of the DEM.

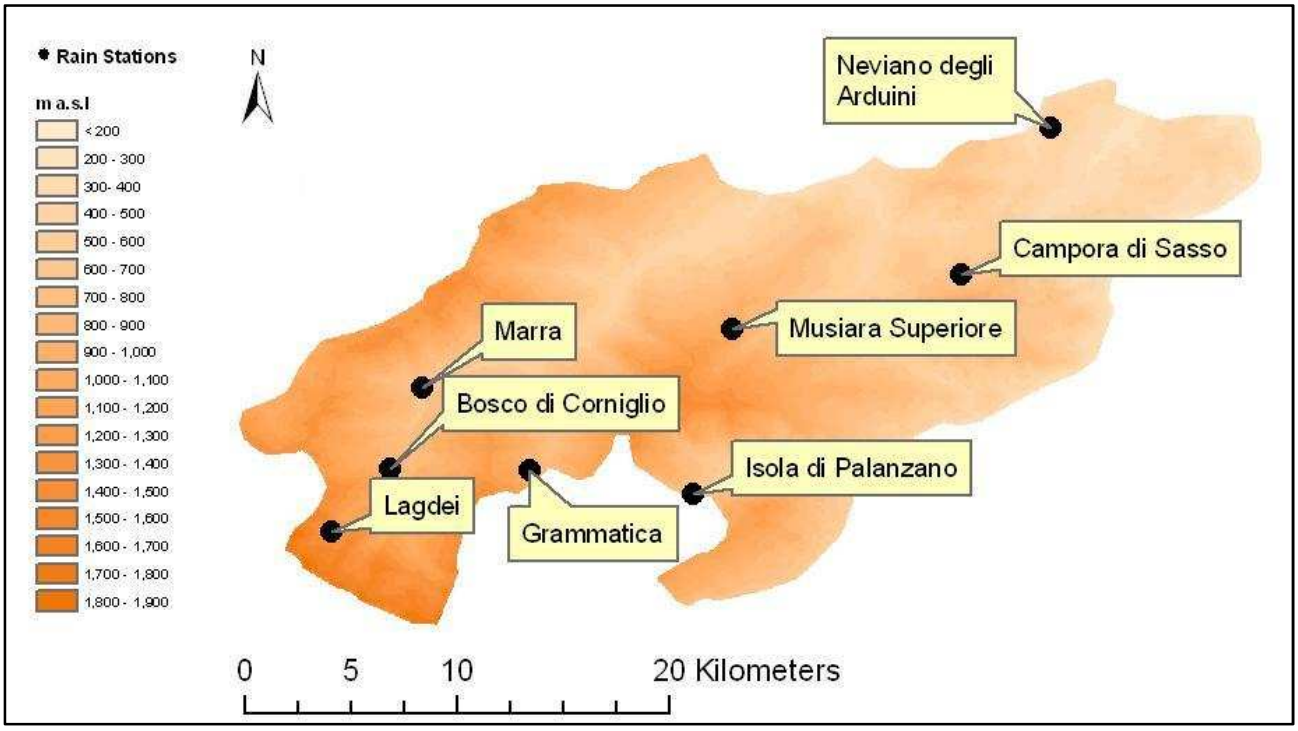

Figure 5.1 DEM and location of rain stations of the study area

In the following figures (5.2-5.8) the 12 hour cumulated rainfalls, for the period March 1st – April 7th 2013, registered at each rain station in the study area are reported. It is evident that there is an abundance of rainfall in the month preceding the landslide events that triggered mostly in the first week of April with two peaks, one around the 19th of March and a second one in the night between the 4th and 5th of April.

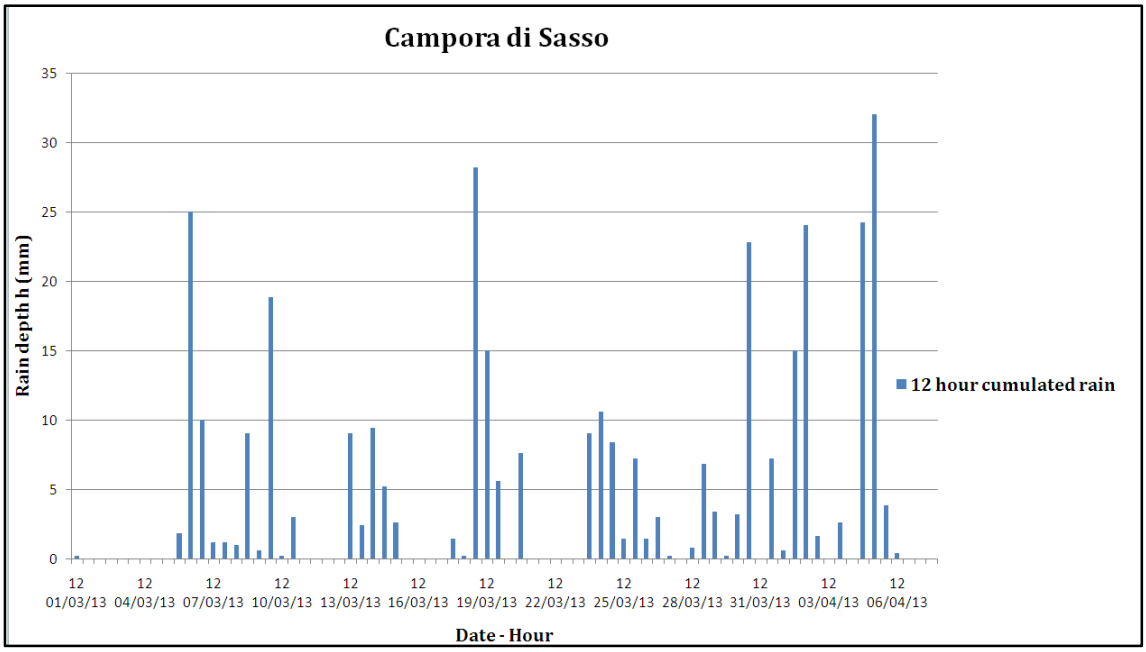

Figure 5.2 12 hour cumulated rainfall registered at the Campora di Sasso rainfall station between March 1st and April 7th 2013

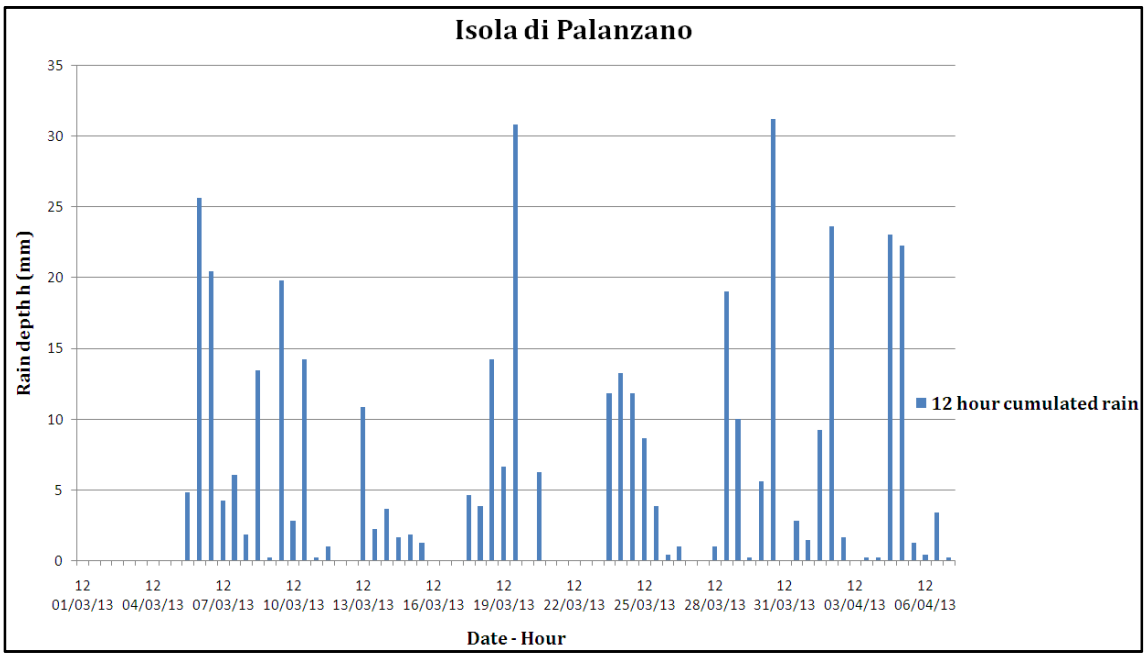

Figure 5.3 12 hour cumulated rainfall registered at the Isola di Palanzano rainfall station between March 1st and April 7th 2013

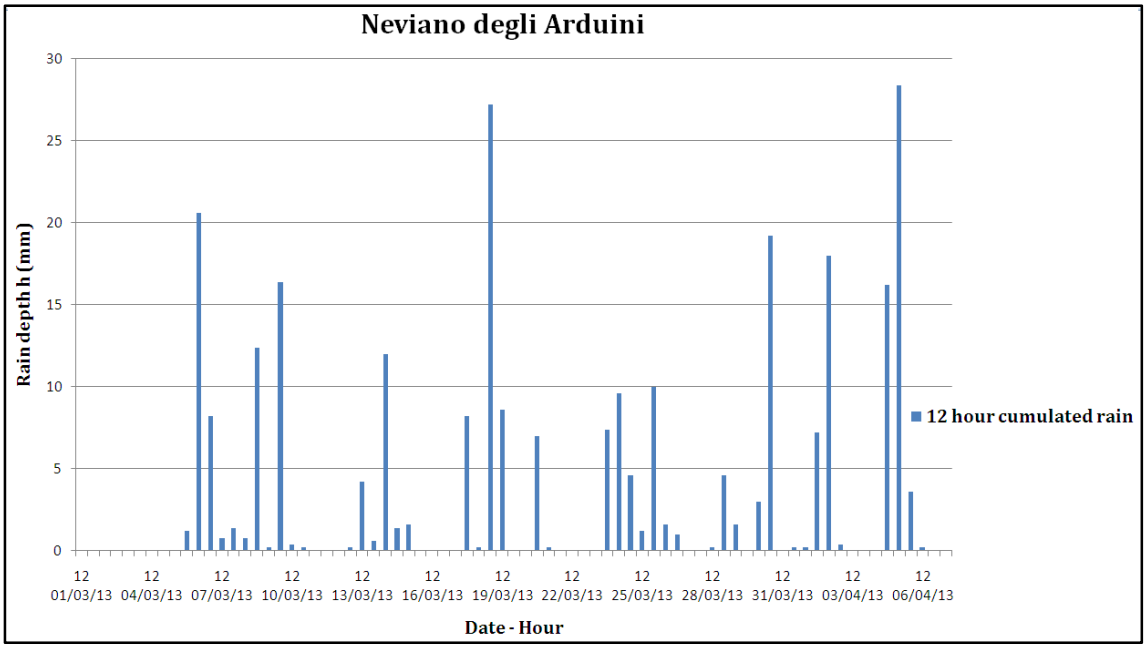

Figure 5.4 12 hour cumulated rainfall registered at the Neviano degli Arduini rainfall station between March 1st and April 7th 2013

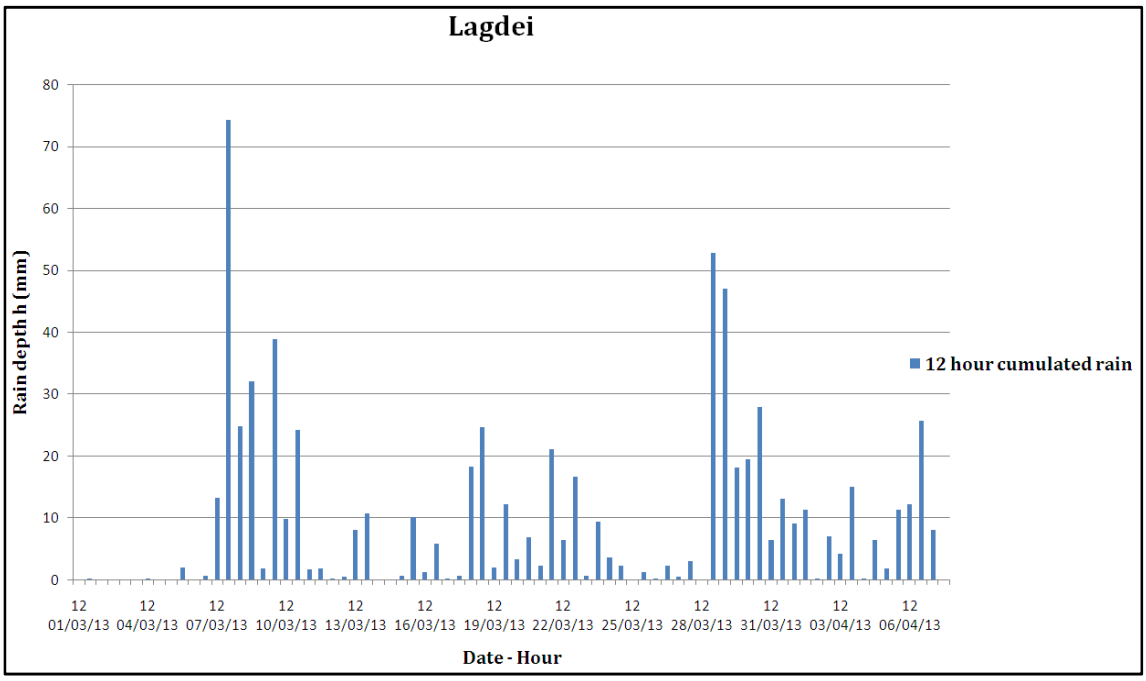

Figure 5.5 12 hour cumulated rainfall registered at the Lagdei rainfall station between March 1st and April 7th 2013

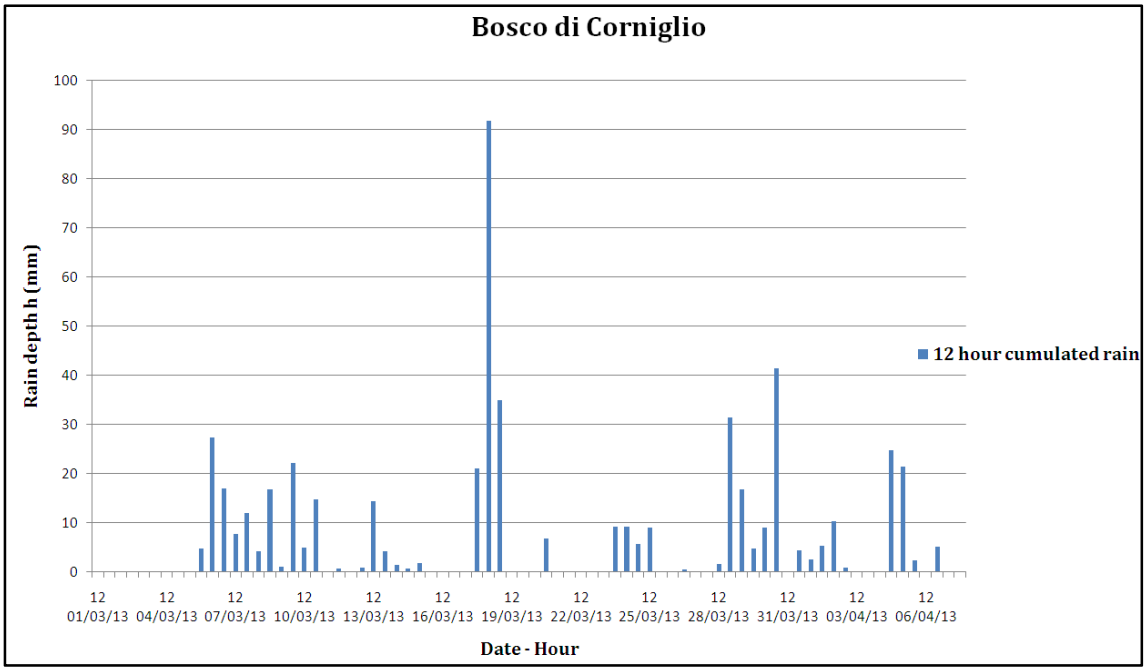

Figure 5.6 12 hour cumulated rainfall registered at the Bosco di Corniglio rainfall station between March 1st and April 7th 2013

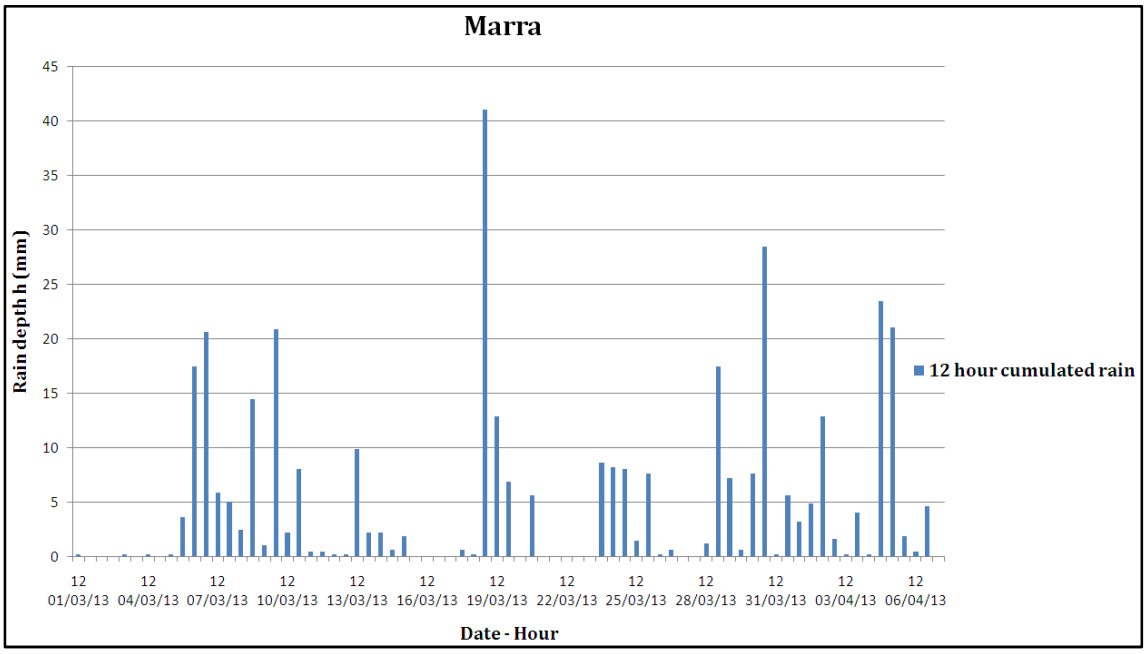

Figure 5.7 12 hour cumulated rainfall registered at the Marra rainfall station between March 1st and April 7th 2013

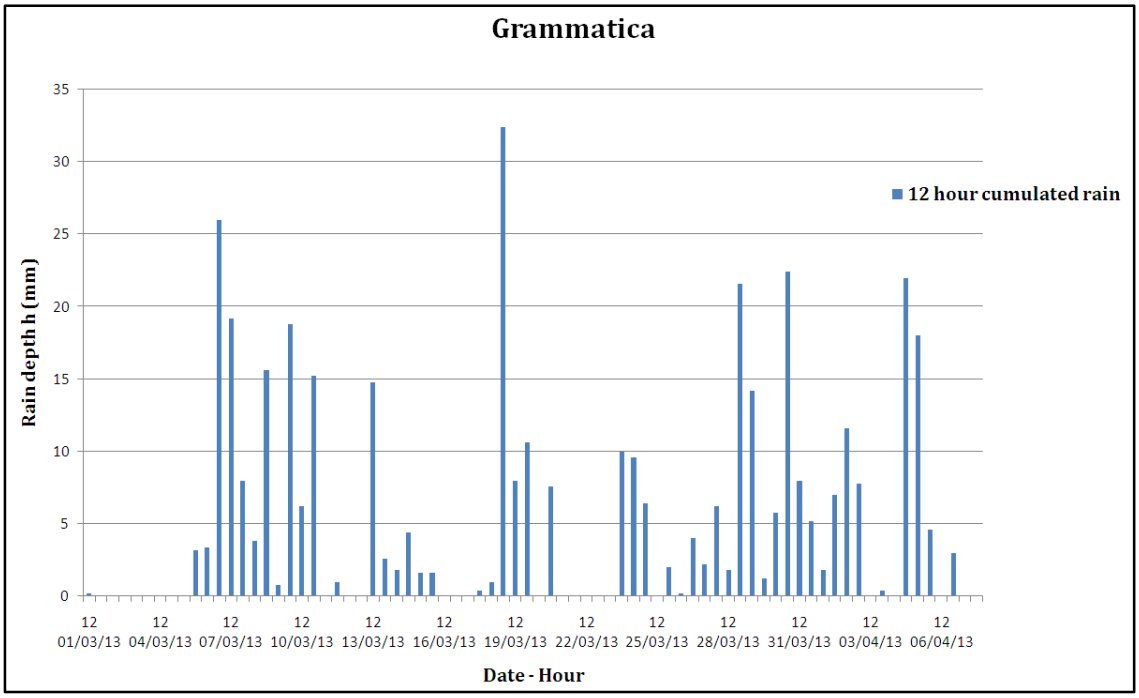

Figure 5.8 12 hour cumulated rainfall registered at the Grammatica rainfall station between March 1st and April 7th 2013

The results of the Musiara Superiore rainfall station are not reported because it only registered the daily cumulated rainfall for this period. In figure 5.9 an example of a rain map used in the SLIP modeling is shown.

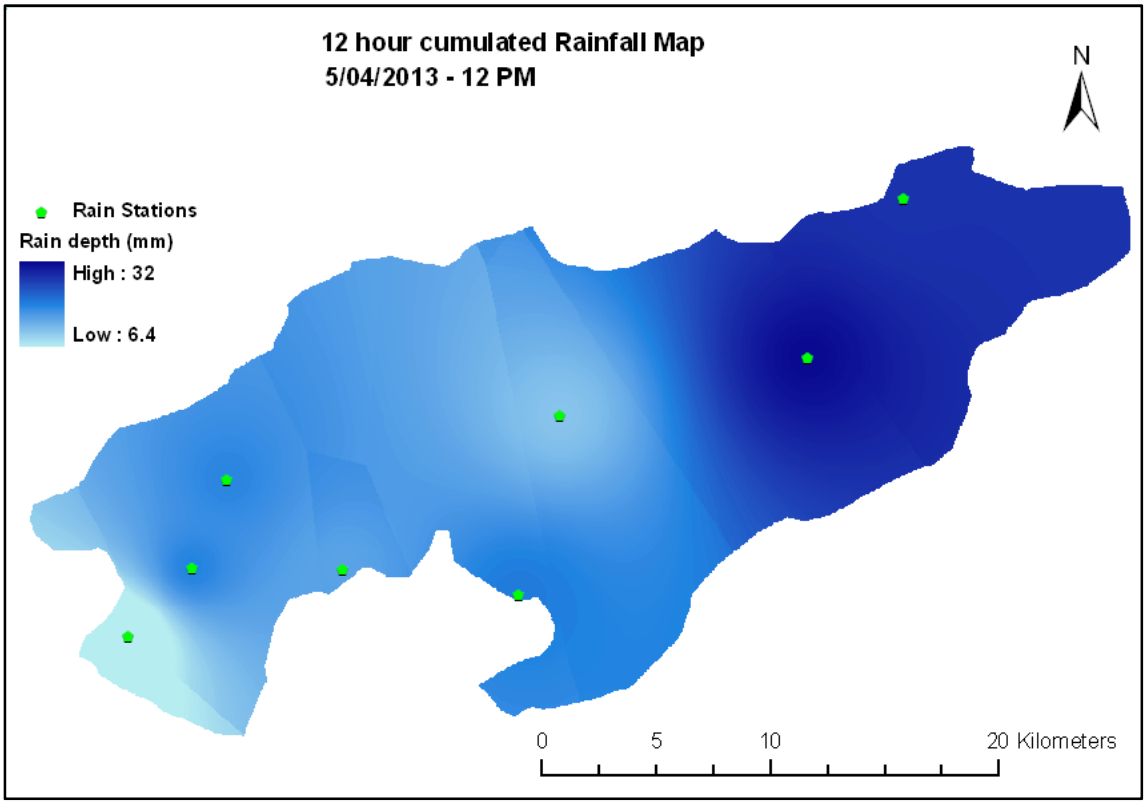

Figure 5.9 Rainfall map of April 5th at 12 PM created using the IDW method

5.2 Input parameters of the SLIP modeling

The first set of input parameters is derived from the information reported in chapter 4 and previous works (Table 5.1).

Input parameter	Description	Value
H	Soil depth	1.5 m
h	rain depth	Spatial/temporal map (m)
β	Slope angle	Spatial map from 5x5 m DEM (°)
n	Porosity	48 (%)
Gs	Solid weight ratio	2.6
Sr	Saturation ratio	Seasonably variable
ξ	Runoff	30 %
c'	Effective cohesion	0 (kPa)
φ’	Internal friction angle	25 (°)
A	Apparent cohesion parameter	100 (kPa)
λ	Apparent cohesion parameter	0.4
α	SLIP parameter	3.4
K_T	Global drainage capacity	$5 \cdot 10^{-7}$ (1/s)

Table 5.1 Set 1 Input parameters

In this study a second set of parameters was found based on an innovative technique used to calibrate some input parameters of the SLIP model. In order to give a further spatial distribution to the input parameters a high-resolution imagery (pre-event orthophotos taken between May and June 2011 (AGEA flight), with 0.5 m of spatial resolution in the RGB-Nir bands) was classified using the Maximum Likelihood algorithm.

Remote sensing is aimed at mapping and monitoring terrestrial, oceanic and atmospheric surfaces; it is therefore implicit that this subject covers a multidisciplinary field of studies. Its applications and techniques represent an important tool in environmental management, providing up-to-date detailed information about land condition and use. With remote sensed data it is possible to acquire information on hardly accessible areas, such as deserts and mountainous environments (Morandi, 2013). One of the main purposes of remote sensing techniques is to produce thematic maps of the investigated surfaces (usually a more or less extensive portion of the earth's surface); the realization of these thematic maps goes through various stages, including data recovery, processing and interpretation. Through the classification of the digital images different surface classes can be

found. Through different procedures developed for this purpose, based on the use of certain algorithms, the pixels of an image are automatically assigned to different categories such as different soil uses, vegetation cover, temperature etc. In supervised classification, the technique used in this study, the operator provides the key to defining the different categories by highlighting a representative number of example pixels directly on the images, named training sets, for each category in which the surface will be divided. It is therefore necessary to identify more than one area referable to the same category on the image, in order to cover all possible aspects of that category. Each training set consists of multiple training sites that must be selected across the whole map in order to be representative of that category. These pixels will be used by the algorithm to classify all the remaining pixels (Figure 5.10). The study area was divided into 4 soil cover classes: (i) Roads, buildings and outcrops (red); (ii) Grass (light green); (iii) Forests (dark green); and (iv) bare soil (brown) (Figure 5.5). Post-classification assessment calculation revealed that the adopted classification technique proved to be successful in discriminating these four land cover classes (Overall Accuracy resulted 92%). Figure 5.10 shows a diagram of the functioning of the program used for classification.

Figure 5.10 Example of image classification: a) a detail of the AGEA flight image, b) examples of training sites of the four classes c) output of the program in which all pixels are classified in one of the four categories.

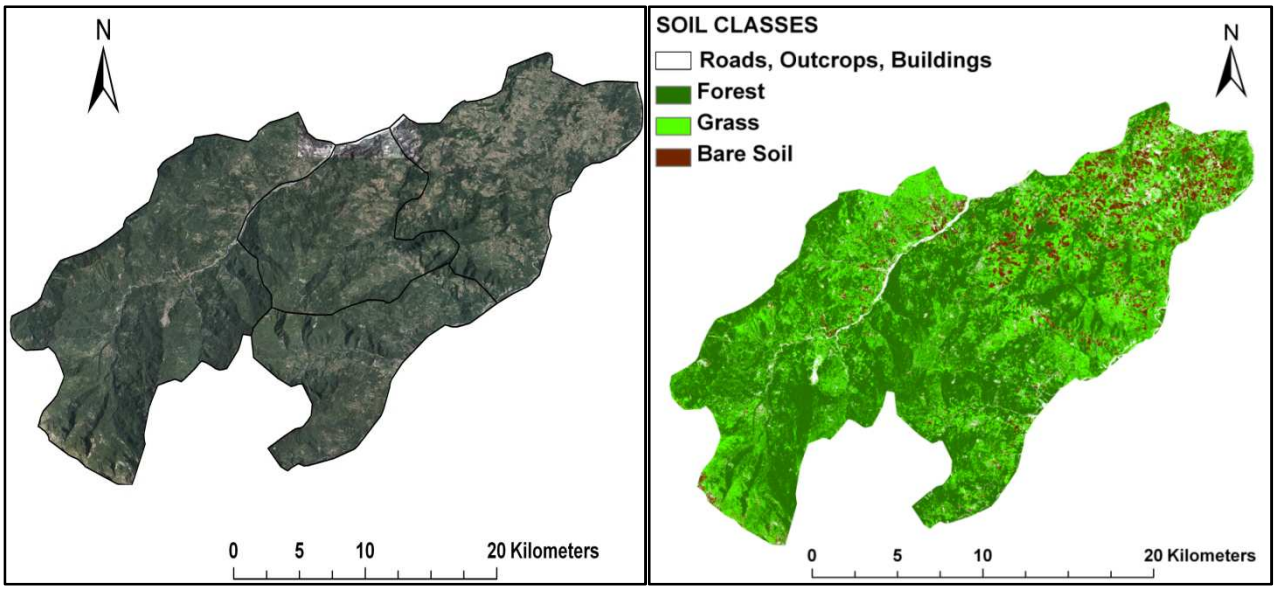

Figure 5.11 Study area flight image and corresponding earth observation classification in 4 cover classes.

The ASCII files prepared in GIS environment are based on a 5x5 m DEM. We considered different values of β* (infiltration rate) across the landscape based on the soil cover classes defined by the earth observation technique, considering a higher infiltration for bare soils and lower infiltration due to vegetation. The values of β* are reported in Table 5.2. Furthermore a contribution of strength named root cohesion of 4 kPa (Cr) was added to the cohesive forces in forest areas hypothesizing a beneficial contribution to slope stability in these areas. The thickness of the fissured sliding material (H) is assumed to be on average 1.5 m, based on site observations. There is no correlation between soil thickness and slope angle because of the absence of an underlying bedrock, differently from the study of Giampilieri presented in the following chapters. Only the first 1.5m are considered to be fissured and this is assumed for each slope angle based on site observations. The input parameters of the model are listed in Tables 5.2-5.5. Except for infiltration rate, root cohesion and soil thickness (H), the values of these parameters are based on previous works and laboratory tests described in chapter 4.3 (Montrasio and Valentino 2008; Montrasio et al. 2009, Losi 2012).

Land cover	Runoff (%)	Root cohesion (kPa)
Forest	40	4
Grass	30	0
Bare Soil	20	0
Outcrops, Buildings, etc.	No calculation performed	

Table 5.2 Input parameters that vary with land cover class

Input parameter	Description	Value
H	Soil depth	1.5 m
h	rain depth	Spatial/temporal map (m)
β	Slope angle	Spatial map from 5x5 m DEM (°)
n	Porosity	48 (%)
Gs	Solid weight ratio	2.6
Sr	Saturation ratio	Seasonably variable (90% in April)
ξ	Runoff	Variable with land cover class
c'	Effective cohesion	0 (kPa)
c_r	Root cohesion	4 (kPa) only in forest areas
φ’	Internal friction angle	35 (°)
A	Apparent cohesion parameter	100 (kPa)
λ	Apparent cohesion parameter	0.4
α	SLIP parameter	3.4
K_T	Global drainage capacity	$5 \cdot 10^{-7}$ (1/s)

Table 5.3 Set 2 input parameters

5.3 Model output: safety factor maps

The output of the SLIP model are time-varying safety factor maps shown in figure 5.12. Figures a, b and c represent the study area respectively at 12 PM on the 4th of April 2013, 12 AM of April 5th 2013 and 12 PM of April 5th 2013, calculated with the first set of parameters while figures d, e and f are calculated with the second set of parameters taking into account spatial variability from flight image classification. Three colors have been used to define the safety factor computation class, namely red for unstable pixels (FS < 1), yellow for areas near instability but still stable (1 < FS < 1.5) and blue for stable pixels (Fs > 1.5). The safety factor maps have a peak number of unstable pixels on April 5th 2013 at 12.00 pm; according to the local newspaper and witnesses, this time corresponds to the time interval when most of the landslides were triggered. A further consideration on SLIP’s ability to predict landslides, in terms of time, can be seen by the time varying FS maps in the days before the landslide event that have low instability. This result highlights the model’s ability prediction of the triggering instant, in fact on April 4th there is no instability detected while the first unstable pixels appear on April 5th at 12.00 am and evolve in maximum instability on April 5th at 12 pm. The instability scenario depicted by the model represents realistically the shallow landslides distribution, triggered by the April 2013 precipitation event. The second set of parameters gives a better prediction resulting in less false alerts showing how a precise spatial

variation gives more accurate results. Nevertheless also in this case there are regions where the instability is clearly over predicted. These results, driven by a high false positive rate, might be related to the accuracy of the mapped landslides (source areas). The surveyed landslides are indeed the ones that were visible from the roads. Since no post-event images are available, we cannot exclude that other unmapped landslides were triggered. The area where the instability is over-predicted corresponds to the uppermost part of a southwest facing hill slope, mainly covered by ploughed fields and distant from the main road network. It would be optimal to retrieve post-event images in order to integrate and complete our landslide database, particularly in those portions of the study area, which are not easily accessible or distant from roads.

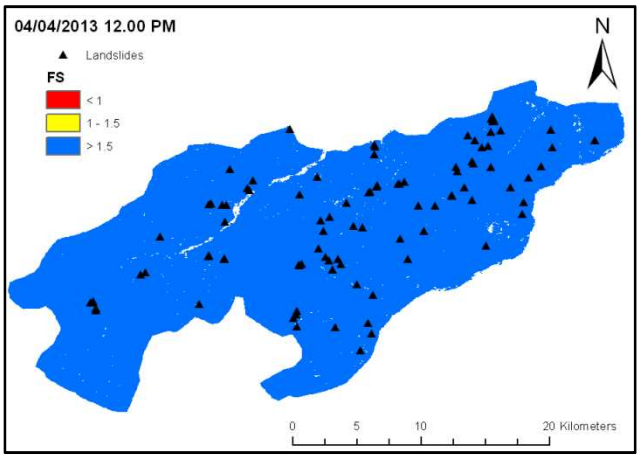

a)

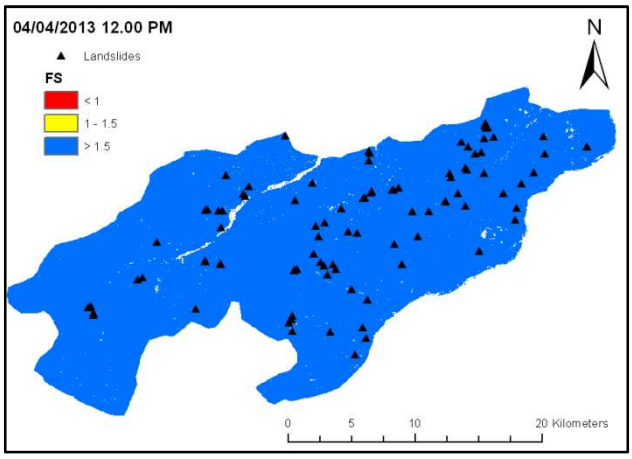

d)

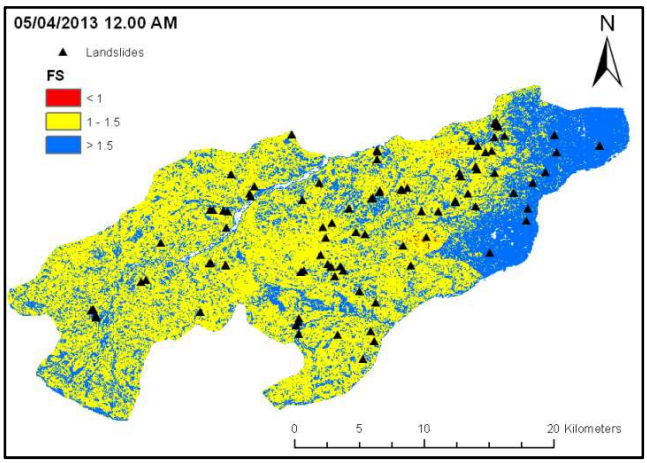

b)

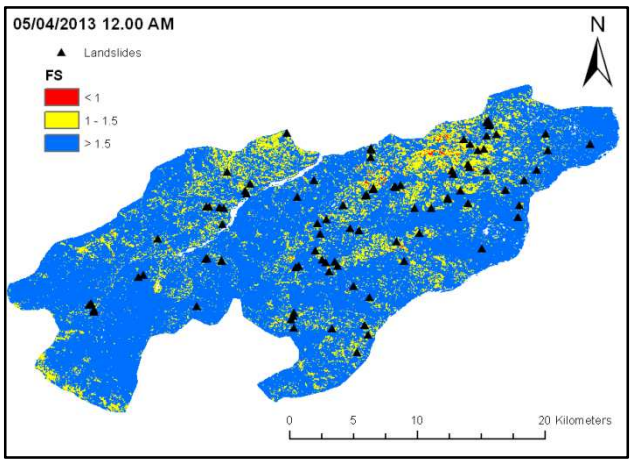

e)

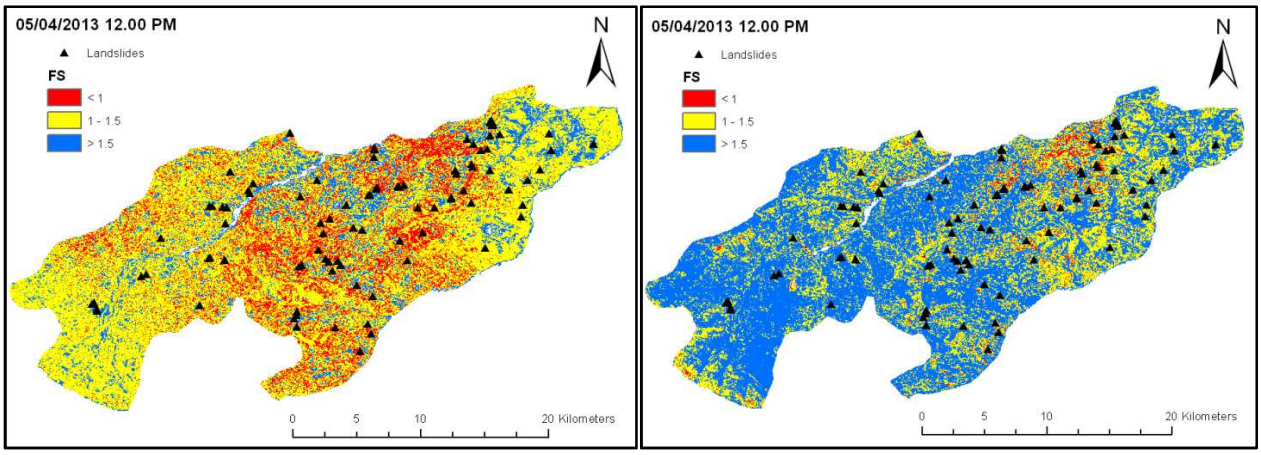

c) *f)*

Figure 5.12 Time varying safety factor maps: a) 04/04/2013 12.00 pm – Set 1 b) 05/04/2013 12.00 am – Set 1 c) 05/04/2013 12.00 pm – Set 1 d) 04/04/2013 12.00 pm – Set 2 e) 05/04/2013 12.00 am – Set 2 f) 05/04/2013 12.00 pm – Set 2

5.4 Validation of the model

Model validation is a fundamental step in any natural hazards study. Validation regards comparing the model predictions (i.e. safety factor maps) with a real-world dataset, (i.e. landslide detachment area inventory map), for assessing its accuracy or predictive power. Validation permits to establish the degree of confidence of the model, which is of great importance for transferring the results to the final users. Also, without a proper validation it is not possible to compare the model with other ones, or even with alternative sets of parameters or predictor variables (Begueria, 2006). The ROC analysis (Receiver Operating Characteristic) has been chosen to analyze the reliability of the safety factor maps, namely to assess how the real landslides are spatially located compared with those predicted by the model. Each pixel of the safety factor map falls within one of these four groups.

1) True Positive (TP) – Correct predictions of instability. These are the pixels with Fs less than 1 (the model assesses them as unstable) which fall within a landslide detachment area of the inventory map. The model considers as unstable areas that were actually mobilized.

2) True Negative (TN) – Correct predictions of stability. These are the pixels with Fs greater than 1 (the model assesses them as stable) which do not fall within a landslide detachment area of the inventory map. The model considers stable areas that did not mobilize.

3) False Positive (FP) - False predictions of instability. These are the pixels with Fs less than 1 (the model assesses them as unstable) that do not fall within a landslide detachment area of the inventory map. The model considers stable areas that actually mobilized.

4) False Negative (FN) – Missed predictions of instability. These are the pixels with Fs greater than 1 (the model assesses them as stable) which fall within the landslide detachment area of the landslide inventory map. The model considers stable areas that were actually mobilized.

After overlaying safety factor maps to the maps of landslide areas, it is possible to assign each pixel to its group. Knowing this information, the two fundamental parameters of the ROC analysis, namely sensitivity and specificity, can be obtained.

Sensitivity, also called true positive ratio, is defined as: $\frac{TP}{TP + FN}$

and represents the ratio between correctly predicted landslides with the total number of landslides of the inventory map.

Specificity, also called true negative rate, is defined as: $\frac{TN}{TN + FP}$

and represents the ratio between correctly predicted stable pixels with the total number of stable pixels of the inventory map.

A high value of sensitivity corresponds to a high number of correct predictions while a high value of specificity corresponds to a low amount of false predictions. The only representative point in the ROC curve is the one corresponding to FS = 1, i.e. considering only the condition of stability or instability. In the following analysis we chose to analyze the specificity and sensitivity for FS values greater than 1, to be able to assess the areas that tend to instability during a meteorological event. A ROC curve is obtained by varying the threshold value of Fs, increasing it gradually, until every landslide source area has a pixel that is less than or equal to the threshold Fs or, in other words, until the analysis reaches maximum sensitivity in correspondence of the maximum value of TP. In this work the following assumption was considered: if a pixel inside a source area is unstable than that landslide is considered as a TP as in Losi (2013) and Montrasio et al. (2014). We used this simplification to overcome spatial positioning errors, due to GPS inaccuracies and spatial resolution of rainfall maps. The area under the ROC curve (AUC) thus obtained, defined as overall accuracy, is a parameter of the model reliability. It can vary from 0.5 (random prediction) to 1 (perfect prediction) and it is also used to compare different models.

Global Accuracy (AUC) (%)	Evaluation
50 < AUC < 60	Fail
60 < AUC < 70	Poor
70 < AUC < 80	Good
80 < AUC < 90	Excellent
90 < AUC < 100	Outstanding

Table 5.4 classes of reliability of ROC prediction based on AUC

According to the ROC evaluation method comparing the safety factor map of 05/04/2013 at 12.00 pm with the landslide inventory map created in GIS based on the surveyed shallow landslides, the AUC is 0.705 for the first set of parameters and 0.77 for the second set of parameters (Figure 5.13), both corresponding to a good prediction but highlighting the beneficial influence of including land cover classes in the modeling. Using the first set of parameters, 74 of 97 landslides are computed as unstable with Fs=1 (sensitivity = 76%) with a specificity of 68% while using the second set of parameters 69 of 97 landslides are computed as unstable with Fs=1 (sensitivity 71%) with a higher specificity (80%)

.

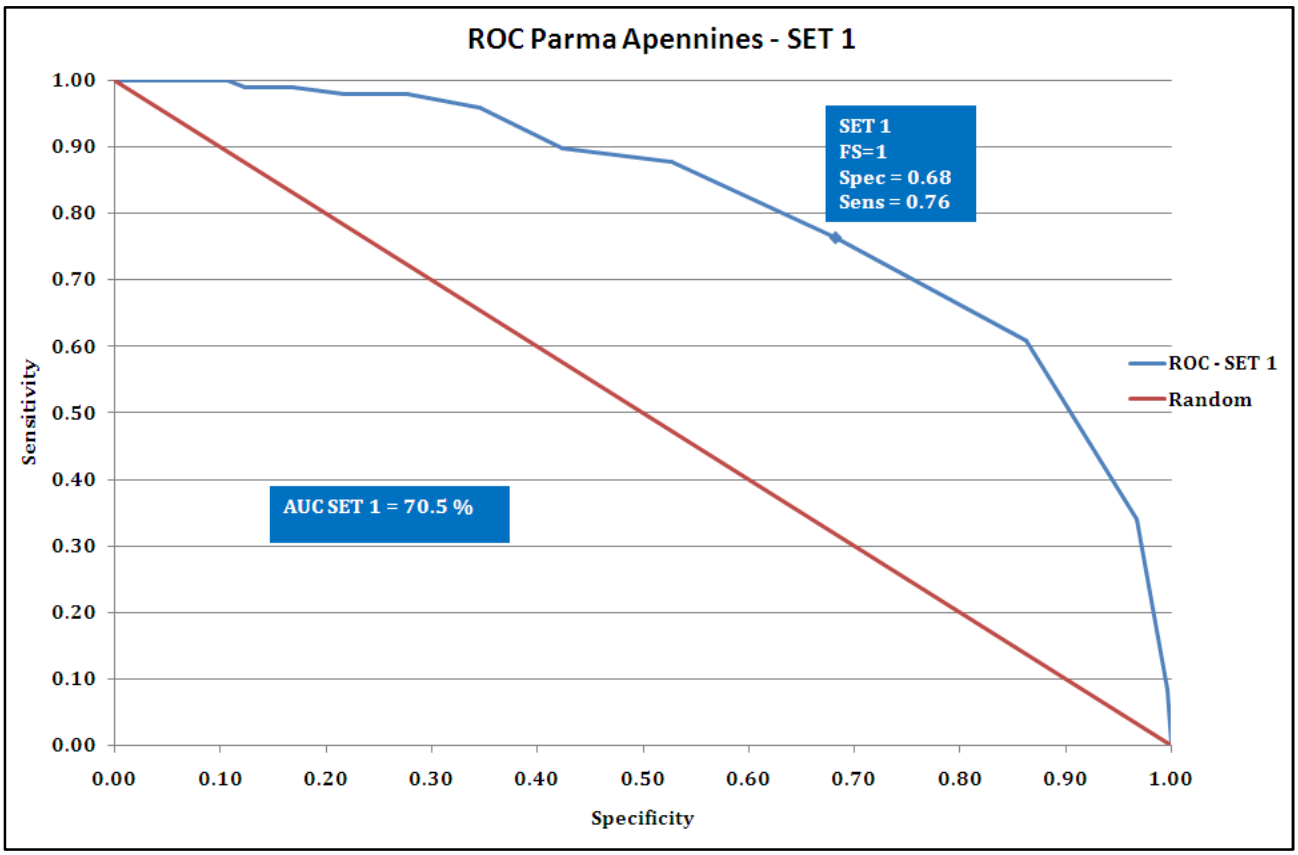

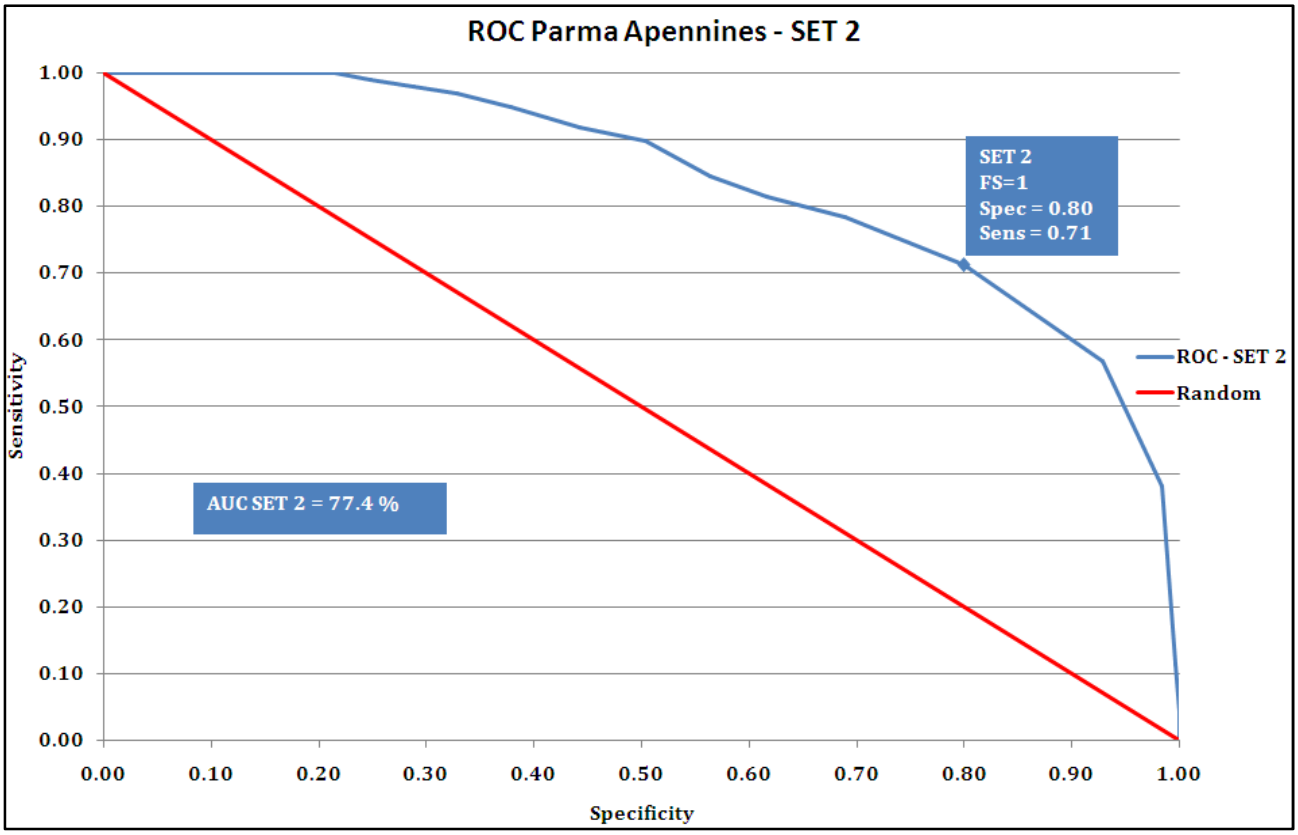

Figure 5.13 ROC curves for the Parma Apennine event of April 5th 2013. a) set 1 and b) set 2

The results highlight a good prediction although there is a high over prediction ratio, that can be related to an incomplete landslide database and spatial errors. From a temporal point of view SLIP correctly predicts the triggering instant. In future analyses a complete landslide database must be used for a correct evaluation of spatial accuracy. Furthermore the second set of parameters give a better overall accuracy due to spatial variation in the input data from land cover classes.

Chapter 6

The Landslide event of Giampilieri (ME) occurred on October 1st 2009

6.1 Study area

Figure 6.1 Aerial view of Giampilieri area a few days after the October 1st, 2009 event (Courtesy of Prof. G. Scarascia Mugnozza)

Giampilieri (Figure 6.1) is a village that has been severely affected by the heavy rainstorm that hit the north-eastern part of Sicily Region and, in particular, the southern Messina area on October 1st, 2009. Hundreds of shallow landslides were triggered by the high intensity rainfall, causing significant damage to infrastructures and civil constructions and causing 37 fatalities, of which 24 only in Giampilieri. The study area (Figure 6.2 a) has an extension of about 8 km^2 and is located in

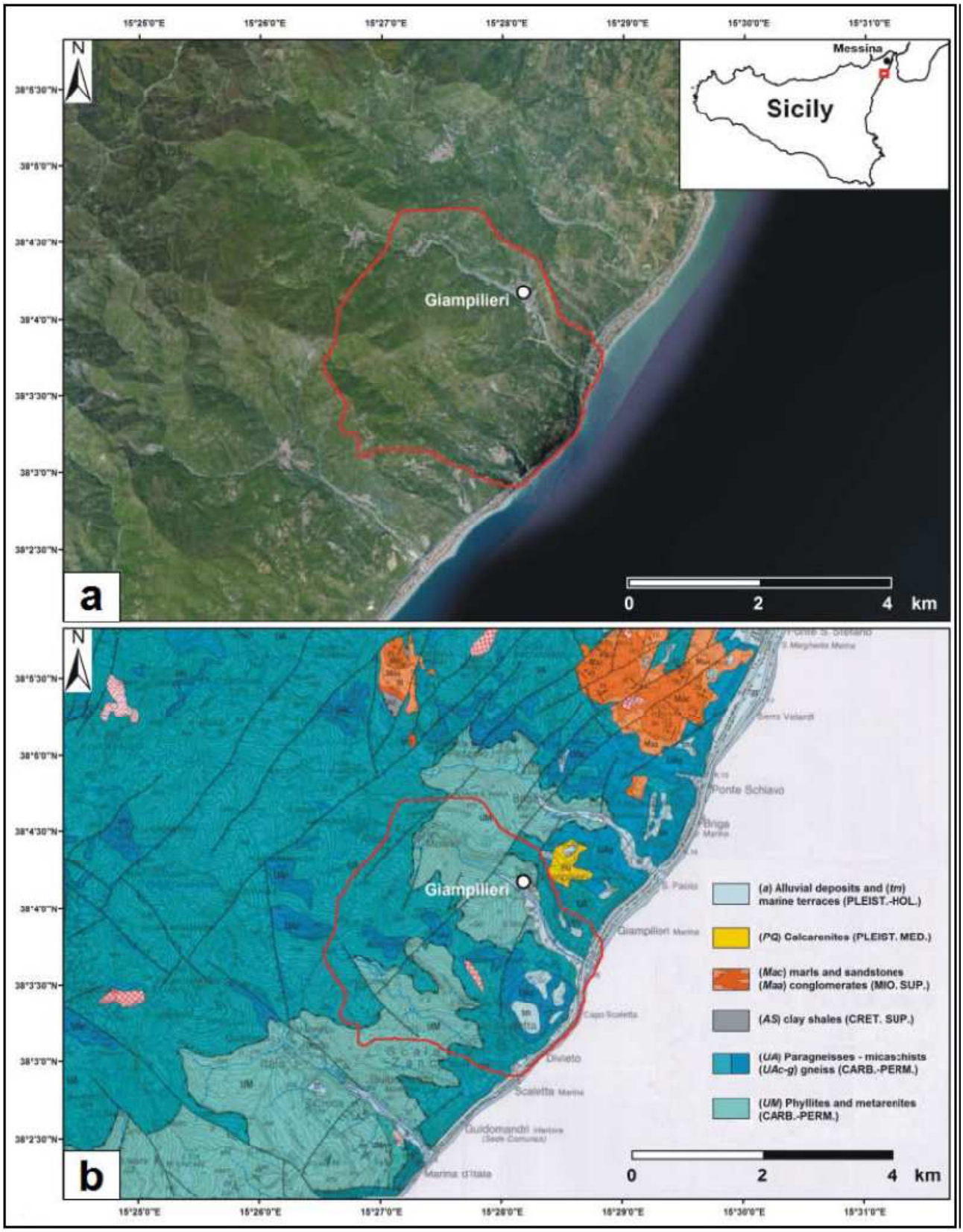

Figure 6.2 a) satellite image of the southern Messina area (from Google Earth ®) b) excerpt of the geological map of Messina Province (from Lentini et al., 2000)

the eastern sector of the Peloritani Mountains, i.e., in the southernmost section of the Calabrian-Peloritan arc (CPA), a complex structure made up of Paleozoic, Mesozoic and recent terrains that connect the NW-SE-trending Apennines with the EW Maghrebide chain of Sicily (Amodio Morelli et al., 1976; Tortorici, 1982; Atzori et al., 1984). It is important to underline the presence of a thin (0.5-2 m) cover of eluvial and colluvial deposits resulting from the weathering of metamorphic rocks. This is a remarkable feature of the area, because the weathered deposit represents the main constituent of the shallow landslides occurred during the October 1st, 2009 event (Figure 6.3).

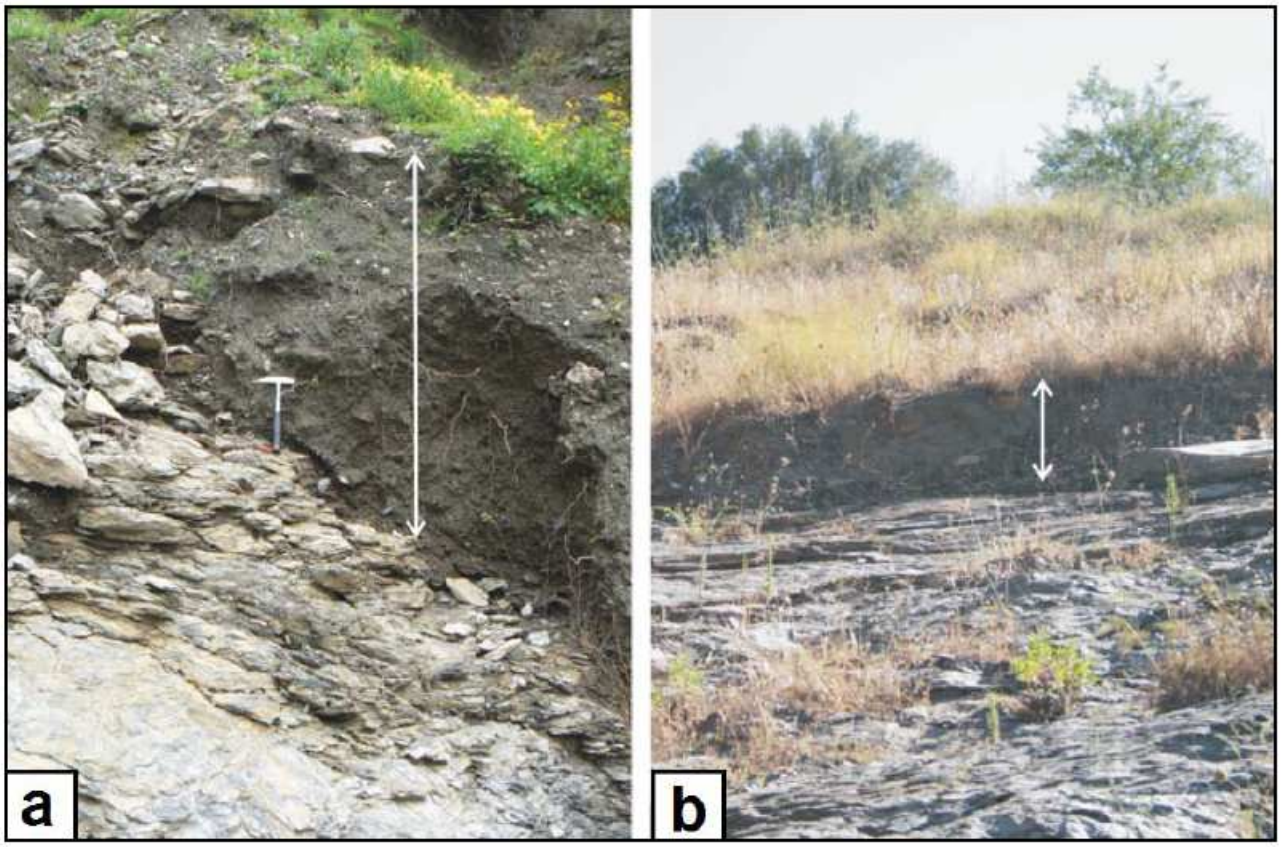

Figure 6.3 L**ateral (a) and frontal (b) view of shallow landslide scars. The sharp contact between the eluvial-colluvial deposit (approximately 1 m thick) and the metamorphic bedrock can be noted (from De Guidi & Scudero, 2013)**

6.2 Geotechnical characterization

To analyze in detail the triggering of the shallow landslides occurred during the October 1st, 2009 event, it is important to characterize the material involved in the landslide movement. Thus, laboratory tests have been performed to measure physical and mechanical properties of the soil cover (see Table 6.1). The following tests have been performed:

- Tests for the determination of unit volume weights;
- Grain size distribution with sieving and sedimentation;
- Drained consolidated triaxial tests.

Unit volume weights

To determine the unit volume weight of soil particles six tests have been carried out using pycnometers:

Test	**Unit**	**1**	**2**	**3**	**4**	**5**	**6**
Pycnometer volume at 20° C	ml	250	250	250	150	150	150
Pycnometer weight	g	84,10	84,81	84,67	102.09	102.35	102.83
Pycnometer and dry soil weight	g	144,88	145,51	145,07	125.13	125.36	125.85
Pycnometer, soil and water weight	g	371,51	372,01	371,65	264.39	262.481	264.8
Pycnometer and water weight	g	333,15	333,55	333,33	249.87	247.9	250.19
Dry soil weight	g	60,78	60,70	60,40	23.04	23.01	23.02
Unit volume weight	Kg/m^3	2,71	2,73	2,74	2.70	2.73	2.74
Unit volume weight	kN/m^3	26,59	26,77	26,83	26.52	26.78	26.85
Mean unit volume weight	kN/m^3	26,73		**Gs**	**-**	**2,725**	

Table 6.1 Pycnometer test results.

Gs, the ratio between the solid particle unit volume weight and water unit volume weight is:

$$G_s = \frac{\gamma_s}{\gamma_w} = 2{,}725 \qquad (6.1)$$

Grain size distribution

Figure 6.4 shows the grain size distribution curve obtained by sieving and X-ray analysis ran at the University “Sapienza” of Rome and the grain size distribution of the same soil obtained by sieving and sedimentation at the University of Parma.

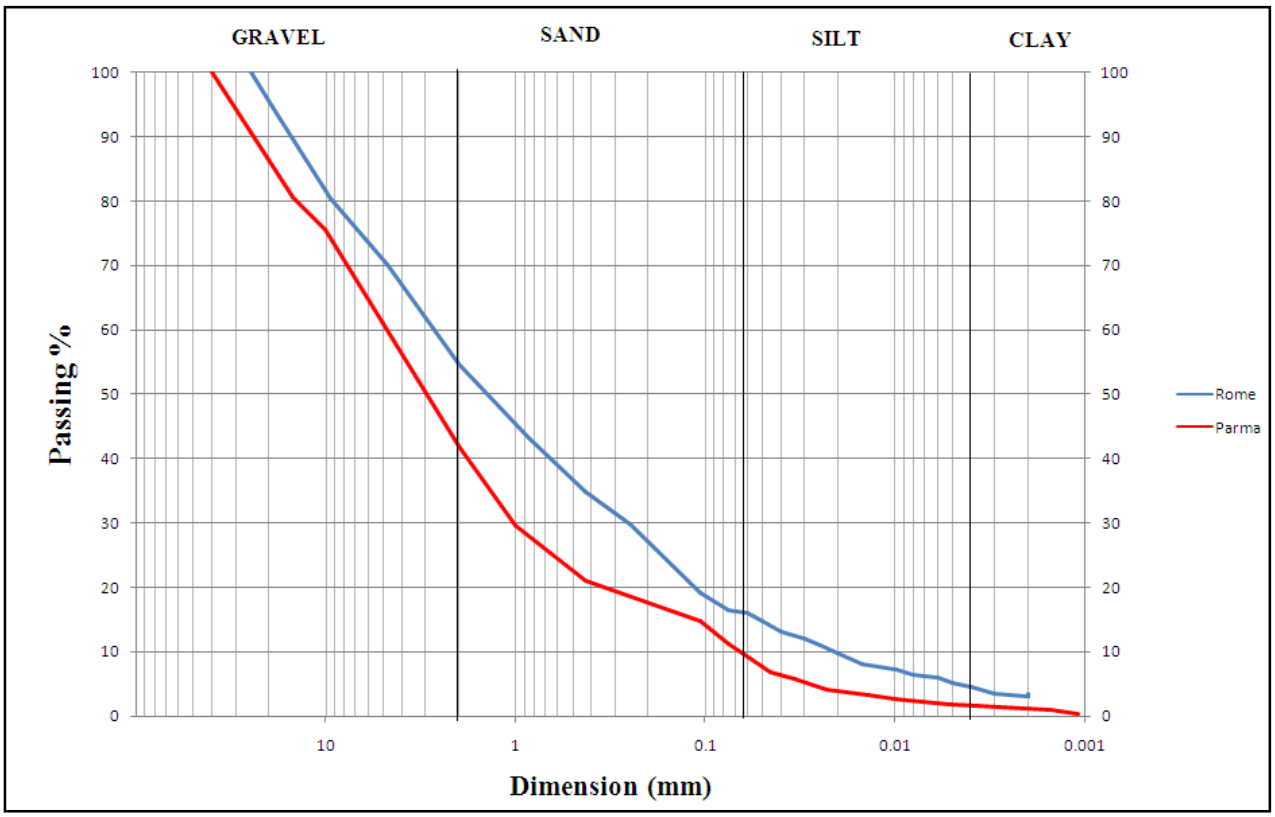

Figure 6.4 Grain size distribution curves

UNIVERSITY	Gravel %	Sand %	Silt %	Clay %	d_{10} [mm]	d_{50} [mm]	d_{60} [mm]	$Cu=d_{60}/d_{10}$ [-]
ROME	45,39	38,12	11,99	4,50	0,021	1,55	2,95	140
PARMA	58,13	30,59	9,48	1,80	0,066	3,28	4,85	74

Table 6.2 Grain size distribution results

The results of the two obtained curves are very similar confirming the heterogeneous nature of this soil which is mainly composed of gravel (51,7%) and sand (34.4%) with minor components of silt and clay (10,7% and 3.2% respectively). These characteristics are typical of soils deriving from the weathering of a metamorphic bedrock, and explain the triggering of shallow landslides after intense imbibition processes, as occurred during the October 1st, 2009 event. Due to the coarse-grained nature of the soil Atterberg limits were not found for this soil.

Consolidated drained triaxial tests

Regarding the mechanical properties, in the same study area several authors (Aronica et al., 2012; Peres & Cancelliere, 2014; Penna et al., 2014) have reported values ranging between 30° and 40° for the friction angle and between 0 and 5 kPa for the cohesion. These different values depend on both the natural spatial variability of soil shear strength parameters and the type of deposit, characterized by an extremely variable texture resulting from erosion and weathering processes.

Independent tests have been executed in triaxial cells both at the University of Parma by our research group and by a private laboratory in Rome (Geostudi SRL – report number 1718 Rome, Italy).

Standard specimen triaxial tests (H=76mm, d=38mm)

In the geotechnical laboratory of the University of Parma three reconstituted standard cylindrical specimens (H = 76mm; d = 38 mm) where tested. The first operation was the preparation of the specimens. The tested material was sieved leaving the maximum grain size of 3.8mm equal to 1/10 of the diameter of the specimen. The tested soil is a loose sand with 25% of fine grained particles. To reconstitute the specimen the soil was compacted inside a mould in 4 layers of decreasing depth, in order to consider undercompaction (Figure 6.5).

Figure 6.5 The triaxial reconstituted specimen (d = 38 mm, h = 76 mm)

In this way three identical specimens with 37% of porosity (n), 12% of water content (w) and 55% of initial saturation ratio (S_{ri}) were made (table 6.3).

Initial Property	Value
w	0.12
Gs	2.67
Sr	0.55
n	0.37
e	0.59
H	76 (mm)
d	38 (mm)

Table 6.3 initial Soil properties for triaxial tests - Parma

The specimens were saturated controlling the B parameter and once a satisfactory value (i.e. 0.95) was reached the specimens were consolidated at three different cell pressures, namely 105, 205 and 300 kPa and then tested.

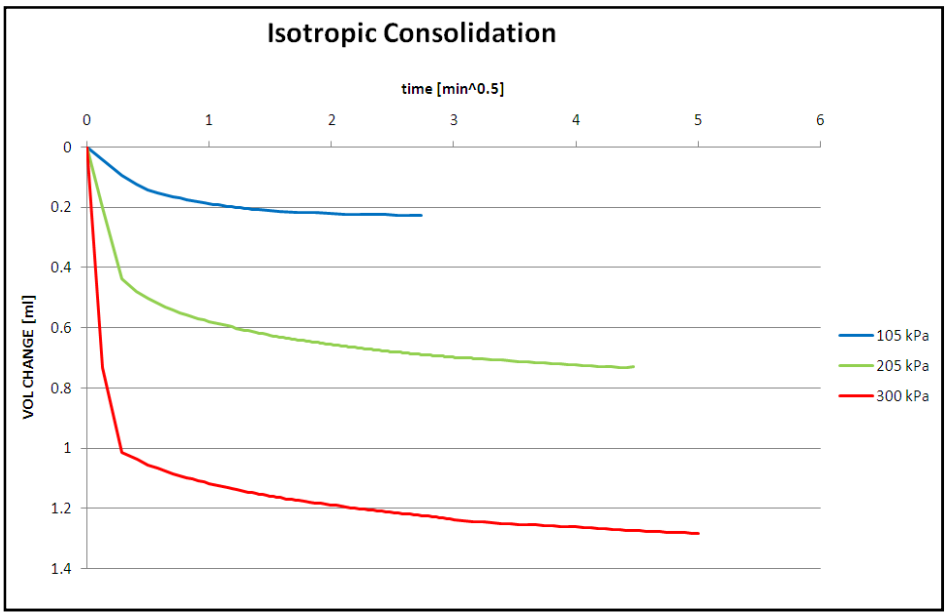

Figure 6.6 Consolidation phase: Volume change vs. time^{0,5}

During the consolidation phase, the three specimens lose small amounts of water (Figure 6.6) and the consolidation occurs very quickly, due to the high permeability of the granular material.

Figure 6.7 The specimen at the end of compression. The specimen assumes the typical "barrel shape" configuration of loose sands.

In table 6.4 the results of the three tests are reported:

Specimen	Cell Pres. [kPa]	Back Pres. [kPa]	$p_i'=\sigma_r$ [kPa]	q_f [kPa]	σ_{af} [kPa]	C [kPa]	r [kPa]	c' [kPa]	φ' [kPa]
1	160	55	105	430	535	320	215	0	42.2
2	280	75	205	830	1035	620	415	0	42.0
3	405	105	300	1037	1337	818.5	518.5	0	39.3
						Mean	Value	0	41.1

Table 6.4 Results of the three triaxial tests performed in Parma

Where p_i' is the effective initial isotropic pressure applied to the specimen, q_f is the final deviatoric pressure, σ_a and σ_r are namely the axial and radial pressures, σ_{af} is the final value of the axial pressure, C is the center of the Mohr Circle and r is the radius of the Mohr Circle:

$$p' = \frac{\sigma_a + 2 \cdot \sigma_r}{3} \tag{6.2}$$

$$q = \sigma_a - \sigma_r \tag{6.3}$$

$$C = \frac{\sigma_a + \sigma_r}{2} \tag{6.4}$$

$$r = \frac{\sigma_a - \sigma_r}{2} \tag{6.5}$$

c', the effective cohesion and φ', the internal friction angle have been found on the Mohr-Coulomb plane:

$$c' = 0 \tag{6.6}$$

$$\varphi' = \arcsin\left(\frac{r}{C}\right) \tag{6.7}$$

The soil behaves like a loose sand with deviatoric shear resistance (q_r) that grows with confining cell pressure and no peak is registered. During shear, at lower cell pressures, water enters the specimen and a slight increase in volume is registered (less than 1% of total volume). The value of the internal friction angle decreases slightly with growing effective confinement typical of a non-linear resistance behavior. Nevertheless an approximate linear failure envelop with null cohesion and internal friction angle = 41.1° (the mean value of the three tests) is plotted (Figure 6.10).

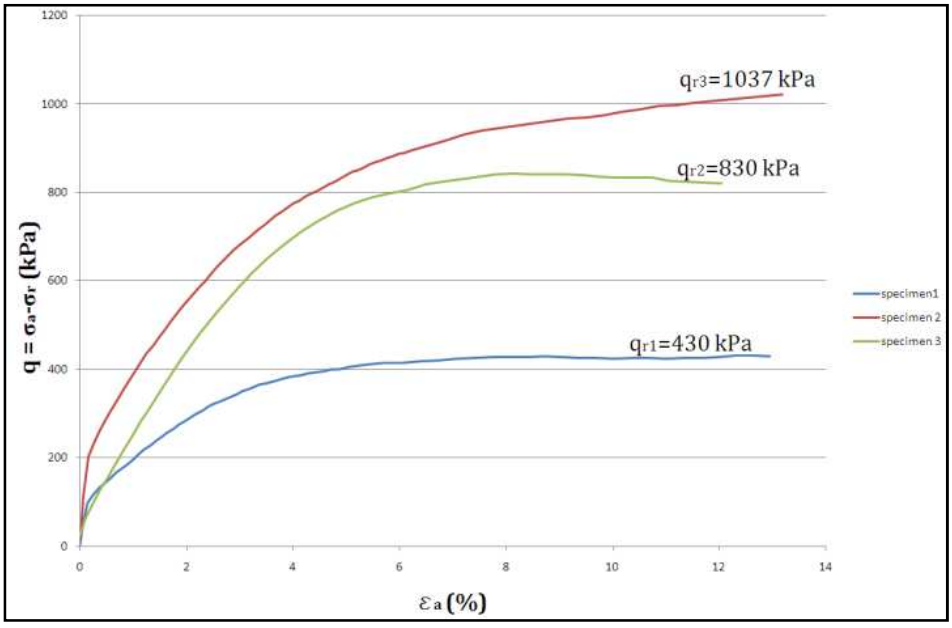

Figure 6.8 Results of triaxial tests: Deviatoric stress vs. axial strain

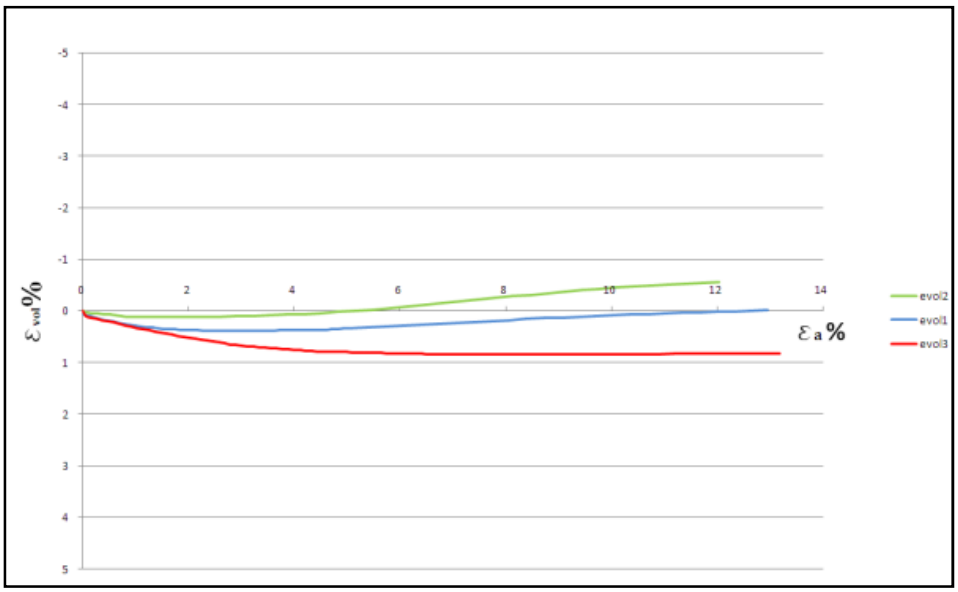

Figure 6.9 Results of triaxial tests: volumetric strain vs. axial strain

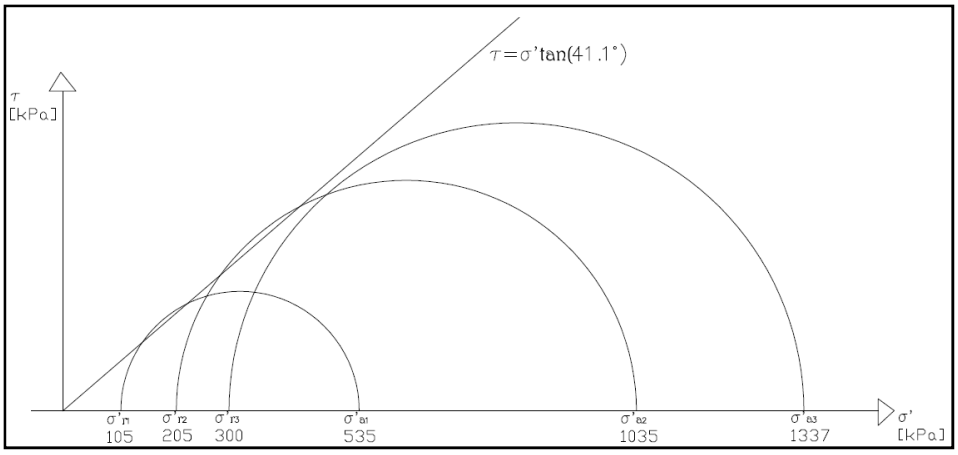

Figure 6.10 Results of triaxial tests: Mohr circles

Large specimen triaxial tests (H=200mm, d=100mm)

Three reconstituted large cylindrical specimens (H = 200mm; d = 100 mm) where tested in the geotechnical laboratory near Rome, (Figure 6.11). The first operation was the preparation of the specimens. The tested material was sieved leaving the maximum grain size of 10mm equal to 1/10 of the diameter of the specimen. The tested soil is a loose sand with 9% of fine grained particles. To reconstitute the specimen the soil was compacted inside a mould in many layers of decreasing depth, in order to consider undercompaction (Figure 6.11).

Figure 6.11 The triaxial reconstituted specimen (d = 100 mm, h = 200 mm)

In this way three identical specimens with 33% of porosity (n), 7% of water content (w) and 38% of initial saturation ratio (S_{ri}) were made (table 4.5).

Initial Property	Value
w	**0.07**
Gs	**2.67**
Sr	**0.38**
n	**0.33**
e	**0.49**
h	**200 (mm)**
d	**100 (mm)**

Table 6.5 Initial Soil properties for triaxial tests - Rome

The specimens were saturated both by flushing and by applying a counter-pressure, controlling the B parameter and once a satisfactory value (i.e. 0.90) was reached the specimens were consolidated at three different cell pressures, namely 49,101 and 196 kPa and then tested.

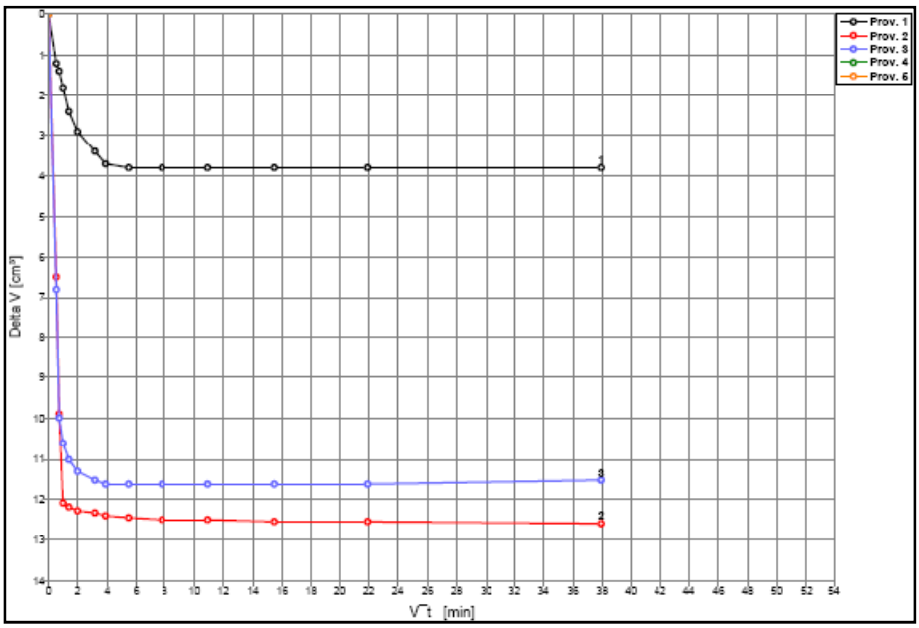

Figure 6.12 Consolidation phase: Volume change vs. time^0,5

Figure 6.13 Triaxial testing chambers

In table 6.6 the results of the three tests are reported:

Specimen	Cell Pres. [kPa]	Back Pres. [kPa]	$p_i'=\sigma_r$ [kPa]	q_f [kPa]	σ_{af} [kPa]	C [kPa]	r [kPa]	c' [kPa]	φ' [kPa]
1	343.2	294.2	49	146.8	195.8	122.4	73.4	0	36.8
2	392.2	294.2	98	271.4	369.4	233.7	135.7	0	35.5
3	490.3	294.2	196.1	574.8	770.9	483.5	287.4	0	36.5
						Mean	Value	0	36.3

Table 6.6 Results of the three triaxial tests performed near Rome

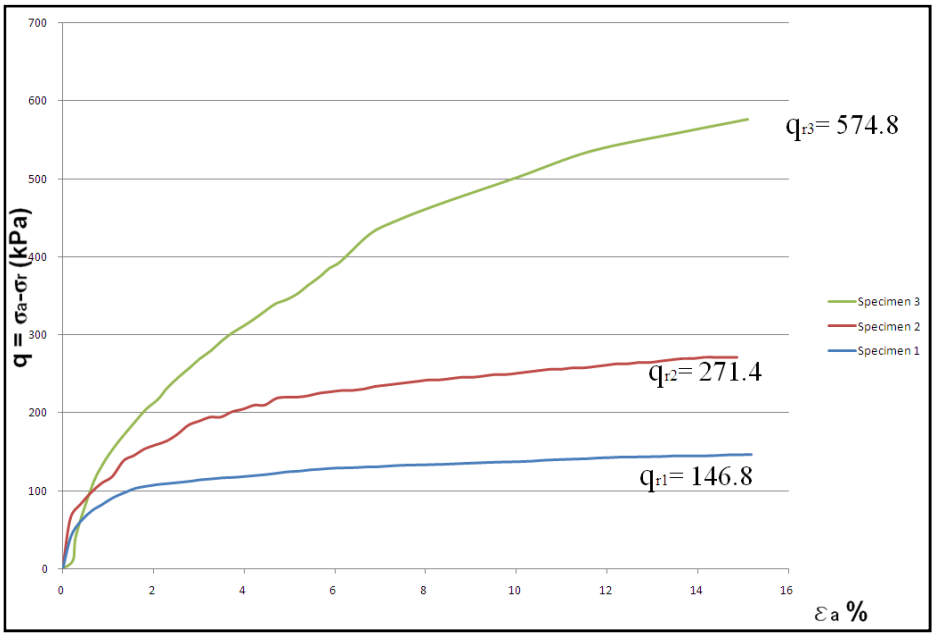

Figure 6.14 Results of triaxial tests: Deviatoric stress vs. axial strain

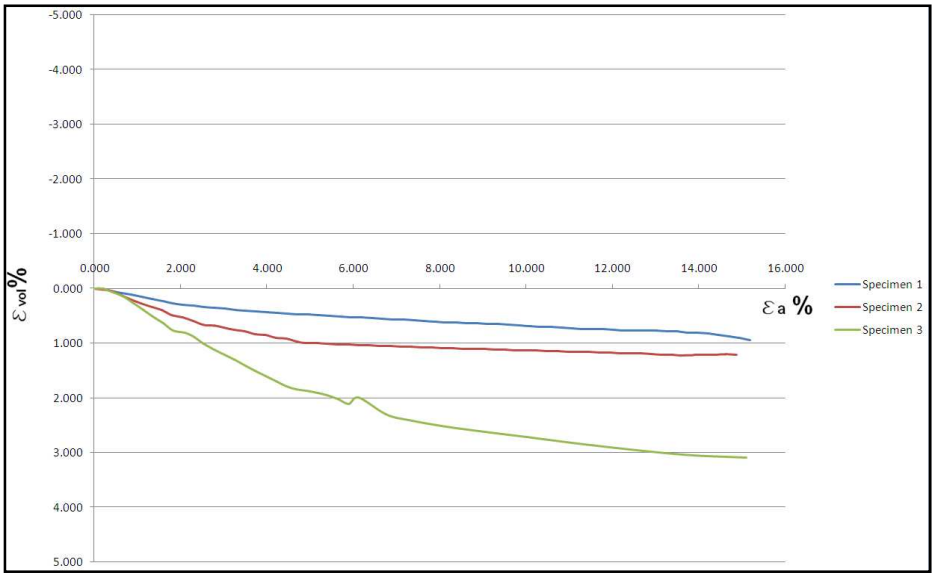

Figure 6.15 Results of triaxial tests: volumetric strain vs. axial strain

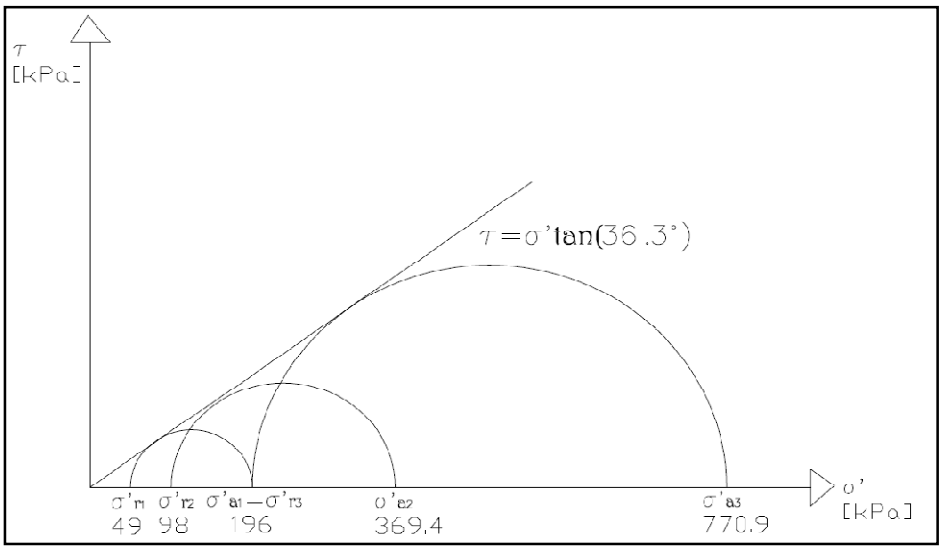

Figure 6.16 Results of triaxial tests: Mohr circles

Where p_i' is the effective initial isotropic pressure applied to the specimen, q_f is the final deviatoric pressure, σ_a and σ_r are namely the axial and radial pressures, σ_{af} is the final value of the axial pressure, C is the center of the Mohr Circle and r is the radius of the Mohr Circle:

$$p' = \frac{\sigma_a + 2 \cdot \sigma_r}{3} \tag{6.8}$$

$$q = \sigma_a - \sigma_r \tag{6.9}$$

$$C = \frac{\sigma_a + \sigma_r}{2} \tag{6.10}$$

$$r = \frac{\sigma_a - \sigma_r}{2} \tag{6.11}$$

c', the effective cohesion and φ', the internal friction angle have been found on the Mohr-Coulomb plane:

$$c' = 0 \tag{6.12}$$

$$\varphi' = \arcsin\left(\frac{r}{C}\right) \tag{6.13}$$

The soil behaves like a loose sand with deviatoric shear resistance (q_r) that grows with confining cell pressure and no peak is registered. During shear, water exits the specimen and a slight decrease in volume is registered (max 3% of volumetric deformation Figure 6.15). This behavior is slightly different from the results obtained in Parma, principally due to the percentage of fine material that is much less than the specimens tested in Parma. The value of the internal friction angle can be well

approximated by a linear failure envelop with null cohesion and internal friction angle = 36.3° (mean value of the three tests). This value is smaller than the obtained value in Parma but the different nature of the tests justifies these slightly different results. (Figure 6.16).

On the basis of both these experimental results and values reported in literature (Aronica et al.,2012; Peres & Cancelliere, 2014; Penna et al., 2014) the following geotechnical values can be assumed (Table 6.7):

Physical properties	**Solid unit weight γ_s (kN/m^3)**	**26.73**
	Porosity, n (%)	35
Grain Size distribution	Gravel (%)	50
	Sand (%)	35
	Silt (%)	10
	Clay (%)	5
Mechanical Properties	Internal Friction Angle, φ' (°)	30-41
	Effective cohesion, c' (kPa)	0-5

Table 6.7 Range of values of physical and mechanical parameters of Giampilieri soil

6.3 Meteorological event

The regional climatic setting of north-eastern Sicily is influenced by different local features, including a complex orographic setting coupled with a marine effect. Rainfall is concentrated during the autumn/winter period, which is when extreme rainfall events generally occur. On the afternoon of October 1st, 2009 a deep cyclone developed in the southern part of the Mediterranean basin, producing an extremely severe rainstorm that hit north-eastern Sicily and, in particular, the southern Messina area. The ten-minute rainfall data made available by S.I.A.S. (*Servizio Informativo Agrometeorologico Siciliano*) describe a particularly strong rainfall event. For instance, the Santo Stefano di Briga and Fiumedinisi monitoring stations, which are the rain gauges closest to the study area (located approximately 3 km north and 7 km west of the study area, respectively),

recorded 225 mm and 150 mm of rain depth that fell in seven hours, respectively (Figure 6.17).

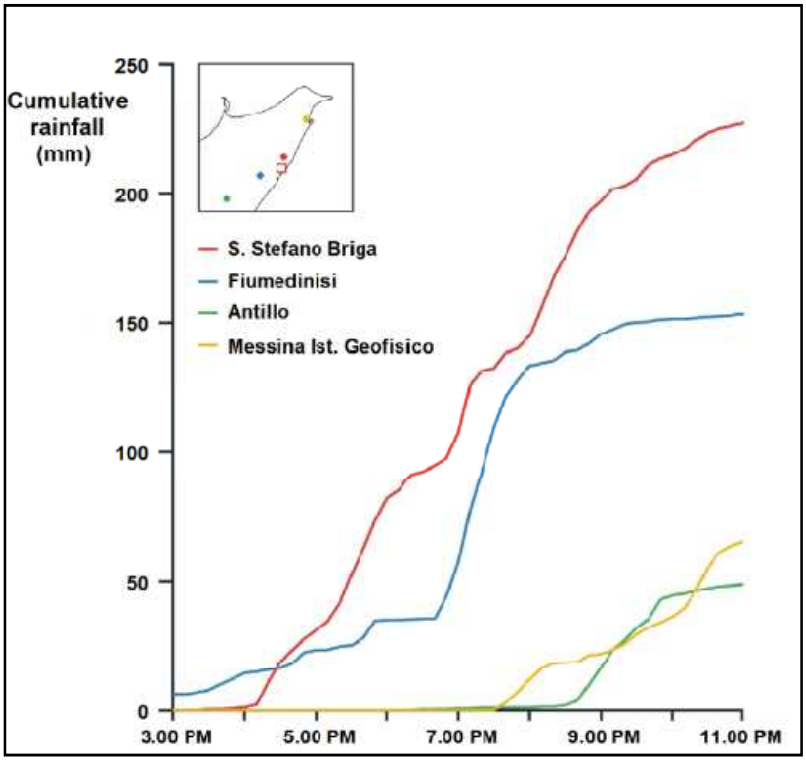

Figure 6.17 Cumulative hyetographs recorded at the 4 rain gauge stations (Santo Stefano di Briga, Fiumedinisi, Antillo and Messina Istituto Geofisico), whose location is shown in the upper left sketch (the red square represents the study area);

At the Santo Stefano di Briga station, the rainfall event began at approximately 4.00 p.m. and ended at about midnight. The maximum intensities were recorded before 11.00 pm, with 225 mm of cumulative rain in eight hours and a mean rainfall intensity of 32.2 mm/h. The event was also characterized by very high intensity peaks; for example, 18.5 mm of rain fell between 7.00 pm and 7.10 pm, corresponding to an intensity of approximately 2 mm/min. The rainfall event began slightly earlier (approximately 3.00 pm) at the Fiumedinisi monitoring station and ended at approximately 11.00 pm. The maximum rainfall intensities were recorded between 6.50 pm and 8.00 pm, with approximately 100 mm of cumulative rain in just one hour. This station also recorded extremely high rainfall peaks; 20.6 mm of cumulated rain was recorded between 7.00 pm and 7.10 pm, corresponding to an intensity of more than 2 mm/min. The analysis of the rainfall data shows the localized nature of the event, as demonstrated by the low precipitation values recorded in two rain gauge stations approximately 20 km from the study area (Antillo and Messina Istituto Geofisico monitoring stations, see Figure 6.17). Satellite data observations also highlight the reduced extent of the rainfall field. It is worth noting that in the days preceding the debris-flow event, the area was affected by two intense rainfall events: one on September 16th and one on the night between September 23rd and September 24th. According to the precipitation data from the

Fiumedinisi rain gauge station, the cumulative rain in this period was approximately 300 mm. Thus, the total rainfall from September 15th to October 1st amounted to approximately 500 mm, which is approximately 80 mm higher than the average October-December rainfall (421 mm), calculated from 79 years of historical precipitation data from the Santo Stefano di Briga monitoring station. These data are directly available on the website of the Sicily Region:

(*http://www.osservatorioacque.it*).

As far as the reconstruction of the October 1st, 2009 event is concerned, it is difficult to define precisely the temporal and spatial evolution of the event based only using the information reported to the authorities by witnesses. Furthermore the fact that most of landslides occurred in the evening must be considered, so the observations reported by witnesses took place in partial darkness within or close to their homes and often while involved in rescuing relatives or themselves. However, it is possible to distinguish and define substantially three main phases (Schilirò et al, *in press*):

1) critical conditions rapidly developed over 1-2 hours, approximately between 5.00 pm and 7.00 pm, due to a large increase in precipitation. According to witnesses, approximately at 6.00 pm the Divieto torrent level (the stream that flows into the Ionian Sea near Scaletta Marina village, see Figure 6.18) was already high due to the presence of high quantity of mud and debris;

2) After 7.00 pm the stream flow (progressively increased in volume by sediments) became so strong that it began to capture cars along the inundated streets both in Scaletta Marina and Giampilieri village. Meanwhile, first important landslide events occurred. For instance, a witness asserts that the debris-flow in Via Puntale in Giampilieri (Figure 6.18 b) occurred between 7.10-7.15 pm;

3) After a further rainfall peak (at approximately 7.40 pm, when the water level reached the level of car windows), large portions of the Racinazzo watercourse rapidly failed, followed by rapid debris-flow development, which occurred between 8.00 pm and 8.15 pm. Several witnesses heard a loud rumbling noise at approximately 8.00 pm, slightly before the debris-flow reached the town of Scaletta Marina, crushing buildings and infrastructure (Figure 6.18c-d) and killing 14 people. This scenario is confirmed by the Santo Stefano di Briga rain monitoring data (3 km north of the site), in which a high-intensity rainfall peak is clearly visible at 8.00 pm (Figure 6.17). Meanwhile, also in Giampilieri many shallow landslides occurred, whereas in Molino village the main slope instabilities were recorded slightly later, approximately between 8.30-8.45 p.m. The temporal shift between these events depends on the movement of the perturbation cloud towards the inner areas. The experiences reported by witnesses along with the damage to buildings, particularly in the area

reached by the debris-flow fans (Figure 6.19), both indicate very fast-moving debris-flows. Further researches to find five missing people and broader studies on the submarine slope stability (Casalbore et al., 2011) have shown evidence of a high-energy flow, even on the sea slope.

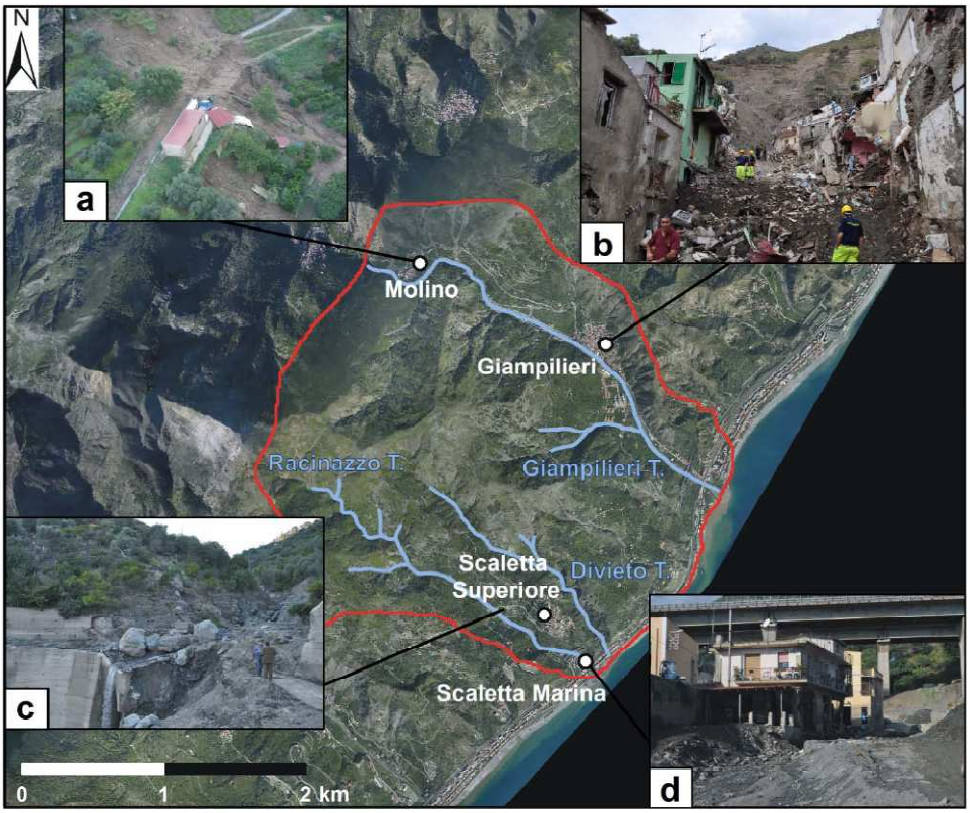

Figure 6.18 Aerial photograph of the study area after the October 1st, 2009 event. Some locations affected by shallow landslides a) debris avalanche in Molino village; b) debris-flow in Via Puntale, Giampilieri, c) bridge destroyed by a debris-flow along the road towards Scaletta Superiore village, d) the effect of the same debris-flow in Scaletta Marina village (Courtesy of Prof. G. Scarascia Mugnozza)

Figure 6.19 Aerial view of the debris-flow fan that flows into the sea (Courtesy of Prof. G. Scarascia Mugnozza)

Chapter 7

Laboratory flume tests on Giampilieri soil

7.1 Modeling at the laboratory scale: flume testing on Giampilieri soil

To better understand the mechanisms and conditions that lead to shallow landslide triggering, over the past decades several laboratory-scale landslide studies were performed using experimental apparatuses, generally composed of a tiltable flume and a sprinkler system that simulates the rainfall input. For instance, (Eckersley, 1990) and (Iverson et al., 2000) conducted large-scale experiments to quantify the importance of the initial state (initial void ratio) and drainage conditions, whereas (Wang & Sassa, 2001, 2003) and (Olivares & Damiano, 2007) triggered a number of shallow landslides in sandy soils using a small flume, demonstrating how the failure mode and the pore water pressure generation (during and immediately after slope failure) depend not only on the initial density but, greatly, on the grain size and fine particle content, that can have a significant impact also on the mobility of rainfall-induced landslides and (Olivares et al., 2009) analyzed the fundamental aspects of the mechanics of rainfall-induced failure in pyroclastic soils in initially unsaturated granular deposits and the transition to a flow-like landslide. Using the same techniques, other authors focused on different aspects related to shallow landslide initiation, like the effect of soil depth on failure mode and sediment discharge (Acharya et al., 2009) or the pore water pressure generation at the interface of layers of different permeability (Lourenco et al., 2006).

In this thesis the experimental flume was not used to simply analyze the behavior of an elementary soil volume but as a simulator of the real scale phenomenon through some expedients that create similar infiltration mechanisms as those that occur in the real slopes, i.e. through the insertion of preferential infiltration macro-channels and by reproducing a scaled hyetograph of the real rainfall. Consequently a calibration in back analysis of some of the input parameters of the SLIP model was accomplished. In the following paragraphs the experiments are presented.

Numerous flume tests have been performed to analyze in detail the triggering mechanisms of the material involved in the shallow landslides occurred during the October 1st, 2009 event of Giampilieri (Messina); the results have been also used to calibrate some parameters of the physically-based models (TRIGRS and SLIP). The employed flume test apparatus (Figure 7.1a) is composed of a plexiglass flume, 136 cm long, 50 cm wide and 35 cm high, connected to a threaded rod that allows to change the flume angle. To assure the same friction between the soil particles and the base of the flume as of that of particles inside the flume, a rough plastic panel was applied to the

surface of the flume base. A stiff permeable barrier was fixed in front of the soil to contain it after the failure, whereas a video camera was used to monitor failure initiation time and location. The tested material (Figure 7.1b) was sampled in the study area and sieved to obtain a maximum grain size of 1 cm. Thus, the coarser fraction (cobbles and boulders) was removed due to technical aspects related to the size of the flume. However, on the basis of the grain-size distribution curve obtained in laboratory, the resulting material represents approximately 80% of the real soil. The flume angle was kept constant at 38° (i.e. the average slope observed within the landslide source areas) whereas the soil thickness (13 cm) was equal to approximately 1/6 of the real average soil thickness (80 cm). The rainfall simulator consists of a spray nozzle (Albuz ATR 80° CLIPS, gently provided by Braglia SRL) placed above the flume (Figure 7.1c). Keeping the supplied water pressure constant by means of a pressure regulator, the resulting artificial rainfall can be considered homogeneous, on the basis of different checking tests made with 13 bins fixed at the base of the flume (Figure 7.1d). The actual rainfall intensity was measured, resulting for a specific water pressure of 3.2 bar, equal to 1.1 mm/min. Once the rainfall system had been calibrated, 29 flume tests were performed varying the initial soil conditions (porosity and water content), simulating the presence/absence of preferential flow directions of infiltrating water and using two different rainfall hyetograph inputs (Table 7.1). During each test, the failure mode was observed and the triggering time was measured. To investigate a wide range of initial soil conditions, in the first test series 4 different porosity values (i.e. 30, 35, 37 and 40%) and 5 initial water contents (4, 6, 8, 10 and 12%) were used, whereas in the subsequent tests only the initial conditions considered representative of the investigated problem (i.e. porosity of 35% and water content not exceeding 10%) were imposed. Before placing the soil into the flume, the established water content was obtained by wetting a specific quantity of oven-dried soil with the quantity of water necessary to reach the desired water content value. After the soil was set into the flume, the water content was checked by sampling the soil in different points. The initial porosities were obtained by placing the soil in 2-cm compacted layers parallel to the flume base. Considering that the test geometry is fixed, each layer occupied a known volume and then for each test the exact weight of soil (having a specific water content) required to fill that volume was calculated.

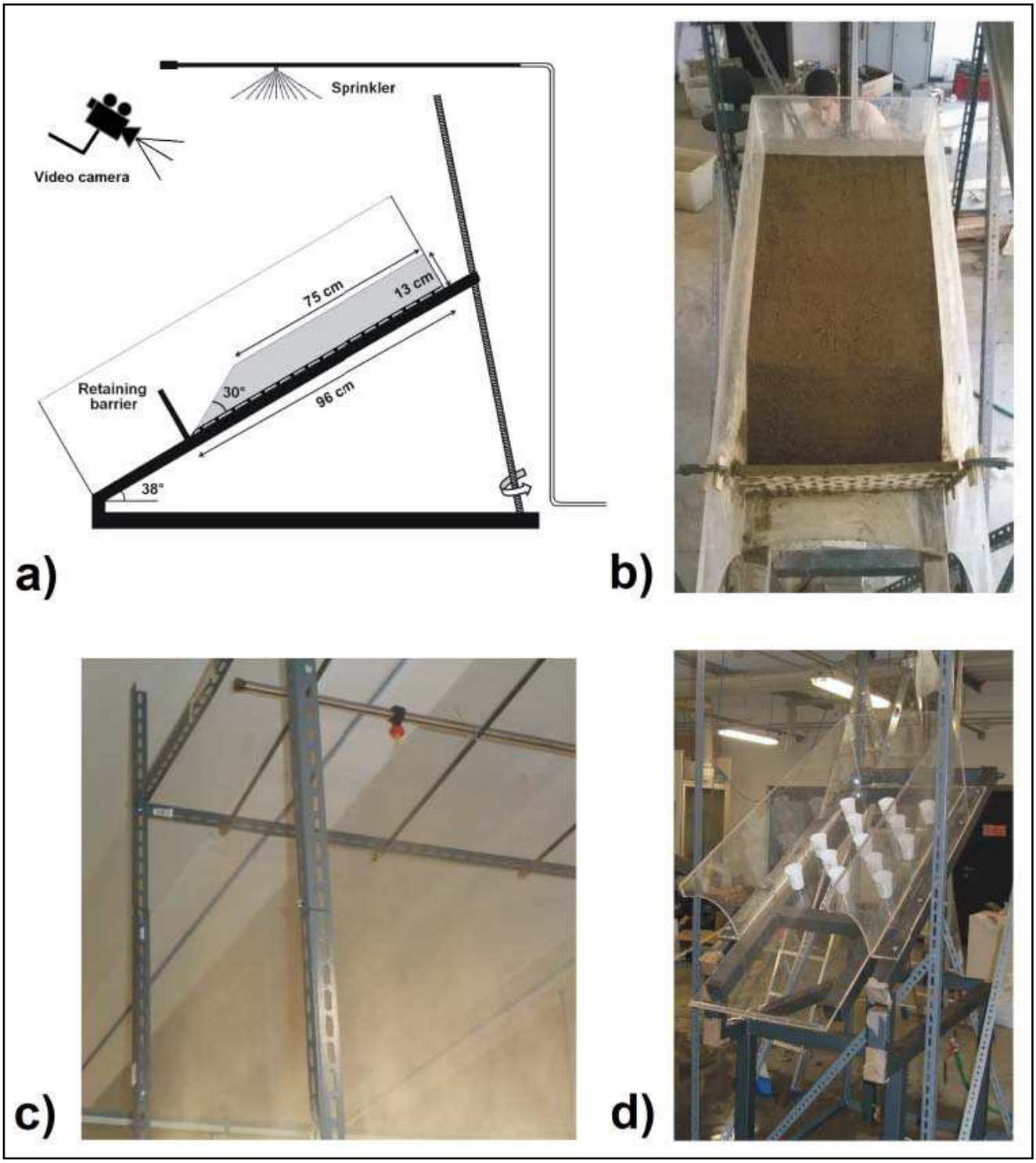

Figure 7.1 a) scheme of the experimental flume; b) top view of the soil slightly before the test; c) water spray nozzle for simulated rainfall; d) rainfall homogeneity and intensity measurement configuration

Test	Type	n (%)	w (%)	Sr (%)	Test	Type	n (%)	w (%)	Sr (%)
1	CN	30	8	50.8	16	CN	40	10	40.9
2	CN	30	10	63.6	17	CN	40	12	49.0
3	CN	30	12	76.3	18	GN	35	4	20.2
4	CN	35	4	20.2	19	GN	35	6	30.4
5	CN	35	6	30.4	20	GN	35	8	40.5
6	CN	35	8	40.5	21	GN	35	10	50.6
7	CN	35	10	50.6	22	CD	35	4	20.2
8	CN	35	12	60.7	23	CD	35	6	30.4
9	CN	37	4	18.6	24	CD	35	8	40.5
10	CN	37	6	27.8	25	CD	35	10	50.6
11	CN	37	8	37.1	26	GD	35	4	20.2
12	CN	37	10	46.4	27	GD	35	6	30.4
13	CN	40	4	16.3	28	GD	35	8	40.5
14	CN	40	6	24.5	29	GD	35	10	50.6
15	CN	40	8	32.7					

Table 7.1 Initial soil conditions and rainfall input of the 29 flume tests performed. CN=Constant rainfall with no preferential infiltration channels; GN= Giampilieri hyetograph rainfall input with no preferential infiltration channels. CD= Constant rainfall with presence of the preferential infiltration channels; GD = Giampilieri hyetograph rainfall input with presence of the preferential infiltration channels.

Obviously, six 2-cm layers and one 1-cm layer at the top of the soil were necessary to obtain the final geometry. As regards the artificial rainfall, tests have been performed using a constant rainfall input or conveniently opening-closing the rainfall simulator to reproduce the Santo Stefano di Briga 15-minute hyetograph related to the main phase of the October 1st event, i.e. between 4.00 pm and 9.00 pm (Figure 7.2 a-b). To keep the same rainfall intensity recorded on site and considering that the test soil thickness is approximately 1/6 of the real average soil thickness, a simulation time step of 2.5 minutes (15/6) was defined, during which the spray nozzle (that produces a constant rainfall input of 1.1 mm/min) has been activated for the time necessary to reach 1/6 of the real rain quantity fallen in the corresponding 15 minutes. However, only in the case of the highest rainfall peak (7.00-7.15 pm) it was necessary to increase the rainfall intensity to achieve the exact rainfall amount in 2,5 minutes by increasing the rainfall intensity to 1.4mm/min. Opening and closing phases of the rainfall simulator (Figure 7.2 c) are defined in such a way as to center the rainfall peak within the time step. Finally, the presence of preferential flow directions of infiltrating water has been simulated to account for the natural macropore structure of soils (Flury et al., 1994). To simulate

these preferential flow channels six small drains have been made, approximately 30 cm long and 1 cm wide, composed of gravel enveloped in a plastic net (Figure 7.3a) and placed into the soil according to a fixed scheme (Figure 7.3 b-c). In the following paragraph a detailed synthesis of the tests and main results is reported.

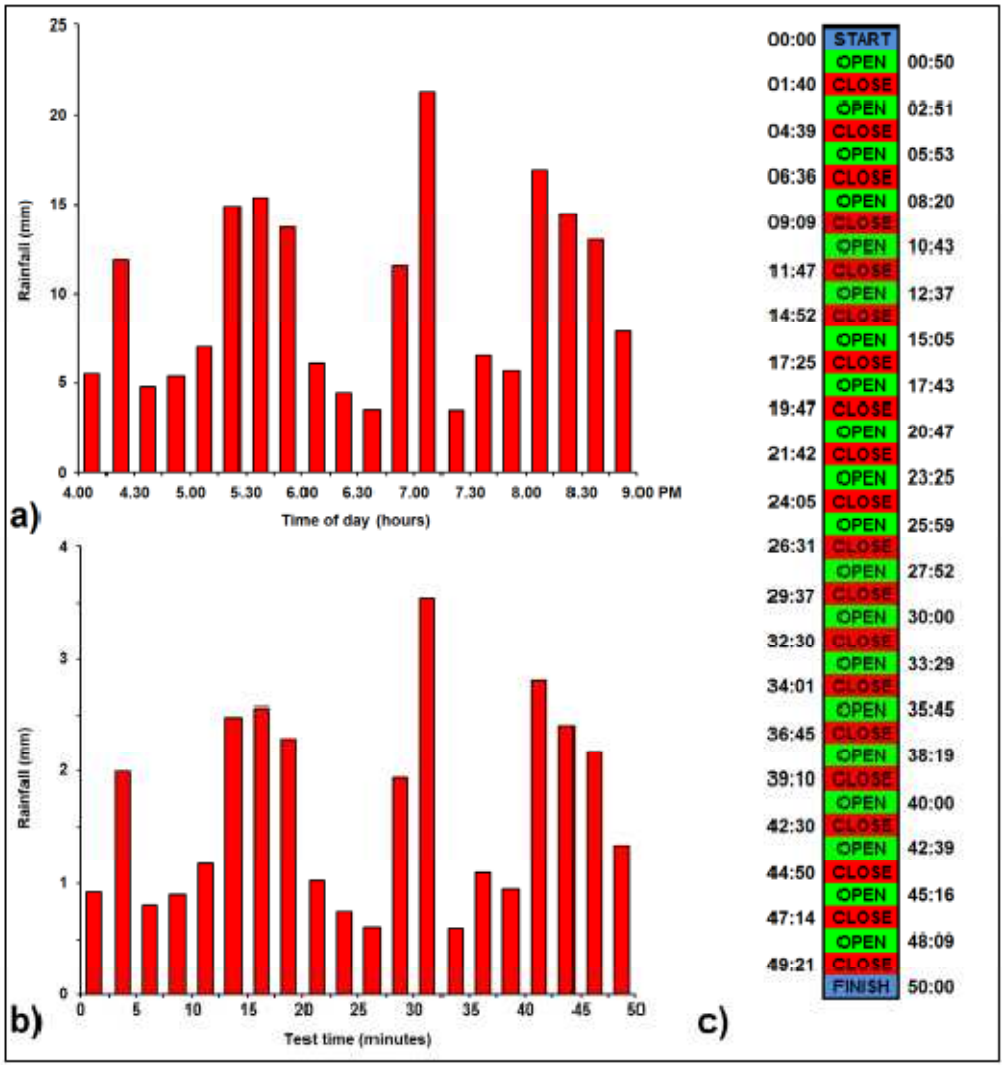

Figure 7.2 a) 15-minute hyetograph recorded at Santo Stefano di Briga between 4.00 and 9.00 pm of October 1st 2009; b) laboratory hyetograph used in the flume tests; c) opening-closing phases of the rainfall simulator to reproduce the Santo Stefano di Briga 15-minute hyetograph

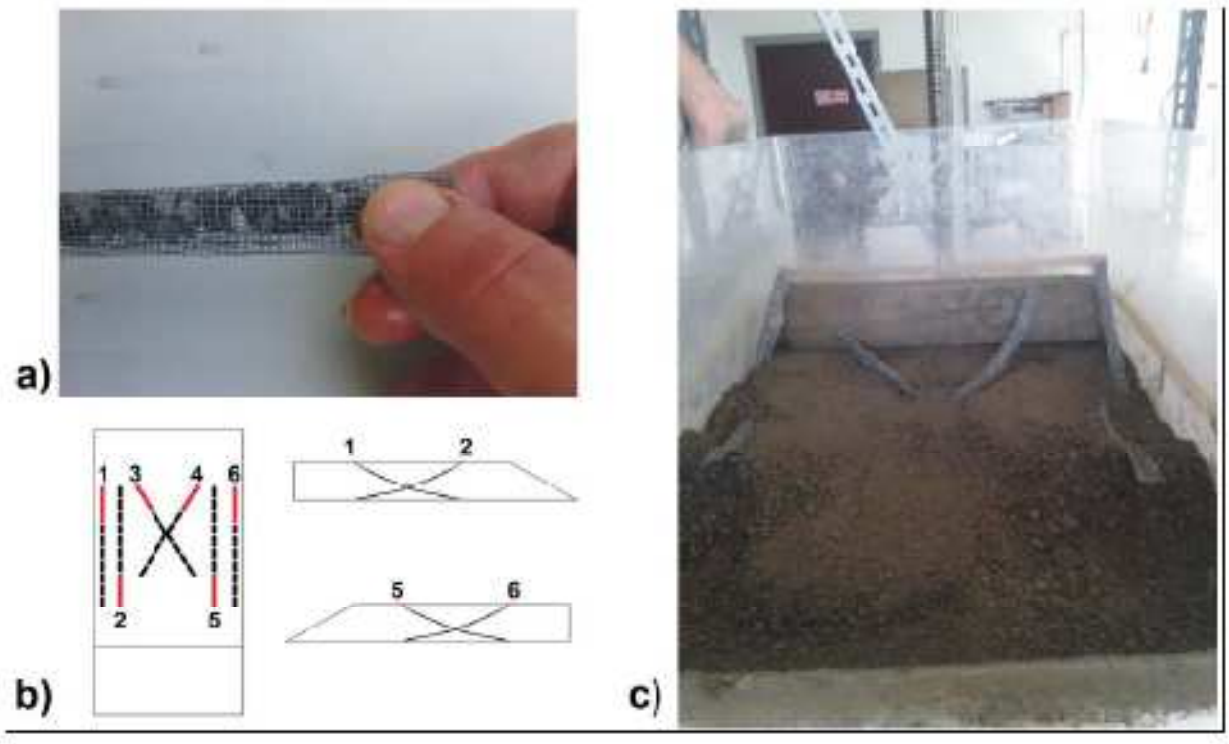

Figure 7.3 a) detail of a drain used during the tests; b) disposition scheme of drains within the soil (Left: top view, right: side view). Red and black colors indicate the part oriented towards the surface and the flume base, respectively c) disposition of the drains during the placing of soil into the flume

7.2 Flume tests: main results and considerations

The triggering mechanisms of landslides induced by rainfall have been analyzed in detail through 29 flume tests performed using the soil sampled in Giampilieri. The first observation is that the failure mode is generally extremely rapid, with no evidence of incipient instability (Figure 7.4 a-c), and involves a soil thickness between 7 and 10 cm (figure 7.4 d-e); thus, considering that the total soil thickness was 13 cm, the failure surface develops always within the soil profile, and not at the contact between soil and flume base. Furthermore, it is worth noting that, if the initial water content was low (e.g. 4%), failure typically occurred in the upper part of the flume, and vice versa (Figure 7.4 f-g). As regards the first set of tests (constant rainfall and absence of preferential flow directions), a wide range of initial soil conditions have been investigated (Table 7.2), thus, different observations can be made:

Test	n (%)	w (%)	Sr (%)	Tf (min)	Test	n (%)	w (%)	Sr (%)	Tf (min)
1	30	8	50.8	-	10	37	6	27.8	13
2	30	10	63.6	-	11	37	8	37.1	11
3	30	12	76.3	-	12	37	10	46.4	7
4	35	4	20.2	29	13	40	4	16.3	12
5	35	6	30.4	22	14	40	6	24.5	9
6	35	8	40.5	13	15	40	8	32.7	6
7	35	10	50.6	7.5	16	40	10	40.9	4
8	35	12	60.7	3	17	40	12	49.0	-
9	37	4	18.6	17.5					

Table 7.2 Initial soil conditions and failure time (Tf) for each of the 17 tests performed with constant rainfall and absence of preferential flow channels (CN).

1) As the initial water content (w) or porosity (n) increases the failure time decreases on equal porosity or water content, respectively (Figure 7.5). Although these results appear obvious, it is worth noting that the widest range of failure times is observed for n = 35%; thus, this specific porosity level is particularly sensitive to variations in the initial water content. It is also worth noting that time of failure is not strictly linked to soil saturation (figure 7.4b) but is dependent on both porosity and saturation;

2) n = 30% can be considered a too low porosity value for the investigated phenomenon. In fact, the excessive soil consolidation results in a very high runoff (and, consequently, in an extremely low infiltration rate), that does not produce a landslide type instability but a gradual erosion type mass movement of the superficial layers of the toe (Figure 7.6a,b) even with the wettest initial soil conditions. On the other hand, tests with n = 40%, w = 12% have not been performed because failure occurred during the flume tilting, due to the excessive looseness and wetness of the material, represented by a detachment of the soil from the uphill barrier (Figure 7.6 d-e);

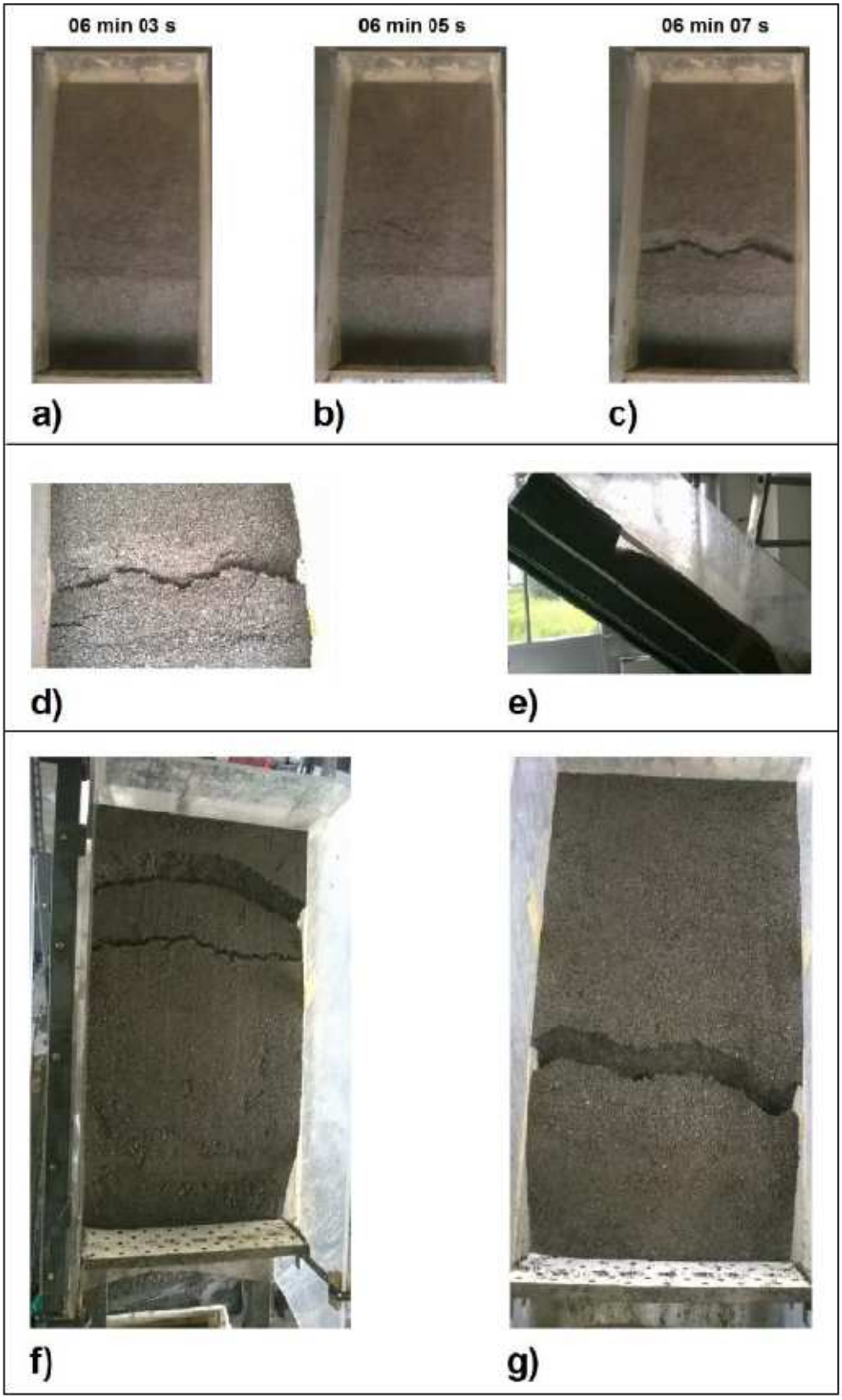

Figure 7.4 a-c) temporal evolution of failure in soil with n: 40% and w: 8% (test n. 15); d-e) detail showing the depth of the failure surface in soil with n: 35% and w: 8% (test n. 6); f-g) localization of failure in soils with n: 35% and different initial water content (left: w: 4% - test n.18; right: w: 8% - test n. 20)

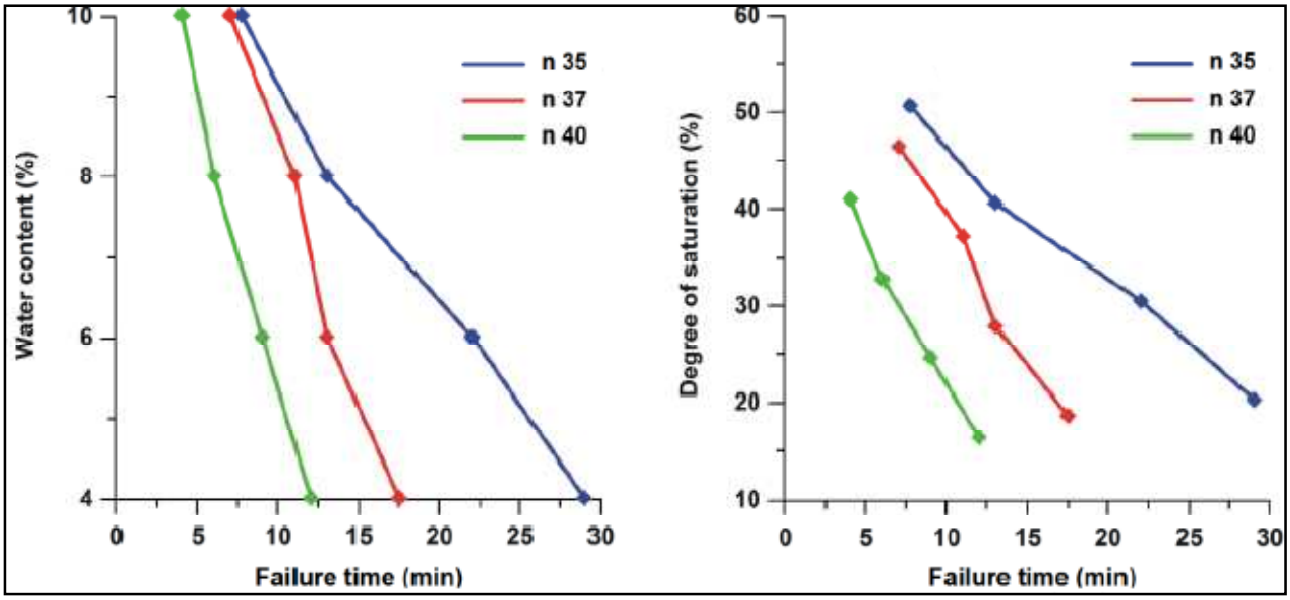

Figure 7.5 a) Failure time versus water content and b) versus degree of saturation for different initial porosity values (35, 37 and 40%)

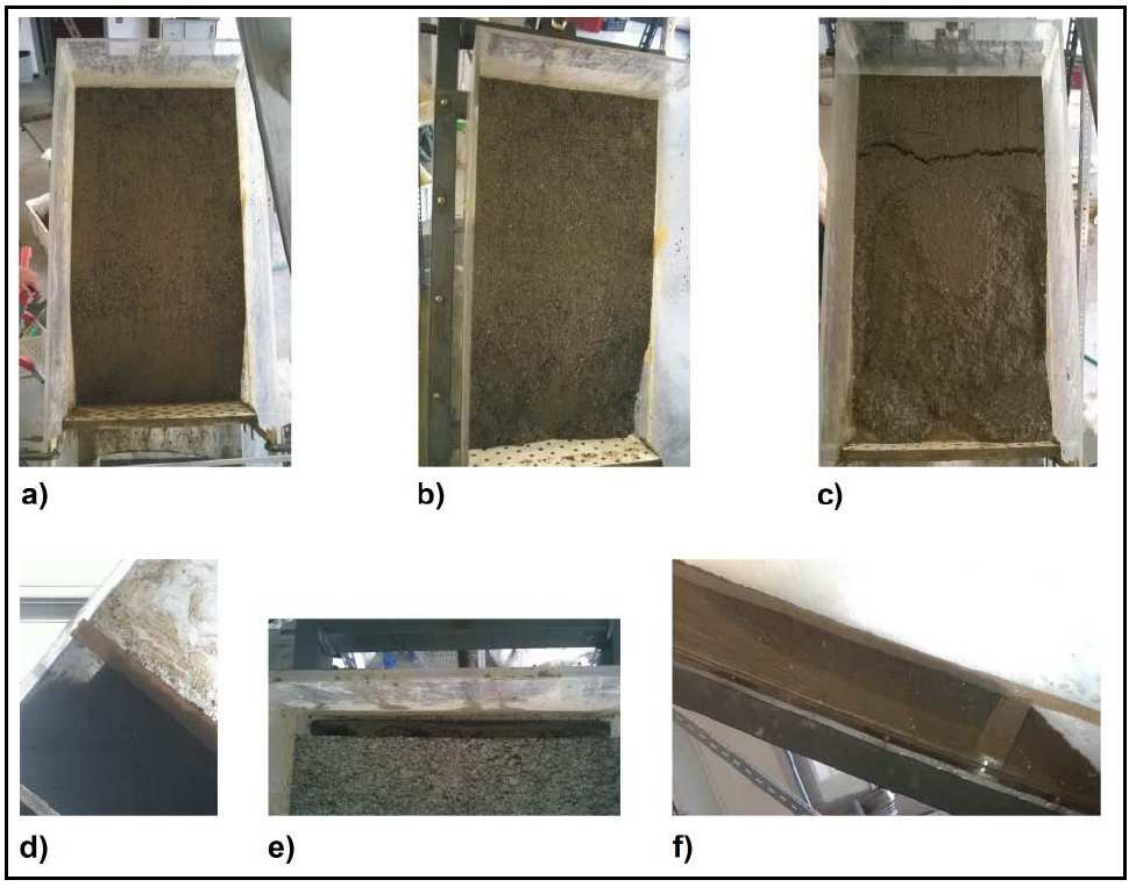

Figure 7.6 a) initial and b) final configuration of soil with n: 30% and w: 12% (test n. 3): no failure occurs; c) shallow flows in soil with n: 37% and w: 4% (test n.9); d-e) Soil detachment during flume tilting for soil with n: 40% and w: 12% (test n. 17); f) wetting front within the soil during test n. 9

3) In tests with n = 37 – 40 % and w = 4%, after about 10 minutes a superficial fracture in the upper part of the flume appeared. This fracture did not induce the detachment of soil. Instability occurred by means of progressive shallow flows (Figure 7.6 c) caused by the advance of the wetting front (Figure 7.3 f). This phenomenon can be explained with the scarce coherence of the material, that favors the formation of a saturated superficial zone wetter than the underlying one, causing instability only in the upper part of the soil profile.

On the basis of these first results (CN), a second set of tests were made (tests 18-21, GN, "Giampilieri scaled hyetograph" rainfall and absence of preferential flow directions), considering only the most representative initial conditions of the investigated phenomenon, i.e. porosity equal to 35% and water content not exceeding 10%. Unlike the "constant rainfall input", in the second type of tests opening and closing stages of rainfall system have been conveniently alternated to reproduce the Santo Stefano di Briga 15-minute hyetograph; thus, both the cumulative opening time of rainfall system (T_c) and the total test duration (T_f), that is hypothetically corresponding to an equivalent real time, have been measured for each test (Table 7.3).

Test	n (%)	w (%)	Sr (%)	Tc (min)	Tf (min)	Equivalent real time
18	35	4	20.2	26	44	8.15-8.30 PM
19	35	6	30.4	19	36	7.30-7.45 PM
20	35	8	40.5	12	22	6.15-6.30 PM
21	35	10	50.6	5	13	5.15-5.10 PM

Table 7.3 Initial soil conditions, cumulated rainfall failure time (Tc), total failure time (Tf) and equivalent real time for each of the 4 tests performed with "Giampilieri scaled hyetograph" rainfall input and absence of preferential flow channels (GN).

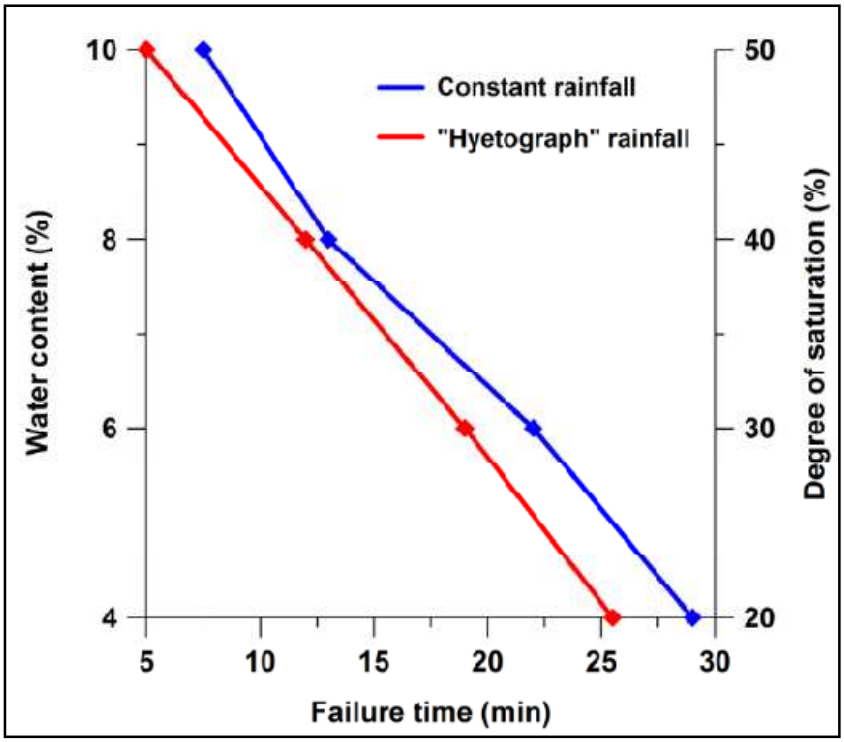

Figure 7.7 Failure time versus water content-saturation ratio for constant and "Giampilieri scaled hyetograph" flume tests in absence of preferential infiltration channels

The results shows how an initial water content varying between 4% and 8% induces instability in a real time corresponding interval compatible with the real landslide event, whose main phase occurred between 6.00 pm and 9.00 pm. On the other hand, a water content equal to 10% does not seem to be as representative because failure occurs too early (13 minutes, equivalent to 5.15 pm-5.30 pm). Moreover, comparing the cumulative opening times of rainfall system (T_c) with the failure times obtained in the constant rainfall tests (Figure 7.7), it is immediately noted that trends are very similar, but failure times are slightly lower in the case of "hyetograph" rainfall tests. This feature can be explained considering that during the closing stages water continues to infiltrate, reducing the runoff component.

In the following tests, the presence of preferential flow directions has been simulated introducing six small "drains" into the soil(Figure 7.3).

Test	n (%)	w (%)	Sr (%)	Tc (min)	Test	n (%)	w (%)	Sr (%)	Tc (min)
22	35	4	20.2	28	**24**	35	8	40.5	12
23	35	6	30.4	20	**25**	35	10	50.6	10.5

Table 7.4 Initial soil conditions and failure time (Tf) for each of the 4 tests performed with constant rainfall and presence of preferential flow channels (CN).

In the case of a constant rainfall input (tests 22-25 CD, Table 7.4), the resulting failure times are slightly lower than those obtained in absence of preferential flow directions, excluding the w = 10% case, where the instability is delayed by about 3 minutes (Figure 7.8). It is fundamental noting that

in all 4 tests, the mobilized soil volume is greater (about 10 cm) than that of the preceding tests (about 7 cm) indicating that the preferential channels do not influence the triggering time but influence the infiltration process mobilizing greater volumes of soil. Furthermore, it has been observed that with w = 8-10% a unique fracture develops in correspondence of the drains located in the upper part of the flume (Figure 7.9 a), whereas with lower water contents failure occurs with a double fracture system, where the second failure surface is located in correspondence of the drains placed in the lower part of the flume (Figure 7.9 b). This difference is probably due to the greater water infiltration within the drier soils, that succeeds to saturate also the lower part of the soil slope.

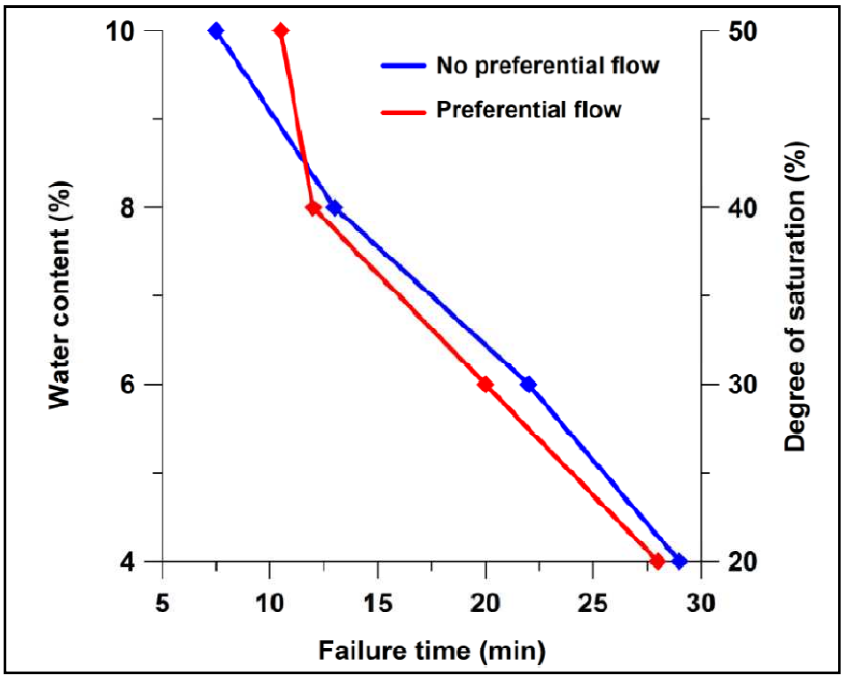

Figure 7.8 Failure time versus initial water content-saturation ratio for constant rainfall input flume tests in absence(blu) and presence (red) of preferential infiltration channels

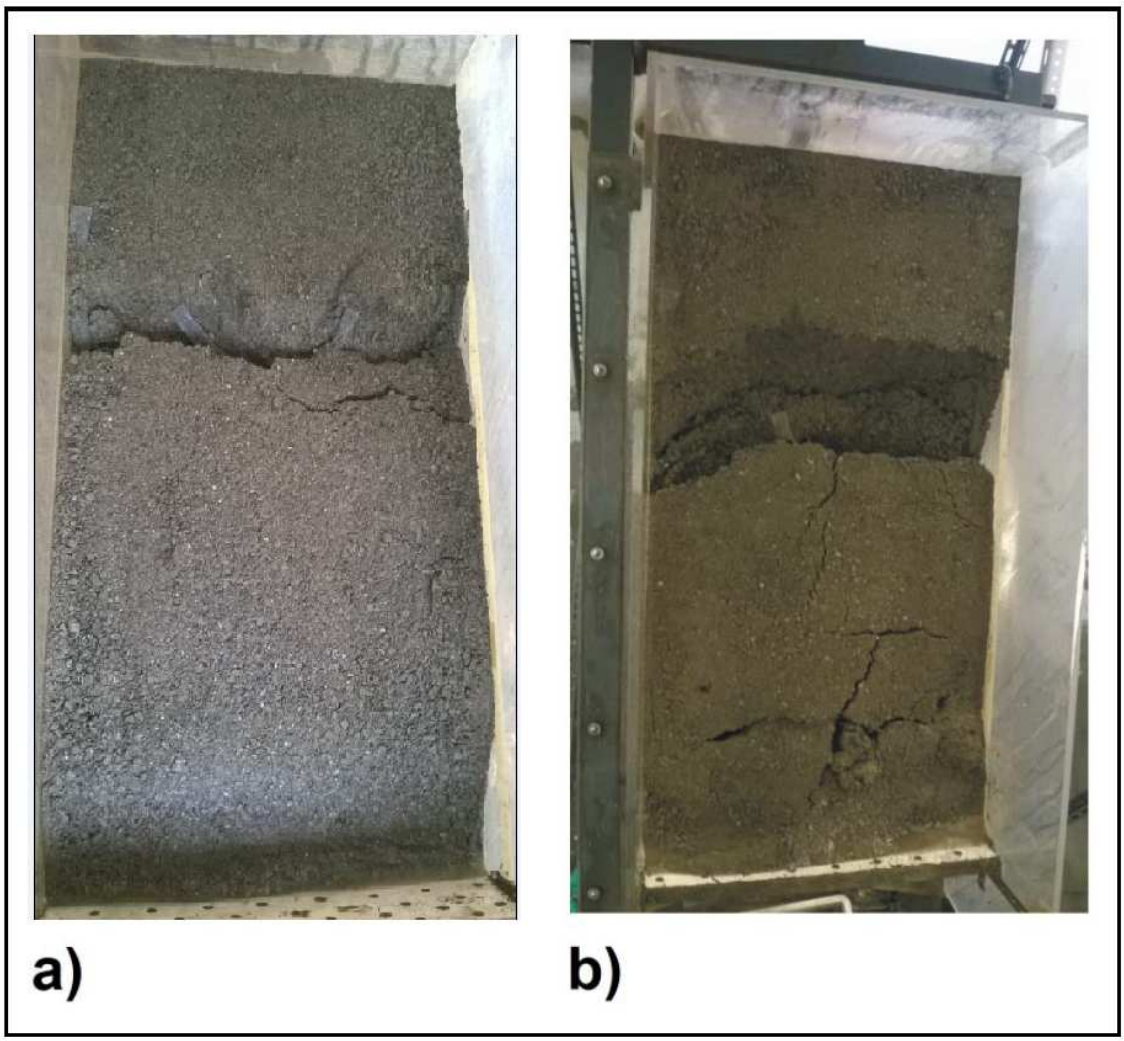

Figure 7.9 Post-failure images of tests with preferential flow channels and constant rainfall a) w=8%, test 24 and b) w=6% test 23

Finally, the same configuration with preferential infiltration channels has been tested using the "Giampilieri scaled hyetograph" rainfall input (tests 26-29, GD, Table 7.5). Also in these tests, only the failure time of test with initial water content w = 10% substantially deviates from the time measured in the corresponding test with no preferential flow directions (Figure 7.10). However, in this case the delay is higher (about 7 minutes). In this case when the initial conditions are dry w= 4 - 6 % the triggering mechanism is multi-fractured while in wetter cases w=8-10% the infiltration pores channel water to the toe of the slope that saturates quickly causing a sudden fracture and subsequent instability in the lower part of the flume). In both cases the mobilized soil volume is greater than the cases without infiltration channels (Figure 7.11 a-b).

Test	n (%)	w (%)	Sr (%)	Tc (min)	Tf (min)	Equivalent real time
26	35	4	20.2	27	46	8.30-8.45 PM
27	35	6	30.4	18	31	7.00-7.15 PM
28	35	8	40.5	13	23	6.30-6.45 PM
29	35	10	50.6	12	19	5.45-6.00 PM

Table 7.5 Initial soil conditions, cumulated rainfall failure time (Tc), total failure time (Tf) and equivalent real time for each of the 4 tests performed with "Giampilieri scaled hyetograph" rainfall input and presence of preferential flow channels (GD).

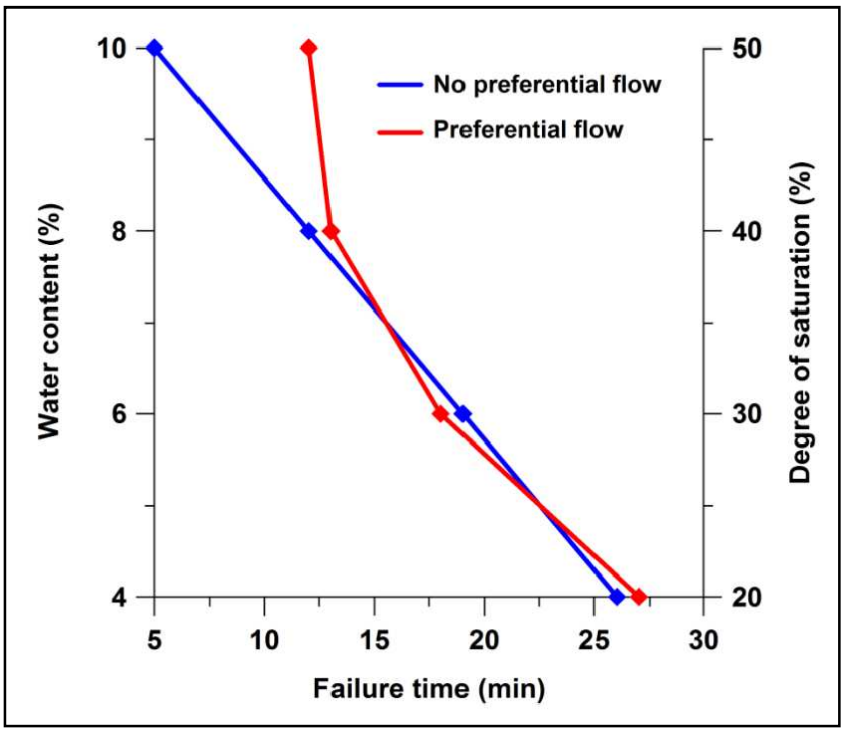

Figure 7.10 Failure time versus initial water content-saturation ratio for "Giampilieri scaled hyetograph" rainfall input flume tests in absence (blue) and presence (red) of preferential infiltration channels (GD)

During tests with w = 4%, due to the light brown initial color of the soil, a qualitative view of the infiltration trend was possible through the lateral plexiglass walls of the flume that became dark brown while wetting. In absence of the preferential channels a top-bottom infiltration process was registered while in presence of infiltration channels both the top soil and the bottom soil around the channels became wet, indicating an effective influence of the channels in infiltration process.

Figure 7.11 Post-failure images of tests with presence of infiltration channels and "Giampilieri scaled hyetograph". a)test 26, w = 4% b) test 28 w = 8%

In synthesis, the results of flume tests show the influence of initial soil conditions (porosity, water content) on times and modalities of slope failure. In particular, the alternation of rainfall peaks produces an increase of water infiltration, causing the mobilization of greater soil volumes rather than significant variations in failure time. This effect is emphasized in the case of preferential flow directions, where for higher slip thickness a substantial delay in failure time occurs only in one case (the wettest conditions, w = 10%). As regards the soil conditions before the October 1st, 2009 event, the results of "Giampilieri scaled hyetograph" rainfall tests suggest that the initial water content could vary between 4% and 8%, corresponding to a degree of saturation of 20.2% - 40.5%. These values substantially agree with the degree of saturation (41.5%) obtained using HYDRUS model (Chapter 8.3). Finally, it is important to note that test reproducibility has been assessed repeating the most complex tests (i.e. "hyetograph" rainfall and presence of preferential flow directions) and measuring the difference between failure times: in all of 4 tests, this difference is lower than one minute.

Chapter 8

Application of the physically based models to the Giampilieri landslide event of October 2009

In this chapter the results of the application of two physically based models, TRIGRS and SLIP, to the Giampilieri event occurred on October 1st 2009 are presented.

Shallow rainfall-induced landslides commonly occur under transient infiltration conditions into initially unsaturated soils (Baum et al., 2010). The infiltration process of water into soil during a rainfall event is highly dependent on the hydraulic properties of the material, the steady-state water-table depth and the initial soil moisture conditions. Thus, these parameters strongly influence the triggering conditions of shallow landslides and are required as essential inputs for physically-based modeling. In fact, these models generally couple an infinite slope stability model for the computation of the Safety Factor with a hydrologic model for the analysis of pore-water pressure regime.

8.1 Calibration of input parameters based on flume test observations

The input parameters of the SLIP model have been found by using data provided from preceding works (Montrasio & Valentino, 2007; Montrasio et al., 2014) and by calibration based on the results of flume tests. More specifically, α and λ have been assumed equal to 3.4 and 0.4 respectively, according to experimental tests (Montrasio & Valentino, 2007), whereas A, K_T, ξ and Sr_m have been adjusted through a procedure of back-analysis, carrying out different numerical simulations to reproduce the performed flume tests. If A and K_T values substantially agree with those referred to this soil type (Montrasio & Valentino, 2008; Montrasio et al., 2011), ξ and Sr_m have been modified for each test according to the varying initial soil conditions (i.e. porosity and presence of preferential flow directions), keeping all the other parameters constant. In fact these two parameters vary with soil density, considering that ξ is the parameter that quantifies the runoff component (ξ=1-β*) whereas Sr_m is a new calibration parameter, introduced for flume test modeling, that determines the initial equivalent value of the initial saturated layer (m_0) according to a water balance between the real amount of water and the fictitious model (Figure 8.1, Equations 8.1, 8.2):

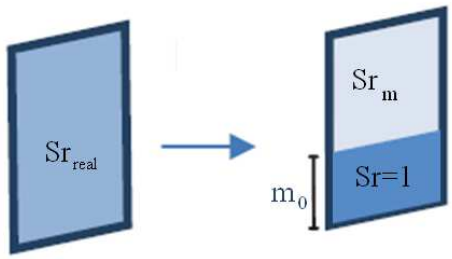

Figure 8.1 Hydraulic scheme of SLIP modeling

$$Sr_{real} \cdot n \cdot H = Sr_m \cdot n \cdot (1 - m_0) H + Sr_{sat} \cdot n \cdot m_0 \cdot H \tag{8.1}$$

$$m_0 = \frac{(Sr_{real} - Sr_m)}{(1 - Sr_m)} \tag{8.2}$$

where Sr_{real} is the real initial saturation ratio of the soil for each flume test, depending on the initial water content, porosity (n) and the unit weight of soil solids and Sr_m is a fictitious initial degree of saturation of soil, that allows the separation in two layers: the first $(1\text{-}m_0)\cdot H$ assumes the form of partially saturated layer ($Sr=Sr_m$) that contributes to shear resistance through apparent cohesion and the second, whose thickness is equal to $m_0 \cdot H$, assumes the form of a saturated layer at the bottom of the soil. This assumption was made in order to compare tests with same initial porosity keeping constant all the input parameters (with the only exception of m_0 function of the initial varying water content). A certain time lapse passed between the putting of the soil into the flume, and the opening of the simulated rainfall thus allowing some pore water to reach the lower layers of the soil strengthening this hypothesis. For each test, the simulated failure time has been compared with the real one, calibrating ξ and Sr_m with the aim to minimize the times difference. Tables 8.1 and 8.2 report the calibration results for flume tests with porosity equal to 35%. This calibration gives encouraging results being the mean variation between real and predicted failure time comprised between 1.4 and 2.2 minutes in absence and presence of preferential flow directions respectively, confirming the good predictive capability of the model for flume tests. Furthermore, these results have also been obtained by varying the rainfall input (constant or "Giampilieri scaled hyetograph") and maintaining all the other input parameters constant. The calibrated value of ξ is lower in the case of presence of preferential flow directions, considering that a soil with higher macro-porosity is affected by a lower surface runoff.

Test	Type	n (%)	w (%)	Sr_{real} (%)	Sr_m (%)	m_0	ξ (%) (runoff)	Tf_{real} (min)	Tf_{pred} (min)	Δt (min)
4	CN	35	4	20.2	15	0.06	20	29	28	1
5	CN	35	6	30.4	15	0.18	20	22	21	1
6	CN	35	8	40.5	15	0.30	20	13	14	1
7	CN	35	10	50.6	15	0.42	20	7.5	8	0.5
18	GN	35	4	20.2	15	0.06	20	44	47	3
19	GN	35	6	30.4	15	0.18	20	36	38	2
20	GN	35	8	40.5	15	0.30	20	22	24	2
21	GN	35	10	50.6	15	0.42	20	13	14	1
								Mean	1.4 min	

Table 8.1 Initial soil conditions, calibrated input parameters (Sr_m, m_0, ξ) real failure time (Tf_{real}), predicted failure time (Tf_{pred}) and time difference for each flume test performed with 35% porosity and absence of preferential flow channels (CN constant rain, GN Giampilieri scaled hyetograph rain).

Test	Type	n (%)	w (%)	Sr_{real} (%)	Sr_m (%)	m_0	ξ (%) (runoff)	Tf_{real} (min)	Tf_{pred} (min)	Δt (min)
22	CD	35	4	20.2	15	0.06	10	28	25	3
23	CD	35	6	30.4	15	0.18	10	20	19	1
24	CD	35	8	40.5	15	0.30	10	12	12	0
25	CD	35	10	50.6	15	0.42	10	10.5	6	4.5
26	GD	35	4	20.2	15	0.06	10	46	44	2
27	GD	35	6	30.4	15	0.18	10	31	32	1
28	GD	35	8	40.5	15	0.30	10	23	22	1
28	GD	35	10	50.6	15	0.42	10	19	14	5
								Mean	1.4 min	

Table 8.2 Initial soil conditions, calibrated input parameters (Sr_m, m_0, ξ), real failure time (Tf_{real}), predicted failure time (Tf_{pred}) and time difference for each flume test performed with 35% porosity and presence of preferential flow channels (CD constant rain, GD Giampilieri scaled hyetograph rain).

The results obtained reproducing the flume tests with porosity equal to 37% (Table 8.3) and 40% (Table 8.4) are substantially similar: in this case, the mean difference is lower than 2.5 minutes. However, it is worth noting that, as the porosity increases, not only ξ, but also Sr_m decreases, considering that a greater porosity corresponds to a lower degree of saturation, on equal initial water content.

Test	Type	n (%)	w (%)	Sr_{real} (%)	Sr_m (%)	m_0	ξ (%) (runoff)	Tf_{real} (min)	Tf_{pred} (min)	Δt (min)
9	CN	37	4	18.6	10	0.09	10	17.5	22	4.5
10	CN	37	6	27.8	10	0.20	10	13	16	3
11	CN	37	8	37.1	10	0.30	10	11	11	0
12	CN	37	10	46.4	10	0.40	10	7	5	2
								Mean	2.4 min	

Table 8.3 Initial soil conditions, calibrated input parameters (Sr_m, m_0, ξ), real failure time (Tf_{real}), predicted failure time (Tf_{pred}) and time difference for each flume test performed with 37% porosity and absence of preferential flow channels (CN constant rain).

Test	Type	n (%)	w (%)	Sr_{real} (%)	Sr_m (%)	m_0	ξ (%) (runoff)	Tf_{real} (min)	Tf_{pred} (min)	Δt (min)
13	CN	40	4	16.3	5	0.12	0	12	16	4
14	CN	40	6	24.5	5	0.21	0	9	11	2
15	CN	40	8	32.7	5	0.29	0	6	6	0
16	CN	40	10	40.9	5	0.38	0	4	2	2
								Mean		2 min

Table 8.4 Initial soil conditions, calibrated input parameters (Sr_m, m_0, ξ), real failure time (Tf_{real}), predicted failure time (Tf_{pred}) and time difference for each flume test performed with 40% porosity and absence of preferential flow channels (CN constant rain).

On the basis of these results, previous works and laboratory tests, the following input parameters have been assigned for the SLIP model application to the real scale case:

Parameter	Value	
n	35 (%)	
Gs	2.725	
Sr	30 (%)	
ξ	20 (%)	10 (%)
c'	0 (kPa)	
φ	35 °	
A	50 (kPa)	
λ	0.4	
α	3.4	
K_T	$1.5 \cdot 10^{-5}$(m/s)	

Table 8.5 SLIP input parameters

Two different values of the runoff parameter (ξ) and have been assigned to areas where maintained and abandoned terraces are located. This distinction has been made supposing that an abandoned agricultural terrace is affected by higher erosion phenomena, resulting in a greater macroporosity level thus allowing greater infiltration.

8.2 Introduction to TRIGRS

Transient models are able to improve the effectiveness of susceptibility analysis, accounting for the transient effects of varying rainfall on slope stability conditions, although they generally need several and accurate spatial data (Sorbino et al., 2010). In areas where abundant geotechnical information is available, site-specific, empirical models can be used to provide initial and boundary conditions. However, most applications are likely to take place in areas where such information is

lacking: in these cases, process-based theoretical models may provide a way to characterize the spatial variability of hydraulic conditions over large areas (Godt et al., 2008). Recently, physically-based models simulating the water flow into unsaturated porous media have been developed. In these models unsaturated flow is usually described by Richards' equation (Richards, 1931):

$$\frac{\partial}{\partial x}\left[K_x(\Psi)\left(\frac{\partial \Psi}{\partial x}-\sin\delta\right)\right]+\frac{\partial}{\partial y}\left[K_y(\Psi)\left(\frac{\partial \Psi}{\partial y}\right)\right]+\frac{\partial}{\partial z}\left[K_z(\Psi)\left(\frac{\partial \Psi}{\partial z}-\cos\delta\right)\right]=\frac{\partial \vartheta}{\partial \Psi}\frac{\partial \Psi}{\partial t}+S \quad (8.3)$$

where K is the hydraulic conductivity in the three dimensions, Ψ is the negative pressure head or suction head, expressed in terms of equivalent height of a water column, δ is the slope angle, ϑ is the volumetric water content, t is time and S represents the sink term describing water volumetric losses (root uptake, evapotranspiration etc.). This equation describes the variation of pore-water pressure head, and the related volumetric water content, with time. Since it is a three dimensional, parabolic, non linear, partial differential equation, a general analytic solution has not been found. Analytical solutions have been found only under certain hypotheses which allow for its linearization (e.g. Iverson, 2000; Chen et al., 2001). As mentioned in chapter 2.3, TRIGRS (Transient Rainfall Infiltration and Grid-based Regional Slope Model) is a Fortran program for the spatiotemporal modeling of rainfall induced shallow landslides (Baum et al. 2002, 2008). It combines a transient, one-dimensional analytic solution for pore-pressure response to rainfall infiltration with an infinite slope stability calculation. In the original version (Baum et al., 2002), the infiltration model was based on Iverson's (2000) linearized solution of Richards' equation, with implementation of complex storm histories, an impermeable basal boundary at finite depth and a simple runoff routing scheme (Savage et al., 2003; Salciarini et al., 2006). Assuming that Richards' equation can be linearized, the vertical transient flow of groundwater is described by a form of the diffusion equation:

$$\frac{\partial \Psi}{\partial t}=D_1\frac{\partial^2 \Psi}{\partial Z^2} \quad (8.4)$$

where Ψ is the groundwater pressure head, t is time, Z=z/cosδ (where z is the slope-normal coordinate direction and δ is the slope angle) and $D_1=D_0/cos^2\delta$ (where D_0 is the saturated hydraulic diffusivity). Introducing a time-varying rainfall input on the ground surface I_Z, the pressure head response $\Psi(Z,t)$ can be computed using the following input parameters (variable from cell to cell throughout the model):

- slope δ;
- soil layer depth d_{lb};

- depth of the initial steady-state water table d_{wt};
- long term (steady-state) surface flux I_Z;
- saturated hydraulic conductivity Ks.

Iverson's (2000) solution represents a particular case of the general solution for pressure head response, when $d_{lb} \rightarrow \infty$ and surface flux is applied for a single time interval (Salciarini et al., 2008). However, equation 8.4 is appropriate for initial conditions where the hillslope is tension-saturated (Figure 8.2 a).

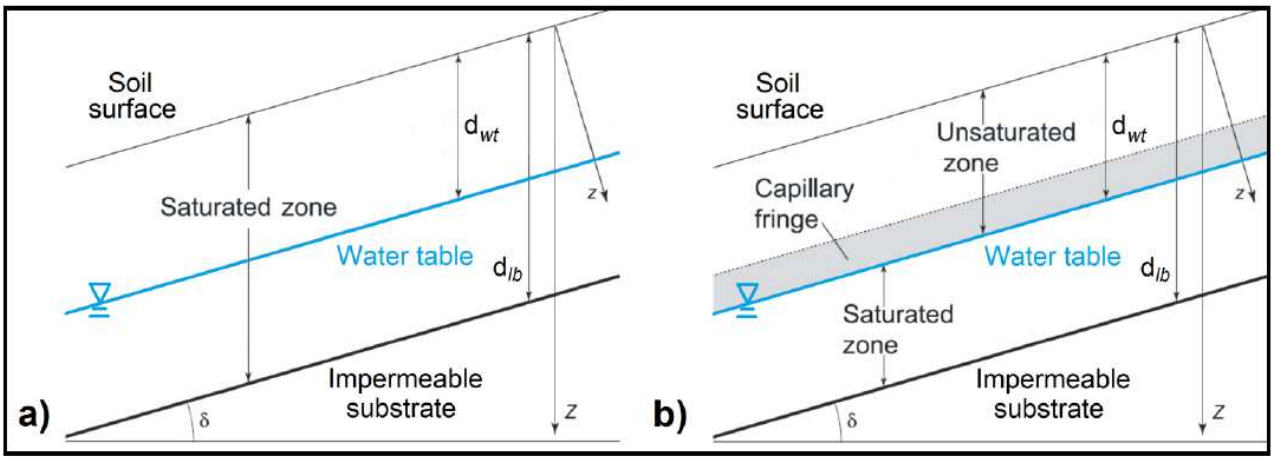

Figure 8.2 Conceptual scheme of TRIGRS hydrological model simulating a) tension-saturated and b) unsaturated soil conditions

In the second version (Baum et al., 2008) TRIGRS model was expanded to address infiltration into a partially unsaturated surface layer above the water table by using an analytical solution of Richards' equation for vertical infiltration. This scheme assumes the soil as a three-layer system consisting of an impermeable stratum at a certain depth d_{lb} overlain by a saturated zone with a possible capillary fringe above the water table, itself overlain by an unsaturated zone that extends to the ground surface (Figure 8.2 b). The unsaturated zone absorbs part of the water that infiltrates the ground surface and the remaining water passes through the unsaturated zone and accumulates at the base of the unsaturated zone above the initial water table. In this case, the one dimensional form of Richards' equation is expressed by (Freeze & Cherry, 1979):

$$\frac{\partial \vartheta}{\partial t} = \frac{\partial}{\partial Z}\left[K(\Psi) \cdot \left(\frac{1}{\cos^2 \delta} \frac{\partial \Psi}{\partial Z} - 1 \right) \right] \qquad (8.5)$$

where ϑ is the volumetric water content and $K(\Psi)$ is the hydraulic conductivity function. TRIGRS uses four hydrodynamic parameters (ϑs, ϑr, α_G and Ks) to linearize Richards' equation through the unsaturated zone, according to the hydraulic model proposed by Gardner (1958):

$$\begin{cases} K(\Psi) = K_S \exp(\alpha_G \cdot \Psi^*) \\ \vartheta = \vartheta r + (\vartheta s - \vartheta r)\exp(\alpha_G \cdot \Psi^*) \\ \Psi^* = \Psi - \Psi_0 \end{cases} \quad (8.6)$$

where ϑs and ϑr are the saturated and residual water content and α_G is a constant related to the pore size distribution of the medium where $1/\alpha_G$ represents the vertical height of the capillary fringe above the water table. Ψ_0 is a constant that can assume zero-value in the case of absence of capillary fringe or equal to $-1/\alpha_G$ and thus, at the top of the capillary fringe, the pressure head is $\Psi_0 = -1/\alpha_G$. In the unsaturated zone, the pressure head response is expressed by:

$$\Psi(Z,t) = \frac{\cos\delta}{\alpha_1} \ln\left[\frac{K(Z,t)}{K_S}\right] + \Psi_0 \quad (8.7)$$
$$\alpha_1 = \alpha_G \cos^2\delta$$

where the hydraulic conductivity $K(Z,t)$ solution is given by (Srivastava & Yeh, 1991). Both in the saturated and unsaturated configuration, TRIGRS imposes as additional physical limitation that the resulting pressure head cannot exceed that which would result from having the water table at the ground surface and subject to the long-term hydraulic gradient (Baum et al., 2008):

$$\Psi(Z,t) \le Z\cos\delta\left(\cos\delta - \frac{I_Z}{K_S}\right) \quad (8.8)$$

If the amount of infiltrating water reaching the water table exceeds the maximum amount that can be drained by gravity, TRIGRS simulates a rise in the water-table comparing the exceeding water quantity to the available pore space directly above the water table or capillary fringe and then, for each time step, applies the water weight at the initial top of the saturated zone to compute the new pressure head (Baum et al., 2010). Finally, the Safety Factor at a depth Z is calculated by:

$$FS(Z,t) = \frac{\tan\varphi'}{\tan\delta} + \frac{c' - \psi(Z,t)\cdot\gamma_w \cdot \tan\varphi'}{\gamma_s \cdot Z \cdot sen\delta \cdot \cos\delta} \quad (8.9)$$

Where c' is the effective cohesion, φ' is the internal friction angle of the material, γ_w is water unit volume weight and γ_s is soil unit volume weight. The depth Z where the safety factor drops below the unit is identified as the sliding depth. The pressure head $\Psi(Z,t)$ is subject to the limitation imposed by Equation 8.8 and, in the unsaturated configuration, is multiplied by the effective saturation parameter $\chi = (\vartheta - \vartheta r)/(\vartheta s - \vartheta r)$ as suggested by (Vanapalli & Fredlund, 2000). This

approximation is applied to a generalized effective stress law and represents a simplified form of the suction-stress characteristic curve (Lu & Godt, 2008; Lu et al., 2010).

8.3 Calibration of input parameters based on HYDRUS 1D

Among the numerical models that solve Richards' equation at different levels of complexity, HYDRUS-1D (Šimůnek et al., 1998) is one of the most known and used. It is a USDA (United States Department of Agriculture) Salinity Laboratory software that simulates water, heat and solute transport in variably saturated porous media on the basis of finite element method. The software describes infiltration in vadose zone using a modified version of Richards' equation for one dimensional vertical flow:

$$\frac{\partial \vartheta}{\partial t} = \frac{\partial}{\partial z}\left[K(\vartheta)\left(\frac{\partial \Psi}{\partial z} - \cos\delta \right)\right] - S \tag{8.10}$$

where K is the unsaturated hydraulic conductivity given by:

$$K(\Psi, Z) = K_S(z) K_r(\Psi, Z) \tag{8.11}$$

where Kr is the relative hydraulic conductivity and Ks the saturated hydraulic conductivity.

In this study, HYDRUS-1D has been used to evaluate the hydraulic properties and conditions of the soil cover (included the possible presence of a steady-state water table) before the October 1st, 2009 event, for further modeling with TRIGRS. Numerical simulations have been performed for the period September 1st - 30th, 2013 in order to quantify the effect of the preceding rainfall. The van Genuchten-Mualem model (van Genuchten, 1980) was chosen to simulate the water flow and to evaluate the soil hydraulic parameters. This model is given by:

$$\begin{aligned} \chi &= \left[1 + \left(|\alpha_{VG}\Psi|\right)^n\right]^{-m} \\ K_r &= \sqrt{\chi}\left[1 - \left(1 - \chi^{1/m}\right)^m\right]^2 \end{aligned} \tag{8.12}$$

Where:

$$\begin{aligned} m &= 1 - \frac{1}{n} \\ \chi &= \frac{\vartheta - \vartheta r}{\vartheta s - \vartheta r} \end{aligned} \tag{8.13}$$

where χ is the effective saturation, n is a function of pore size distribution and α_{VG} is a parameter related to the pore size. The hydrodynamic parameters ϑs, ϑr, α_{VG}, n and Ks are predicted by Hydrus-1D from soil grain size distribution using the ROSETTA Lite module (Schaap et al., 2001). The ROSETTA module uses a database of measured water retention curves and other properties for a wide variety of soils. For a given grain size distribution and other soil properties the model estimates a retention curve (i.e. the relationship between soil water suction Ψ and the volumetric water content ϑ) with good statistical comparability to known retention curves of other soils with similar physical properties (Nimmo, 2005). In this case, daily rainfall (Figure 8.3) is given as the input for time variable boundary conditions, whereas evapotranspiration is accounted for by inserting the maximum and minimum temperature values recorded during the investigated period into Hargreaves equation (Jensen et al., 1997). As a lower geometrical boundary, a slope normal zero-flux condition is assumed due to the presence of an impermeable bedrock below the soil cover. Finally, a 80-cm soil profile of 38° slope (i.e. the average soil thickness and slope observed within the landslide source areas) is chosen as the geometric configuration, considering it as the most representative for a back-analysis of the conditions prior to the event. In table 8.6 the hydrodynamic properties found by HYDRYS-1D are shown:

ϑ_s (-)	ϑ_r (-)	α_{VG} (m^{-1})	n (-)	K_s (m/s)
0.3904	0.0485	3.47	1.7466	$1.22 \cdot 10^{-5}$

Table 8.6 Soil hydrodynamic properties found using HYDRUS-1D

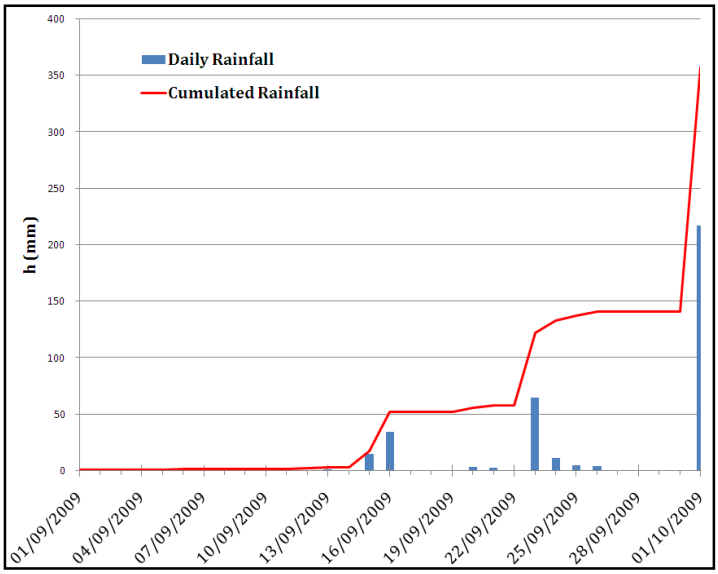

Figure 8.3 Daily and cumulated precipitations for the period 1/9/2009 -1/10/2009 registered at the Santo Stefano di Briga station

According to the simulation results, the absence of a steady-state water table within the soil cover can be assumed, whereas, as regards the initial soil moisture conditions, in Figure 8.4 the resulting water content trend with depth at four different times (September 1st, 24th, 25th and 30th) is reported. The initial soil moisture condition (ϑ = 0.049) is assumed near to the residual water content value considering the hot, dry conditions during the preceding summer months. The effect of the preceding rainfall results in an increase in soil water content, that is equal to 0.202 on September, 25th (the day after the second rainfall peak) and a decrease to 0.145 on September 30th. It is worth noting that the water content values are averaged approximately for the first 30 cm (September 24th) and 50 cm (September 25th) of soil, considering the evident non-homogeneous trend due to the advance of the wetting process. On the other hand, the water content trend is much more homogeneous in the first 70 cm of soil on September 30th, resulting in an average value of 0.145, that corresponds to a degree of saturation (Sr) equal to about 41.5% (on the basis of physical properties reported in Chapter 4, Table 4.7) a similar value than that evaluated from flume tests.

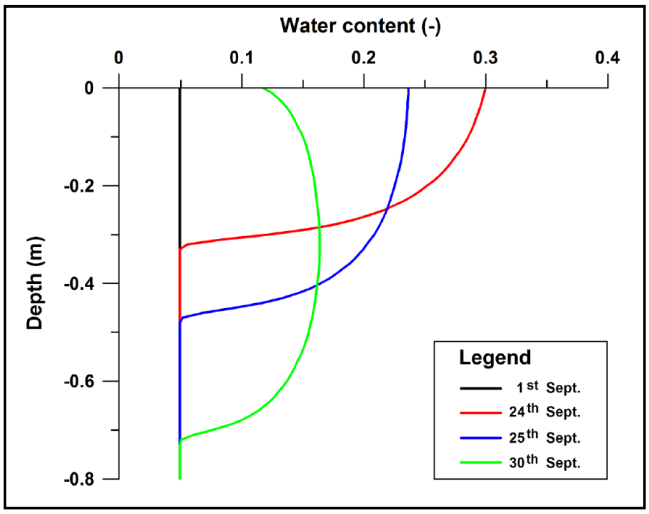

Figure 8.4 Results of the HYDRUS 1D simultaiton: Volumetric water content vs depth at different days prior to the Giampileiri landslide event (1/10/2009).

Date	ϑ (-)	w % (-)	Sr
Sept. 1st	0.049	1.8	14.0
Sept. 24th	0.26	9,7	74.3
Sept. 25th	0.202	7,4	7.457.8
Sept.30th	0.145	5,3	41.5

Table 8.7 Results of the HYDRUS 1D simulation: Volumetric (ϑ) and massic (w) water contents and saturation ratio at different days prior to the Giampilieri landslide event (1/10/2009).

Thus, on the basis of these results it is possible to state that the preceding rainfall had an effect on the hydraulic conditions of the Giampilieri soil cover at the triggering instant. This effect has been taken into account in the physically-based modeling.

Considering the given porosity (35%), the initial water content (6%) and the unit weight of solids (γ_s= 26.73 kN/m^3) used in SLIP modeling, γ_n, that represents the depth-averaged soil unit weight. is equal to 18.4 kN/m^3. As regards the hydrodynamic parameters, ϑs (saturated water content), ϑr (residual water content) and Ks (saturated hydraulic conductivity) are directly predicted by means of HYDRUS-1D model, as well as the absence of an initial water table, whose depth (d_{wt}) so corresponds to the bedrock-soil interface. To evaluate α_G parameter, that is typical of Gardner hydraulic model, use was made of the conversion formula introduced by (Ghezzehei et al., 2007) and based on the capillary length approach (Warrick, 1995), that defines a correspondence between Gardner and van Genuchten-Mualem models:

$$\alpha_G = \frac{\alpha_{vG}}{-1.674 \cdot m^4 + 7.192 \cdot m^3 - 11.4 \cdot m^2 + 6.852 \cdot m - 0.97} \tag{8.14}$$

$$m = 1 - \frac{1}{n} \tag{8.15}$$

where α_{vG} and n are parameters of the van Genuchten-Mualem model obtained using HYDRUS-1D. On the basis of the results of the same simulations the I_{ZLT} parameter, that represents the long-term background rainfall rate, was assumed equal to the cumulative actual surface flux value (5.3 x 10^{-8} m/s). Finally, the saturated hydraulic diffusivity (D_0) has been calculated according to:

$$D_0 = \frac{K_S \cdot H}{S_y} \tag{8.16}$$

where Ks is the saturated hydraulic conductivity, H the average soil thickness (80 cm) and S_y the specific yield (Grelle et al., 2014). Considering that the investigated soil can be classified as silty sand, the specific yield has been assumed equal to 0.26, on the basis of typical values given by (Johnson, 1967) and (Loheide II et al., 2005) for each soil textural class.

The input parameters used in TRIGRS modeling are shown in Table 8.8:

Parameter	Value
γ_n	18.4 (kN/m^3)
c'	3 (kPa)
φ'	35 (°)
$\mathbf{d_{wt}}$	H (m)
$\mathbf{I_{ZLT}}$	$5.3 \cdot 10^{-8}$(m/s)
$\mathbf{K_S}$	$1.22 \cdot 10^{-5}$(m/s)
$\mathbf{D_0}$	$3.75 \cdot 10^{-5}$(m^2/s)
ϑ_s	0.3904
ϑ_r	0.0485
$\boldsymbol{\alpha_G}$	9.09 (m^{-1})

Table 8.8 TRIGRS input parameters

The value of the effective cohesion (c') is not null because of TRIGRS modeling necessities. This is not coherent with the laboratory results but necessary to have initial stability.

8.4 Common input data

8.4.1 Landslide inventory map

Any type of landslide susceptibility assessment is based on a comprehensive landslide inventory map. As regards the study area, a detailed landslide inventory map was produced after the October 1st, 2009 event (Figure 8.5). The following information was gently provided by the Department of earth Sciences of the University "Sapienza" of Rome. According to the classification by (Hungr et al., 2001), three different types of shallow landslide occurred in the area, mainly debris-flows, but also debris-slides, frequently evolved to debris-avalanches. It is worth noting that for each of more than 700 mapped landslides, the source area has been identified too. The landslide inventory map was produced through analysis of high resolution aerial orthophotos integrated by field surveys in the days after the event. In addition, land cover maps and detailed pre-and post-event Digital Elevation Models (DEMs) are available for the study area. In particular, pre-event DEM has a 2x2 m resolution, whereas the post-event DEM, that derives from airborne LiDAR (Light Detection and Ranging) data taken immediately after the event, has a 1 x 1 m resolution. As regards the land cover map, the basic information derive from the third level of the Corine Land Cover 2000 Project, as the area is characterized by a widespread presence of man-made terraces and their state of preservation

could be relevant in terms of landslide susceptibility. Such information, inferred from the interpretation of the high-resolution orthophotos, was added to the land-cover map. Considering the type of available data, it is worth stressing that: (1) The landslide inventory map, reporting only the shallow landslides triggered on October 1st, can be used to assess the landslide susceptibility of the area to similar magnitude rainfall events; (2) In a shallow landslide susceptibility assessment, using only the source areas data in place of the whole landslide inventory map allows to obtain more accurate and reliable results; (3) The availability of both pre- and post-event DEMs allows to carry out different types of analysis. For instance, the pre-event DEM represents a basic tool for the landslide susceptibility assessment and the back-analysis of the 2009 event. Otherwise, the post-event DEM can be used to evaluate future triggering scenarios.

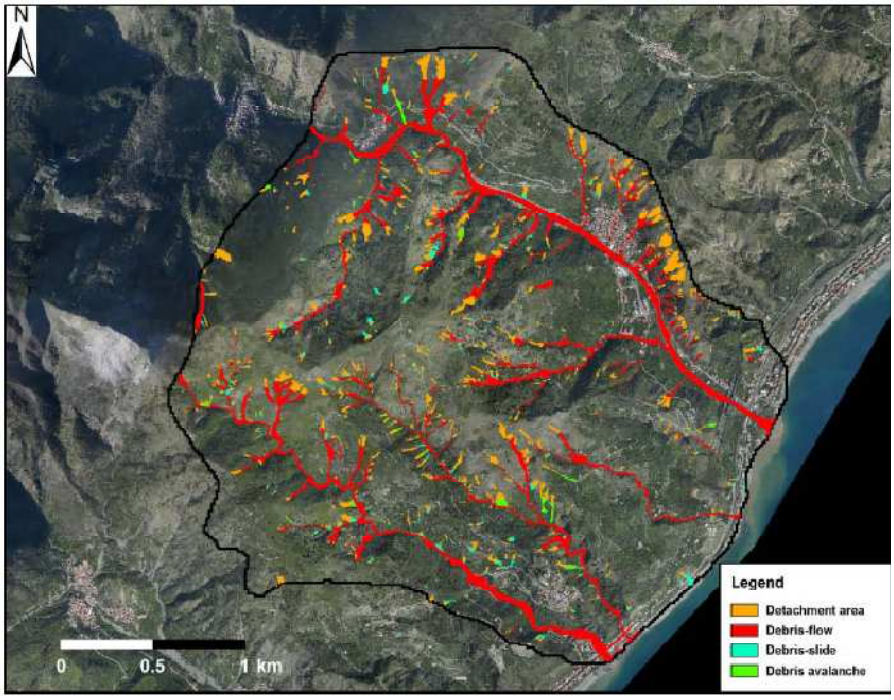

Figure 8.5 Landslide inventory map

8.4.2 Evaluation of spatial variability of soil thickness

Another feature that strongly influences shallow landsliding is soil thickness. In most cases, however, detailed data on this parameter can be difficult to obtain even for small basins (Dietrich et al., 1995). In fact, it can vary as a function of many different interplaying factors, such as underlying lithology, climate, slope, hillslope curvature, upslope area and vegetation cover, making the estimation of this parameter challenging and often unreliable (Catani et al., 2010). To enter soil thickness in basin scale models, many authors rely on straightforward and simplistic solutions such as considering a spatially constant value in the whole studied area (Khazai & Sitar, 2000), using soil thickness classes (Revellino et al., 2008) or assigning a constant value for each geological formation

encountered in the analyzed site (Savage et al., 2004). More complex methods that make use of multivariate statistical analyses (Gessler et al., 2000; Tesfa et al., 2009) or that employ process-based models (Casadei et al., 2003; Pelletier & Rasmussen, 2009) are less frequently used as input data in large scale slope stability analyses because require some effort to be correctly applied and calibrated over large areas. Considering the erosion and weathering processes of bedrock, the resulting eluvial-colluvial deposit generally accumulates on the lower parts of the slopes or in channels associated with weathered terrain. In this study the model proposed by (Saulnier et al., 1997), which correlates soil depth to the local slope angle was used:

$$h_i = h_{\max}\left\{1-\left[\frac{\tan\alpha_i - \tan\alpha_{\min}}{\tan\alpha_{\max} - \tan\alpha_{\min}}\left(1-\frac{h_{\min}}{h_{\max}}\right)\right]\right\} \quad (8.17)$$

where h_i is soil thickness computed at the i-th cell of the mesh, h_{max} and h_{min} are the maximum and minimum soil thickness values measured in the area, α_i is the slope value the i-th cell of the mesh, while α_{max} and α_{min} are the values of the slope angle respective to the cells with depth h_{min} and h_{max}.

Figure 8.6 View of the outcroping bedrock after the triggering of a landslide (Courtesy of Prof. G. Scarascia Mugnozza)

Although this model relies heavily on geomorphological simplifications, it is often used to estimate a spatially distributed soil depth field in basin scale modeling (e.g. Salciarini et al., 2006). In this study, the model has been calibrated using as maximum and minimum slope/soil thickness values those measured within the source areas (17°-58° and 1.5-0.5 m respectively). Thus, the model was applied to the whole study area using the measured values within the source areas as constraints, considering that the shallow landslides occurred in Giampilieri frequently involved the entire soil profile (Figure 8.6). The resulting soil thickness map is reported in Figure 8.7 and it has been used as input data for physically-based modeling.

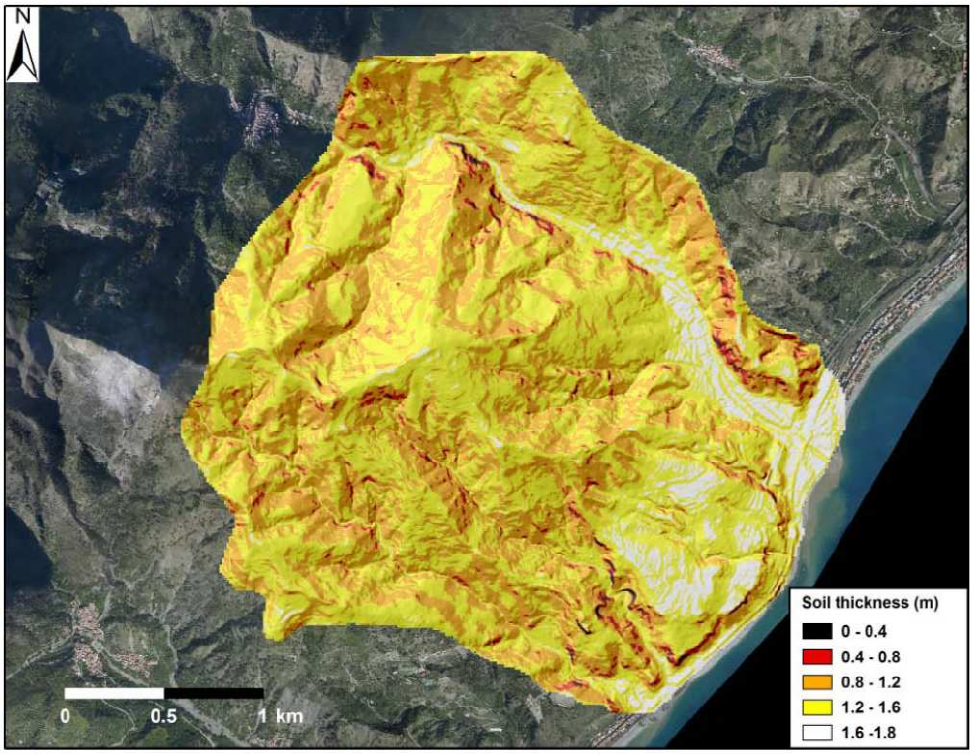

Figure 8.7 Soil thickness map

8.4.3 Evaluation of spatial variability of rainfall during the October 1st, 2009 event

In order to back-analyze the October 1st, 2009 event and, as a consequence, to calibrate the physically-based model, the spatial pattern of the triggering storm has been evaluated to produce more accurate and reliable results. In fact, according to the rain gauge measurements and witnesses reports, the event was characterized by a strong spatial variability. To reproduce the spatial continuity of rainfall fields a number of interpolation techniques, based on rain gauge measurements, are described in literature. Generally these methods can use mathematical functions to create a continuous surface by only using the geometric characteristics of point observations (deterministic methods) or can account for statistical relationships between the measured points (geostatistical methods). Thiessen polygon, Inverse Distance Weighted (IDW) and polynomial interpolation are the most frequently used deterministic methods (Ly et al., 2011), whereas Kriging is the most extensively applied geostatistical interpolation technique. However, even though numerous interpolation methods for estimating spatial rainfall distribution are available, no method is suitable for every circumstance (Nalder & Wein, 1998) and the rainfall characteristics along with geomorphological setting can affect the choice of interpolation method. For instance convective storms (like the one occurred in Giampilieri area) are known to exhibit more significant spatial variability compared to other types of rainfall events (e.g. May & Julien, 1990; Goodrich et al., 1995); otherwise, in mountainous regions, evaluating rainfall distribution is more complicated

because rainfall patterns are influenced by high changes in topographical relief over relatively short distances. Although some authors have proposed modified deterministic techniques to consider the effect of such factors (e.g. Chang, 2005), geostatistical methods are commonly preferred because it allows not only to account for spatial correlation between neighboring observations to estimate values at ungauged locations, but also to include more densely sampled secondary attributes (e.g. weather radar data, elevation) with sparsely sampled measurement of the primary attribute (e.g., rainfall) to improve rainfall estimation (Mair & Fares, 2011). More in particular meteorological satellite radars give a large-scale vision of precipitation fields compared to scattered point estimates from rainfall gauges. Even though this type of data generally underestimates the rainfall intensity due to several well-known sources of error (Habib & Krawjewski, 2002), from 2000s onwards standard range-corrected radar products proved to be sufficiently informative to capture the spatial variability of rainfall to be used in hydrological application (Schuurmans & Bierkens, 2007). In particular, the use of radar products in combination with geostatistical methods proved to be beneficial for spatial rainfall estimation (Velasco-Forero et al., 2009; Verworn & Haberlandt, 2011). On the basis of the above mentioned observations, to reproduce the spatial rainfall distribution of the October 1st, 2009 rainstorm, the conditional merging technique (Ehret, 2002; Pegram, 2003) has been chosen as interpolating method. In this approach, the information from the satellite radar is used to condition the spatial rainfall field obtained by the interpolation of rain gauges. The process is composed of seven steps (Figure 8.8): a) the rainfall field is observed at discrete points from rain gauges; b) the rainfall field is also observed by radar on a regular grid; c) the rain gauge observations are interpolated by Ordinary Kriging on the radar grid; d) the same interpolation technique is applied to the radar pixel values at the rain gauge locations; e) at each radar grid point, the deviation between the observed and interpolated radar value is computed; f) the field of deviations obtained previously is added to the interpolated rainfall field obtained in the first step; g) the resulting rainfall field follows the main field of the rain gauge interpolation along with the spatial structure of the radar field (Sinclair & Pegram, 2005). In this study, the precipitation rate maps deriving from the processing of EUMETSAT (European Organisation for the Exploitation of Meteorological Satellites) satellite data were used. These maps, provided by the National Center of Aeronautical Meteorology and Climatology (CNMCA) of the Italian Air Force, are generated from blending of PMW (passive microwave) measurements and IR (Infrared) brightness temperatures, coupled with the NEFODINA (DYNAmic NEFOanalysis) software, that allows the automatic detection and classification of convective cloud systems reducing the underestimation of precipitation (Mugnai et al., 2013). The accumulated precipitation values are close to those measured by the rain gauges, about 200 mm in less than 6 hours (Melfi et al., 2012). Regarding the

rain gauge data, ten-minute rainfall records of six stations (Antillo, Colle San Rizzo, Fiumedinisi, Ganzirri, Messina Istituto Geofisico and Santo Stefano di Briga) are used, conveniently rescaled into fifteen-minute data to be compared with the corresponding radar rainfall maps. Thus, using the conditional merging method, 32 rainfall maps have been obtained to reconstruct as accurately as possible the development of the October 1st rainfall event between 3.00 pm and 11.00 pm. Each map (Figure 8.9) reports the spatial distribution of rainfall cumulated in 15 minutes and has been used as input for the back-analysis of the event by means of physically-based modeling.

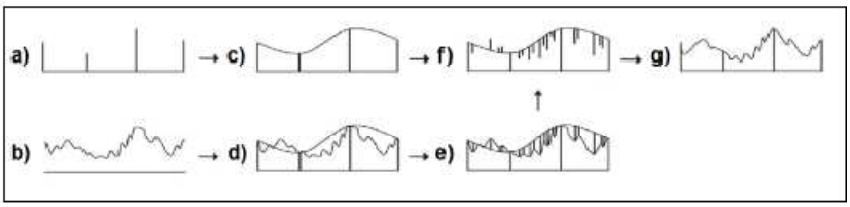

Figure 8.8 Conditional merging technique scheme

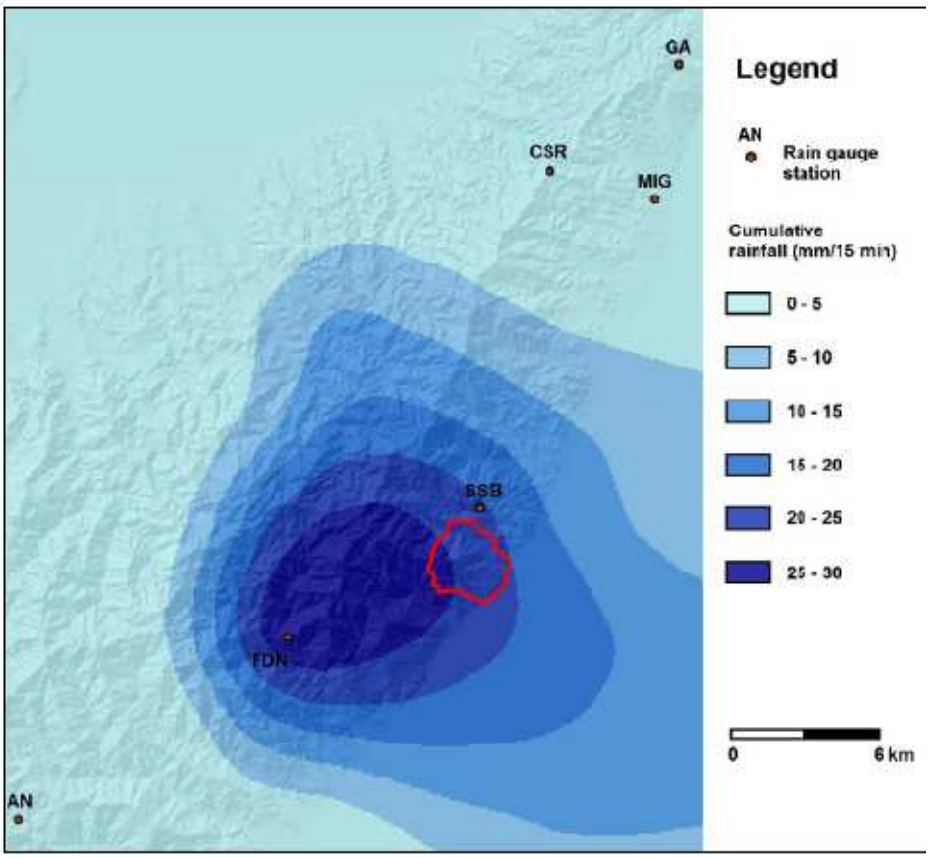

Figure 8.9 Example of satellite rainfall map

8.5 Application of the models

Two physically-based models (TRIGRS and SLIP) have been used to back-analyze the October 1st 2009 event between 3.00 pm and 11.00 pm. Although essential differences exist between the two models, both of them operate on a digital elevation grid and accept input from a series of ASCII text files. In particular, SLIP has been implemented by using Matlab® software and relies on input data prepared in GIS environment. The digital elevation model (DEM) used was the pre-event DEM (resampled to 4x4 m resolution for time computation necessities). Table 8.9 shows the input parameters required by the two models. Soil thickness (*H*) and rainfall intensity (Iz) vary from cell to cell on the basis of the maps obtained according to the methods described above. As regards the geotechnical parameters, according to the available data an average friction angle of 35° has been used in both models, the effective cohesion is 0 kPa in SLIP and 3kPa in TRIGRS (a small amount of effective cohesion is needed in TRIGRS for initial stability), whereas all the other parameters are typical of each model. The output of the models are time-varying safety factor maps whose predictive capability is evaluated by a comparison with the real landslide detachment area maps.

TRIGRS		**SLIP**	
d_{lb} (soil depth)	Spatial map (m)	H (soil depth)	Spatial map (m)
I_Z (rain intensity)	Spatial/temporal map (m/s)	h (rain depth)	Spatial/temporal map (m)
δ (slope)	Spatial map from DEM (°)	β (slope)	Spatial map from DEM (°)
γ_n (unit volume weight)	18.4 (kN/m^3)	n (porosity)	35 (%)
c' (effective cohesion)	3 (kPa)	Gs (solid weight ratio)	2.725
φ' (internal friction angle)	35 (°)	Sr (saturation ratio)	30 (%)
d_{wt} (water table depth)	H (m)	ξ (runoff)	20 (%) or 10 (%)
I_{ZLT} (long term rainfall rate)	$5.3\cdot10^{-8}$(m/s)	c' (effective cohesion)	0 (kPa)
K_S (saturated permeability)	$1.22\cdot10^{-5}$(m/s)	φ' (internal friction angle)	35 °
D_0 (Diffusivity)	$3.75\cdot10^{-5}$(m^2/s)	A (apparent cohesion parameter)	50 (kPa)
ϑ_s (saturated water content)	0.3904	λ (apparent cohesion parameter)	0.4
ϑ_r (residual water content)	0.0485	α (SLIP parameter)	3.4
α_G (hydraulic parameter)	9.09 (m^{-1})	K_T (global drainage capacity)	$1.5\cdot10^{-5}$(m/s)

Table 8.9 Input parameters

Once the input parameters of the two models were defined, the October 1st, 2009 event has been reconstructed in detail and the simulation results, expressed in terms of safety factor (FS), have been compared with the landslide inventory map of the same event for a ROC evaluation.

8.5.1 Application of TRIGRS

Figure 8.10 shows the output of TRIGRS computation, namely time varying safety factor maps between 4.00 pm and 11.00 pm, whereas Table 8.10 reports the number of unstable pixels, percentage of correctly predicted landslides areas and percentage of correctly predicted stable areas. TRIGRS model's prediction is accurate from a temporal point of view developing from 5 pm, with a peak in instability between 7 pm and 8 pm and concluding at 11 pm. This temporal evolution of the phenomenon substantially agrees with both the witnesses and amateur videos, although during the real event no particular increase of slope instability has been registered after 10.00 pm. The modeling underlines the importance of the period between 7.00 pm and 8.00 pm in which most of the shallow landslides triggered. TRIGRS correctly predicts 88% of the stable areas but only 29.9% of landslides pixels at 11 pm showing how, in this case, it underestimates the landslide phenomena.

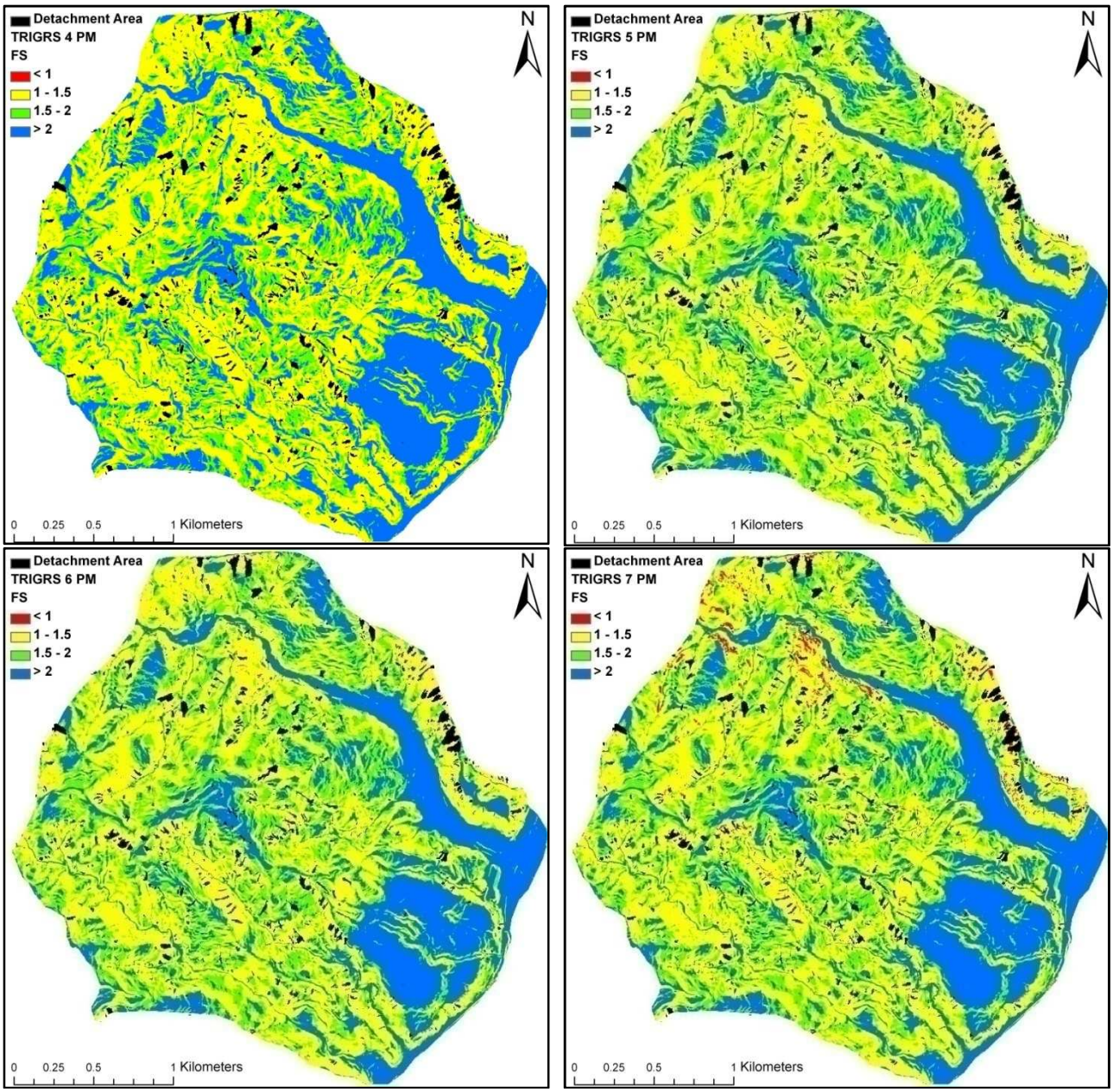

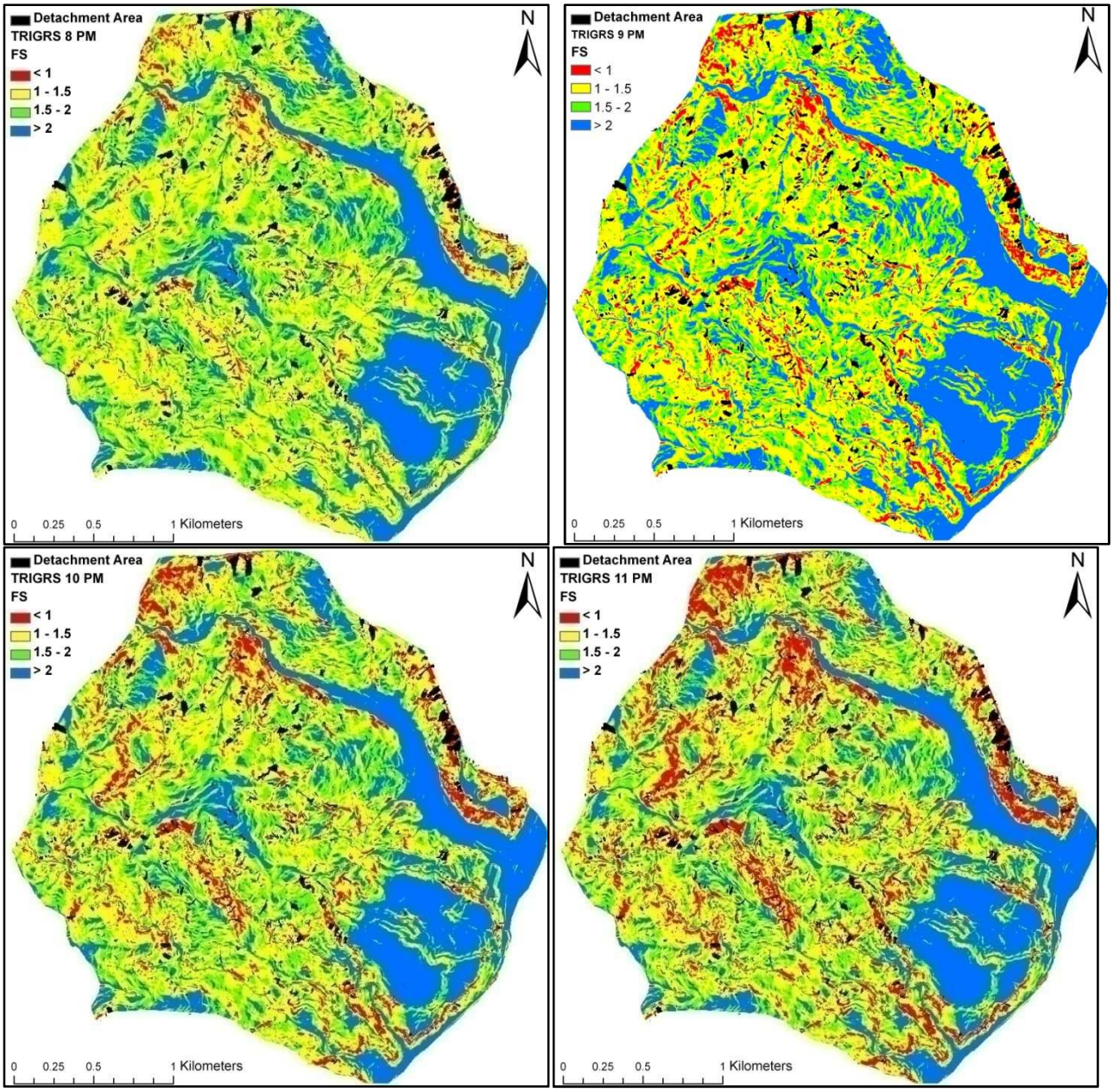

Figure 8.10 TRIGRS output: Time varying safety factor maps from 4.00 pm to 11 pm of October 1st 2009

Time	Predicted instable pixels	Correctly predicted landslide pixels %	Correctly predicted stable pixels %
4.00 PM	0	0	100
5.00 PM	167	0.01	99.96
6.00 PM	420	0.09	99.91
7.00 PM	5202	2.43	98.97
8.00 PM	15655	7.55	96.89
9.00 PM	27849	13.11	94.46
10.00 PM	42150	20.25	91.63
11.00 PM	60723	29.97	87.98

Table 8.10 Temporal evolution of instable pixels, prediction of landslide and stable areas computed by TRIGRS

8.5.2 Application of SLIP

The modeling ran with SLIP is very similar (Figure 8.11 and Table 8.11) to that computed by TRIGRS.

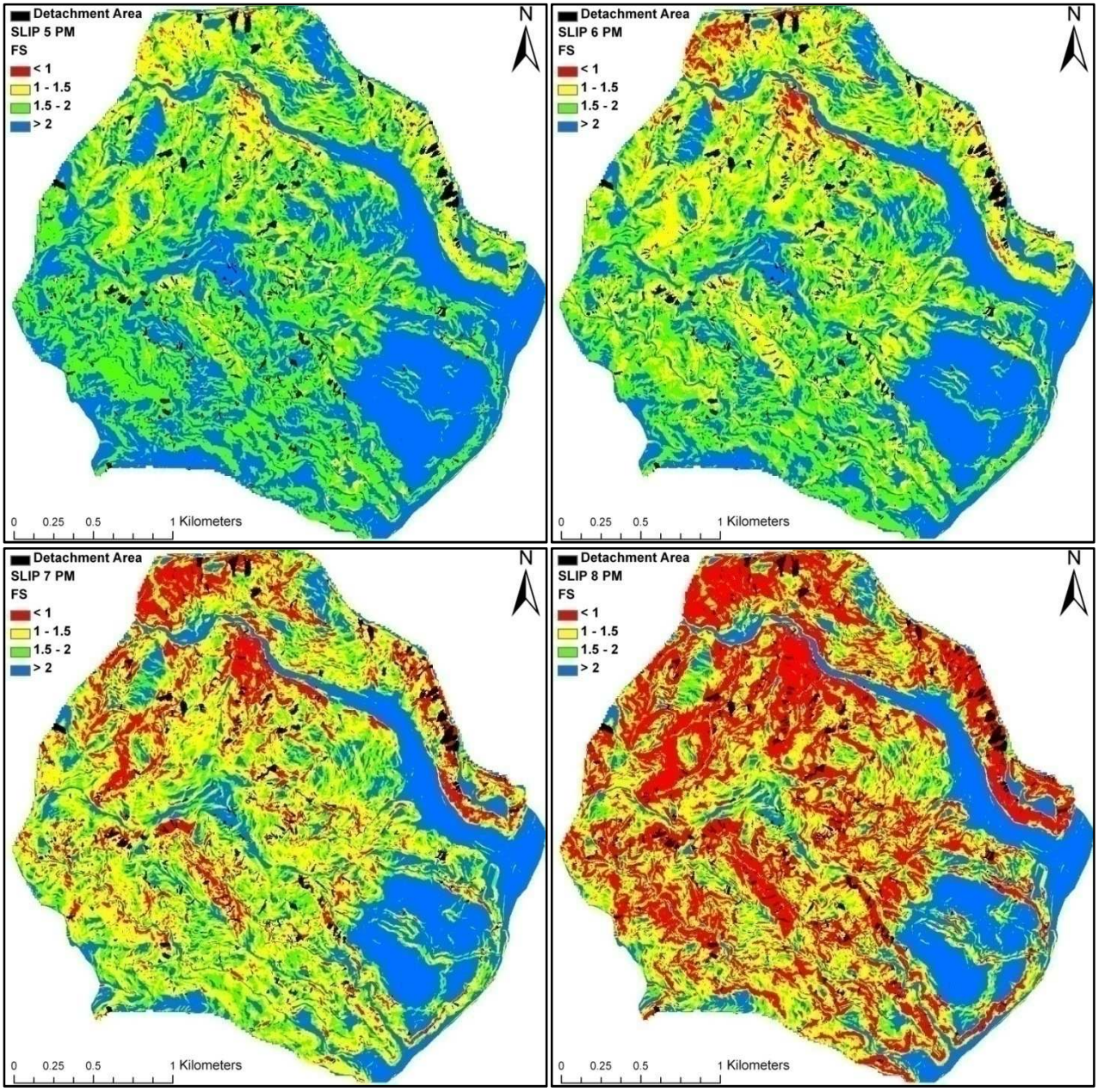

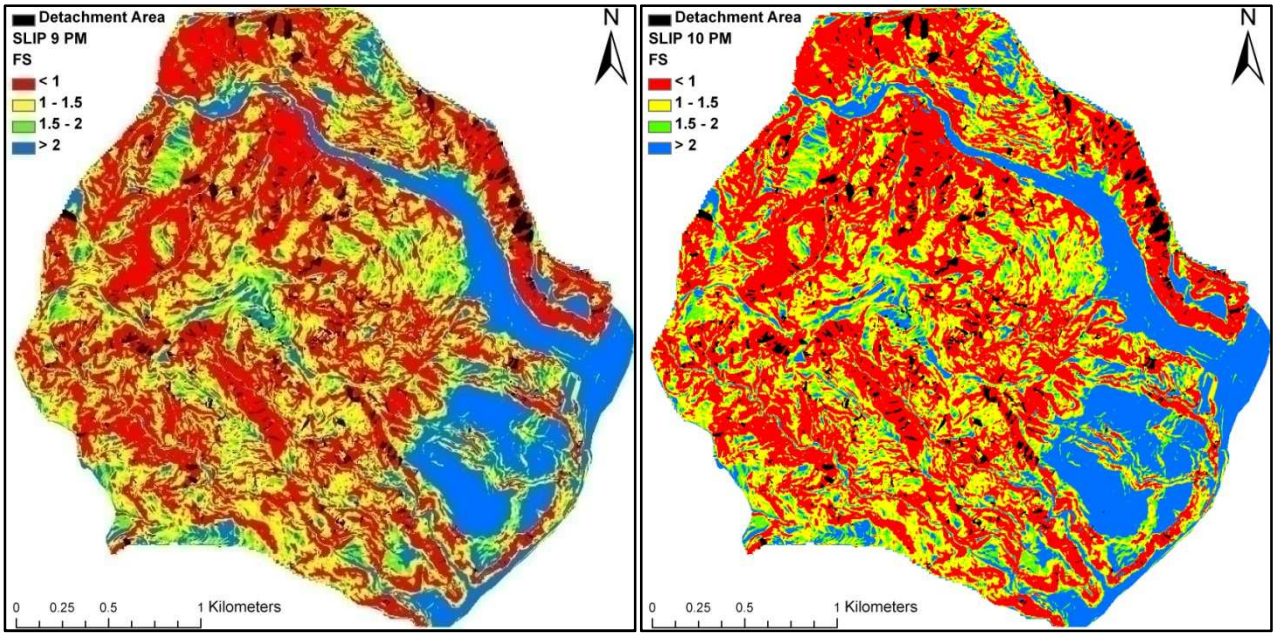

Figure 8.11 SLIP output: Time varying safety factor maps from 5.00 pm to 10 pm of October 1st 2009

Time	Predicted instable pixels	Correctly predicted landslide pixels %	Correctly predicted stable pixels %
4.00 PM	0	0.0	100.0
5.00 PM	1999	0.7	99.6
6.00 PM	11186	5.1	97.8
7.00 PM	65698	36.6	87.1
8.00 PM	170297	75.8	66.0
9.00 PM	185502	82.4	62.9
10.00 PM	211895	84.8	57.3
11.00 PM	211895	84.8	57.3

Table 8.11 Temporal evolution of instable pixels, prediction of landslide and stable areas computed by SLIP

The first observation is that the SLIP model's prediction is accurate from a temporal point of view developing from 5 pm, with a peak in instability between 7 pm and 8 pm and concluding at 10 pm. This temporal reconstruction fits perfectly with the real event evidence provided by witnesses and SLIP underlines the importance of the stage between 7.00 pm and 8.00 pm on the shallow landslides triggering event. SLIP correctly predicts 84.8 % of landslides cells at 10 pm showing how SLIP correctly grasps the landslide areas at the cost of overestimating instable areas. This is seen by the stable area prediction that at 10 pm is 57.3 % of the real stable areas. It must be remarked that these computations are made by comparing the safety factor maps only with the detachment area landslide inventory map.

8.6 Validation of the models

In the following analysis, like in the case of the Parma Apennine events of 2013, we chose to analyze the specificity and sensitivity for FS values greater than 1, to be able to assess the areas that tend to instability during a meteorological event. A ROC curve is obtained by varying the threshold value of Fs, increasing it gradually, until every pixel of the detachment area is less than or equal to Fs* or, in other words, until the analysis reaches maximum sensitivity in correspondence of the maximum value of TP. The area under the ROC curve (AUC) thus obtained, defined overall accuracy, is a parameter of the model reliability.

Figure 8.12 shows the Roc curves for the predictions of TRIGRS and SLIP comparing the final safety factor maps with the landslide detachment area inventory map. The AUC is equal to 74% for TRIGRS prediction. Although the model predicts only about the 30% of real landslides, it is worth noting that the main ones, i.e. those occurred on the slopes above Giampilieri village, are correctly identified. Regarding SLIP, according to the results, the FS map correctly classifies 84.8% of source areas (True Positive) and 57.3% of stable areas (True Negative) with FS = 1, whereas the AUC is equal to 77%. In this case the model predicts more landslides but gives some overprediction. This comparison was made by considering a null value of effective cohesion for SLIP, therefore less stability.

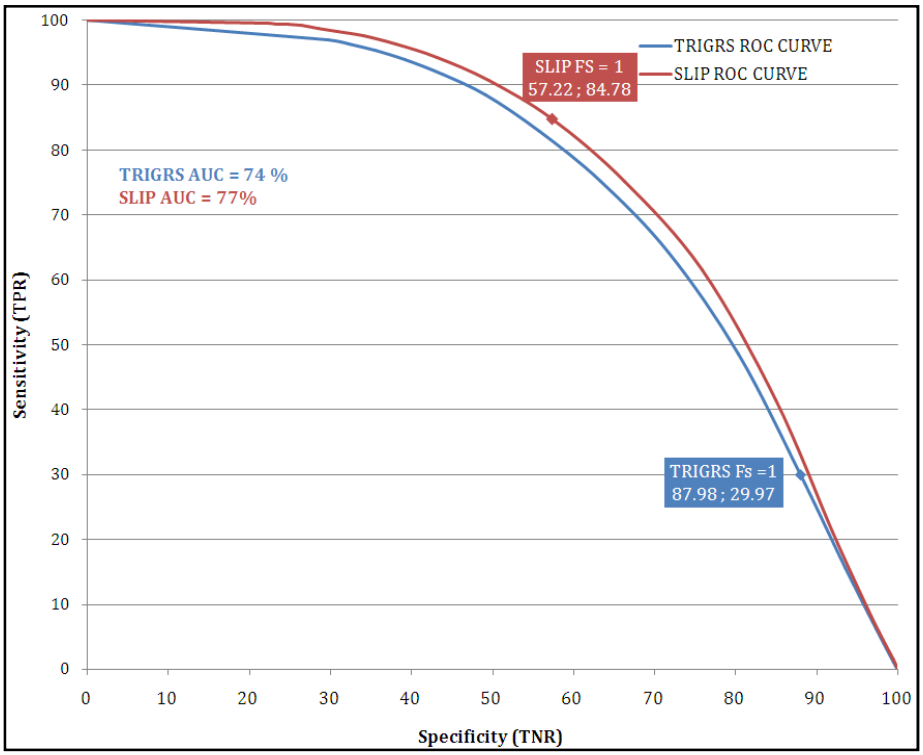

Figure 8.12 ROC curve for TRIGRS and SLIP predictions

A further analyses, plotting the prediction of the daily FS over a time span of 2 years using the SLIP model was made (Figure 8.13). This analysis was made to evaluate if the model could "predict in back-analysis" other landslide events occurred in the same area with different rainfall inputs. Figure 8.11 shows how, in a cell of 40° slope in both well maintained and not maintained terraces, only in 3 days the safety factor falls under 1, thus predicting instability. In two of these days (25/10/2007 and 1/10/2009) there is evidence of actually occurred landslides while the other is probably a false prediction although some non reported instability may have occurred.

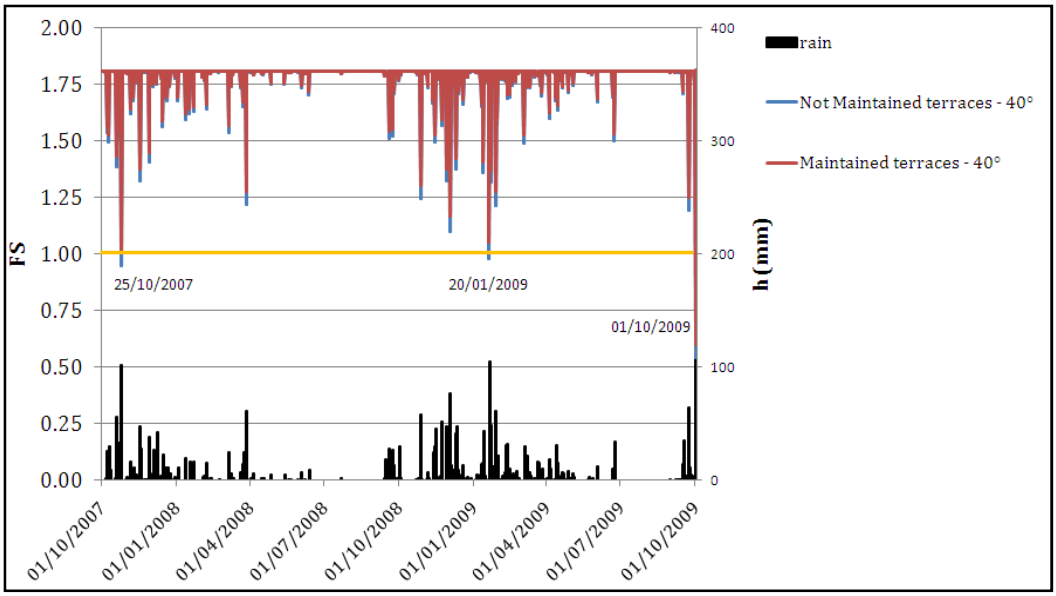

Figure 8.13 SLIP output of annual analysis 1/10/2007-1/10/2009

It is worth noting that the safety factor of the 2007 event is lower than that computed on January 20th 2009, despite the rainfall peak of the latter was slightly higher. These results show how the hydrological scheme of SLIP well models the water content considering the rainfall of preceding days and how, if well calibrated with precise input data, SLIP is capable of predicting correctly instability or stability with different rainfall scenarios. A comparison with TRIGRS output on a yearly basis was not possible due to the extremely high computational time of the model.

A further note on SLIP must be highlighted: the computation times of the models are very short returning the results for Giampilieri area in a few minutes. This means that updated triggering scenario maps can be obtained substantially in real-time. This feature is obviously essential considering a possible integration of the approach with an early warning system. Furthermore, if SLIP model was used in this way, it would operate with forecasted rainfall inputs of few hours, much more reliable than those estimated with a statistical analysis of historical rainfall data which, furthermore, are not always available for a specific area. Ultimately, if coupled with rainfall forecasts SLIP could be used as a "real-time" early warning device for shallow landslide instability.

Chapter 9

Conclusions

This work has focused on validating, on a large scale, the physically based model, named SLIP (Shallow Landslide Instability Prediction) for its future application in real time civil protection integrated platforms, after almost 15 years from its first formulation. Many works have been carried out by our research group using this model to back analyze occurred events and with the correct calibration of its input data the model always gave good results. In this thesis a further validation on various aspects of the model have been carried out from the prediction of instability of simulated landslides in laboratory flume tests to a real scale analysis.

Particularly SLIP has been used to model two case studies, namely the landslide event that hit the Parma Apennines in April 2013 and the event of Giampilieri (ME) occurred the 1st October of 2009.

In the first study case a large gathering of information was carried out from both in situ measurements and laboratory tests on the landslides and its soil. Thanks to an already known background for this type of soil, studied in previous works of our research group, the modeling gave good predictive capability. A new technique that extracted spatial land cover classes from pre-event flight images was consequently used. There was a clear improvement in the overall accuracy of the model between the cases in which this differentiation was used and not showing how a better spatial variation of parameters can improve the model predictive capacity. From a temporal stand point both the parameter sets give excellent results remarking the instability pattern that witnesses and local news provided. The results highlight a good prediction although there is a high over prediction ratio in the first set, and some false alerts in the second set. These problems can be related to an incomplete landslide database and spatial errors due to the absence of post event images.

The calibration of the input parameters of the Giampilieri event was made by laboratory geotechnical characterization, numerical models for hydraulic parameters and by simulating in a small scale flume the triggering of landslides.
Flume tests can be used for multiple purposes, such as to evaluate in back-analysis the initial soil conditions of a reference landslide event, but also to define several input parameters of SLIP model, as well as to analyze in detail the triggering mechanisms of the material potentially susceptible to shallow landslides. Furthermore, the apparatus used in this study is not complex or expensive. With the correct expedients, such as insertion of macro channels, the flume can be used to simulate the real case and to model hypothetical scenarios before they occur in real slopes.

The outcome of flume tests underlines the influence of initial soil conditions on times and modalities of slope failure, as well as indicating how a variable rainfall input produces an increase of water infiltration compared to a constant one of same cumulative depth. The output of two models, SLIP and TRIGRS, a well established model, are shown. The results indicate that the models reconstruct quite well the event, both in terms of temporal evolution and spatial distribution of slope instability, and identify substantially the same areas mostly affected by shallow landslides. The comparison confirms the good predictive capability of the SLIP physically-based model, considering that the two maps converge to the same solution in large part of the study area, although SLIP overestimates spatially the instability while TRIGRS underestimates the landslide occurrence and slightly overestimates temporally the duration of the landslide event. SLIP is a more simple model than TRIGRS requiring less input parameters. The results of a two-year daily analysis are shown only using the SLIP model because a yearly analysis with TRIGRS would require elevated computational time. The results show haw the model well predicts instability capturing both the reported events of this time span and producing only one false alert.

SLIP model returns the results in a few minutes for large areas. This means that updated triggering scenario maps can be obtained substantially in real-time. This feature is obviously essential considering a possible integration of the approach with an early warning system. Furthermore, if SLIP model was used in this way, it would operate with rainfall inputs forecasted for the next hours, then much more reliable than those estimated with a statistical analysis of historical rainfall data which, furthermore, are not always available for a specific area.

Overall, if coupled with forecasted rainfall maps the model could be used as a preliminary early warning system for landslides and could be used to simulate landslide susceptibility over large areas with different rainfall scenarios.

References

Acharya G., Cochrane T.A., Davies T., Bowman E. (2009) *The influence of shallow landslides on sediment supply: a flume-based investigation using sandy soil*. Engineering Geology, 109: 161-169 DOI: 10.1016/j.enggeo.2009.06.008

Ahmadi-Adli M, Toker NK, Huvaj N. (2014) P*rediction of seepage and slope stability in a flume test and an experimental field case*. Procedia Earth Planet Sci;

Airò Farulla C, Rosone M. (2014) *Modeling Round Robin test: an uncoupled approach*. Procedia Earth Planet Sci;

Aleotti, P. (2004). *A warning system for rainfall-induced shallow failures*. Engineering Geology, 73, 247–265.

Alonso EE, Gens A, Josa A. (1990) *A constitutive model for partially saturated soils*. Géotechnique; 40(3):405-430.

Amodio Morelli G., Bonardi G., Colonna V., Dietrich D., Giunta G., Ippolito F., Liguori V., Lorenzoni S., Paglionico A., Perrone V., Piccarreta G., Russo M., Scandone P, Zanettin Lorenzoni E., Zuppetta A. (1976) *L'Arco Calabro-Peloritano nell'orogene Appenninico-Maghrebide*. Memorie della Società Geologica Italiana, 17: 1-60

Aronica G.T., Biondi G., Brigandì G., Cascone E., Lanza S., Randazzo G. (2012) *Assessment and mapping of debris-flow risk in a small catchment in eastern Sicily through integrated numerical simulations and GIS* Physics and Chemistry of the Earth, 49: 52-63 DOI: 10.1016/j.pce.2012.04.002

ARPA Emilia-Romagna, Servizio IdroMeteoClima, (2013) *Rapporto dell'evento meteorologico e idrologico del 4-5 aprile 2013*
http://www.arpa.emr.it/cms3/documenti/_cerca_doc/meteo/radar/rapporti/rapporto_meteo_20130404-05.pdf

ARPA Emilia-Romagna, Servizio IdroMeteoClima, (2013) *Sintesi meteorologica del periodo: 1 Marzo – 7 Aprile 2013*
http://ambiente.regione.emilia-romagna.it/geologia/temi/dissesto-idrogeologico/rapporto-frane-marzo-aprile-2013-1/sintesi-meteorologica-del-periodo-1-marzo-2013-7-aprile-2013

Atzori P., Ferla P., Paglionico A., Piccarreta G., Rottura A. (1984) *Remnants of the Hercynian orogen along the 'Calabrian-Peloritan Arc', Southern Italy: a review* Journal of the Geological Society, 141: 137-145 DOI: 10.1144/gsjgs.141.1.0137

Bagueria, S. (2006). *Validation and evaluation of predictive models in hazard assessment and risk management.* Natural Hazards , 37: 315-329.

Bardou E., Favre-Bulle G., Ornstein P., Rouiller J.D. (2011) *Influence of the connectivity with permafrost on the debris-flow triggering in high-alpine environment*. In: Genevois R., Hamilton D.L., Prestininzi A. (eds.) 5th International Conference on Debris-Flow Hazards Mitigation: Mechanics, Prediction and Assessment. Padua, June 14th - 17th 2011: 13-21 ISBN 978-88-95814-46-9 ISSN 1825-6635

Baum R.L., Savage W.Z., Godt J.W. (2002) *TRIGRS - A Fortran program for transient rainfall infiltration and grid-based regional slope-stability analysis* U.S. Geological Survey Open-File Report 02-424: 61 pp

Baum R.L., Savage W.Z., Godt J.W. (2008) TRIGRS - *A Fortran program for transient rainfall infiltration and grid-based regional slope-stability analysis, version 2.0* U.S. Geological Survey Open-File Report 2008-1159: 75 pp

Baum R.L., Godt J.W. (2010) *Early warning of rainfall-induced shallow landslides and debris flows in the USA* Landslides, 7: 259-272 DOI: 10.1007/s10346-009-0177-0

Baum R.L., Godt J.W., Savage W.Z. (2010) *Estimating the timing and location of shallow rainfall-induced landslides using a model for transient, unsaturated infiltration* Journal of Geophysical Research, 115: F03013 DOI: 10.1029/2009JF001321

Begueria, S., (2006) *Evaluation and evaluation of predictive models in hazard assessment and risk management.* Natural Hazards, 37(3): 315-329.

Berti M., Genevois R., Simoni A., Tecca P.R. (1999) – *Field observations of a debris flow event in the Dolomites* Geomorphology, 29: 265-274 DOI: 10.1016/S0169-555X(99)00018-5

Beven, K. J. and M. J. Kirkby, (1979), *A Physically Based Variable Contributing Area Model of Basin Hydrology*, Hydrological Sciences Bulletin, 24(1): 43-69.

Borga, M., Dalla Fontana, G., Gregoretti, C. and Marchi, L. (2002), *Assessment of shallow landsliding by using a physically based model of hillslope stability*. Hydrol. Process., 16: 2833–2851. doi: 10.1002/hyp.1074

Brand, E.W., 1995. *Slope instability in tropical areas*. In: Bell, D.H. _Ed.., Proc. 6th Int. Symposium on Landslides. Landslides 3. Balkema, Rotterdam, pp. 2031–2051.

Breien H., De Blasio F.V., Elverhøi A., Høeg K. (2008) *Erosion and morphology of a debris flow caused by a glacial lake outburst flood, Western Norway.* Landslides, 5: 271-280 DOI: 0.1007/s10346-008-0118-3

Brunetti M.T., Peruccacci S., Rossi M., Luciani S., Valigi D., Guzzetti F. (2010) *Rainfall thresholds for the possible occurrence of landslides in Italy.* Natural Hazards and Earth System Sciences, 10, pp. 447–458

Buchanan P, Savigny KW (1990) *Factors controlling debris avalanche initiation*. Can Geotech J 27 : 659–675

Caine, N., (1980), *The rainfall intensity duration control of shallow landslides and debris flow*. Geografiska Annaler, 62 (1-2), 659- 675.

Burrough P.A., McDonnell R.A. (1998) *Principles of Geographical Information Systems.* Oxford University Press, Oxford 333pp

Calcaterra D, Parise M, Palma B, Pelella L (2000) *The influence of meteoric events in triggering shallow landslides in pyroclastic deposits of Campania, Italy*. In: Proceedings 8th International Symposium on Landslides, (Bromhead E, Dixon N, Ibsen ML, eds). Cardiff: A.A. Balkema, 1: 209–214

Campbell, R. (1975). *Soil slips, debris flow and rainstorms in the Santa Monica Mountains and Vicinity, Southern California*. U.S. Geological Survey Professional Paper 851.

Cancelli, A., Nova, R. (1985). *Landslide in soil debris cover triggered by rainstorm in Valtellina (Central Alps, Italy).* Proc. IVth Inter. Conf. and Field Workshop on Landslides, Tokyo, 1985.

Cardinali M., Ardizzone F., Galli M., Guzzetti F., Reichenbach P. (2000) *Landslides triggered by rapid snow melting: the December 1996–January 1997 event in Central Italy* In: Claps P. & Siccardi F. (eds.) Proceedings 1st Plinius Conference on Mediterranean Storms, Maratea, Italy, October 14th - 16th, 1999: 439–448 Bios Publisher, Cosenza

Carrara A., Crosta G., Frattini P. (2008) *Comparing models of debris-flow susceptibility in the alpine environment* Geomorphology, 94: 353-378 DOI: 10.1016/j.geomorph.2006.10.033

Casadei M., Dietrich W.E., Miller N.L. (2003) *Testing a model for predicting the timing and location of shallow landslide initiation in soil-mantled landscapes* Earth Surface Processes and Landforms, 28(9): 925–950 DOI: 10.1002/esp.470

Casalbore D., Chiocci F.L., Scarascia Mugnozza G., Tommasi P., Sposato A. (2011) *Flash-flood hyperpycnal flows generating shallow-water landslides at Fiumara mouths in Western Messina Strait (Italy)* Marine Geophysical Research, 32: 257-271 DOI: 10.1007/s11001-011-9128-y

Cascini L., Cuomo S., Pastor M., Sorbino G. (2010) *Modeling of Rainfall-Induced Shallow Landslides of the Flow-Type* Journal of Geotechnical and Geoenvironmental Engineering, 136 (1): 85-98 DOI: 10.1061/(ASCE)GT.1943-5606.0000182

Cascini L., Cuomo S., Della Sala M. (2011) *Spatial and temporal occurrence of rainfall-induced shallow landslides of flow type: A case of Sarno-Quindici, Italy* Geomorphology, 126 (1-2): 148-158 DOI: 10.1016/j.geomorph.2010.10.038

Catani F., Segoni S., Falorni G. (2010) *An empirical geomorphology-based approach to the spatial prediction of soil thickness at catchment scale* Water Resources Research, 46(5): W05508 DOI: 10.1029/2008WR007450

Ceriani M., Lauzi S., Padovan N. *Rainfall thresholds triggering debris flows in the alpine area of Lombardia Region Central Alps–Italy*. I Convegno internazionale per la protezione e lo sviluppo dell'ambiente montano “Man and Mountain”94” (1994), pp. 123–139

Cerrina, Feroni, Vescovi, (2002) *Note illustrative alla Carta Geologica d’Italia Scala 1:50.000 F.217 “Neviano degli Arduini”*.

Chang C.L., Lo S.L., Yu S.L. (2005) *Interpolating precipitation and its relation to runoff and non-point source pollution* Journal of Environmental Science and Health, 40: 1963-1973 DOI: 10.1080/10934520500184673

Chen J., Tan Y., Chen C., Parlange J. (2001) *Analytical solutions for linearized Richards equation with arbitrary time-dependent surface fluxes* Water Resources Research, 37(4): 1091–1094 DOI: 10.1029/2000WR900406

Chiarle M., Iannotti S., Mortara G., Deline P. (2007) *Recent debris flow occurrences associated with glaciers in the Alps* Global and Planetary Change, 56: 123-136 DOI: 10.1016/j.gloplacha.2006.07.003

Clague J.J., Evans S.G., Blown I.G. (1985) - *A debris flow triggered by the breaching of a moraine-dammed lake, Klattasine Creek, British Columbia* Canadian Journal of Earth Sciences, 22 (10): 1492-1502 DOI: 10.1139/e85-155

Corominas, J, Moya, J (1999) *Reconstructing recent landslide activity in relation to rainfall in the Llobregat River basin, Eastern Pyrenees, Spain*. Geomorphology 30: pp. 79-93

Crosta, G. (1990). A *study of slope movements caused by heavy rainfalls in Valtellina (Italy – July 1987).* In: Cancelli A (ed) ALPS 90, Proceedings of 6th International Conference and Field workshop on Landslides, Milan, Ricerca Scientifica ed Educazione Permanente, Suppl. 79b, Milano, 247-258.

Cruden D.M., Varnes D.J. (1996) *Landslides types and processes* In: Turner A.K. & Schuster R.L. (eds.) Landslides investigation and mitigation Transportation Research, US National Research Council, Washington, DC Board Special Report, 247:36-75 ISBN: 0-309-06151-2

De Guidi G., Scudero S. (2013) *Landslide susceptibility assessment in the Peloritani Mts. (Sicily, Italy) and clues for tectonic control of relief processes* Natural Hazard and Earth System Sciences, 13: 949-963 DOI: 10.5194/nhess-13-949-2013

Dietrich W.E., Reiss R., Hsu M.L., Montgomery D.R. (1995) *A process-based model for colluvial soil depth and shallow landsliding using digital elevation data* Hydrological Processes, 9(3-4): 383-400 DOI: 10.1002/hyp.3360090311

DIT-UPC. CODE_BRIGHT (2010). *A 3-D program for thermo-hydro-mechanical analysis in geological media. User's guide*. Barcelona. Centro Internacional de Métodos Numéricos en Ingeniería (CIMNE).

Eckersley D. (1990) *Instrumented laboratory flowslides*, Géotechnique, 40(3): 489-502 DOI: 10.1680/geot.1990.40.3.489

Ehret U. (2002) *Rainfall and flood nowcasting in small catchments using weather radar* PhD Thesis, University of Stuttgart

EM-DAT: *The CRED International Disaster Database*. http://www.emdat.be/database

Fell, R., Corominas, J., Bonnard, C., Cascini, L., Leroi, E., Savage, W.Z. (2008) *Guidelines for landslide susceptibility, hazard and risk zoning for land use planning* Engineering Geology, 102 (3-4), pp. 85-98. doi: 10.1016/j.enggeo.2008.03.022

Fernandes N.F., Guimarães R.F., Gomes R.A.T., Vieira B.C., Montgomery D.R., Greenberg H. (2004) *Topographic controls of landslides in Rio de Janeiro: field evidence and modeling* Catena, 55: 163–181 DOI: 10.1016/S0341-8162(03)00115-2

Flury M, Fluhler H, Jury W, Leuenberger J. (1994) *Susceptibility of soils to preferential flow of water: a field study*. Water Resour Res;**30(7)**:1945-1954.

Fredlund DG, Rahardjo H.*(1993) Soil Mechanics for unsaturated soils.* John Wiley & Sons.

Fredlund DG, Xing A, Fredlund MD, Barbour SL. (1996) *The relationship of the unsaturated soil shear strength to the soil-water characteristic curve.* Can Geotech. J.;**33-3**:440-448.

Freeze R.A., Cherry J.A. (1979) *Groundwater* Prentice Hall, Englewood Cliffs, New Jersey (USA): 604 pp. ISBN: 9780133653120

García-Martínez R., López J.L. (2005) *Debris flows of December 1999 in Venezuela* In: Jacob M. & Hungr O. (eds.) Debris-flow Hazards and Related Phenomena: 519-538 ISBN: 978-3-540-20726-9

Gardner W.R. (1958) *Some steady-state solutions of the unsaturated moisture flow equation with application to evaporation from a water table* Soil Science, 85(4): 228-232 DOI: 0.1097/00010694-195804000-00006

Gavardashvili G., Ayyub B.M. (2011) *The field investigation of erosion and debris flow processes in catchment basin of the Duruji river* In: Genevois R., Hamilton D.L., Prestininzi A. (eds.) 5th International Conference on Debris-Flow Hazards Mitigation: Mechanics, Prediction and Assessment. Padua, June 14th - 17 th, 2011: 63-70 ISBN 978-88-95814-46-9 ISSN 1825-6635

GEO-SLOPE 2007. *SEEP/W*. GEO-SLOPE International Ltd. Calgary. Alberta. Canada; 2007.

Gessler P.E., Chadwick O.A., Chamran F., Althouse L., Holmes K. (2000) *Modeling soil-landscape and ecosystem properties using terrain attributes* Soil Science Society of America Journal, 64: 2046–2056 DOI: 10.2136/sssaj2000.6462046x

Ghezzehei T.A., Kneafsey T.J., Su G.W. (2007) *Correspondence of the Gardner and van Genuchten-Mualem relative permeability function parameters* Water Resources Research, 43: W10417 DOI: 10.1029/2006WR005339

Giannecchini R., Galanti Y., D'Amato Avanzi G. (2012) C*ritical rainfall thresholds for triggering shallow landslides in the Serchio River Valley (Tuscany, Italy)* Natural Hazards and Earth System Sciences, 12: 829–842 DOI: 10.5194/nhess-12-829-2012

Godt J.W., Baum R.L., Savage W.Z., Salciarini D., Schulz W.H., Harp E.L. (2008) *Transient deterministic shallow landslide modeling: requirements for susceptibility and hazard assessments in a GIS framework* Engineering Geology, 112: 214-226 DOI: 10.1016/j.enggeo.2008.03.019

González N. (2011) *Development of a family of constitutive models for geotechnical applications*, Ph.D. Thesis. Barcelona, Spain: Technical University of Catalonia.

Goodrich D.C., Faurès J.M., Woolhiser D.A., Lane L.J., Sorooshian S. (1995) *Measurement and analysis of small-scale convective storm rainfall variability* Journal of Hydrology, 173(1-4): 283-308 DOI: 10.1016/0022-1694(95)02703-R

Govi M., Mortara G., Sorzana P. (1985) *Eventi idrologici e frane* Geologia Applicata & Idrogeologia, 20(2): 359–375

Gray DH, Sotir RB. 1996. *Biotechnical and Soil Bioengineering Slope Stabilization*. John Wiley and Sons: New York; 378 pp.

Grelle G., Soriano M., Revellino P., Guerriero L., Anderson M.G., Diambra A., Fiorillo F., Esposito L., Diodato N., Guadagno F.M. (2014) *Space-time prediction of rainfall-induced shallow landslides through a combined probabilistic/deterministic approach, optimized for initial water table conditions* Bulletin of Engineering Geology and the Environment, 73(3): 877-890 DOI: 10.1007/s10064-013-0546-8

Guadagno F.M., Martino S., Scarascia Mugnozza G. (2003) *Influence of man-made cuts on the stability of pyroclastic covers (Campania, southern Italy): a numerical modeling approach* Environmental Geology, 43: 371-374 DOI: 10.1007/s00254-002-0658-0

Guadagno F.M., Forte R., Revellino P., Fiorillo F., Focareta M. (2005) *Some aspects of the initiation of debris avalanches in the Campania Region: the role of morphological slope discontinuities and the development of failure* Geomorphology, 66 (1-4): 237-254 DOI: 10.1016/j.geomorph.2004.09.024

Guzzetti F., Peruccacci S., Rossi M., Stark C.P. (2007) *Rainfall thresholds for the initiation of landslides in central and southern Europe* Meteorology and Atmospheric Physics, 98(3-4): 239-267 DOI: 10.1007/s00703-007-0262-7

Guzzetti F., Peruccacci S., Rossi M., Stark C.P. (2008) *The rainfall intensity-duration control of shallow landslides and debris flows: an update.* Landslides, 5: 3-17 DOI: 10.1007/s10346-007-0112-1

Habib E., Krajewski W.F. (2002) *Uncertainty analysis of the TRMM ground-validation radar-rainfall products: application to the TEFLUN-B field campaign* Journal of Applied Meteorology, 41: 558-572 DOI: 10.1175/1520-0450(2002)041<0558:UAOTTG>2.0.CO;2

Hoffmann C, Meler N, Pinyol NM, Alonso EE. (2014) *Small scale slope failure benchmark test. Modelling and prediction.* Procedia Earth Planet Sci;

Hungr O., Evans S.G., Bovis M.J., Hutchinson J.N. (2001) *A review of the classification of landslides of the flow type* Environmental & Engineering Geoscience, 7: 221-238 DOI: 10.2113/gseegeosci.7.3.221

Hungr O., McDougall S., Bovis M. (2005) *Entrainment of material by debris flows* In: Jacob M. & Hungr O. (eds.) Debris-flow Hazards and Related Phenomena: 135-158 ISBN: 978-3-540-20726-9

Hungr O., Mcdougall S., Wise M., Cullen M. (2008) *Magnitude-frequency relationships of debris flows and debris avalanches in relation to slope relief* Geomorphology, 96 (3-4): 355-365 DOI: 10.1016/j.geomorph.2007.03.020

Hungr O., Leroueil S., Picarelli L. (2014) *The Varnes classification of landslide types, an update* Landslides, 11: 167-194 DOI: 10.1007/s10346-013-0436-y

Hürlimann M., Rickenmann D., Graf C. (2003) *Field and monitoring data of debris-flow events in the Swiss Alps* Canadian Geotechnical Journal, 40: 161-175 DOI: 10.1139/T02-087

Iovine G., Di Gregorio S., Lupiano V. (2003) *Debris-flow susceptibility assessment through cellular automata modeling: an example from 15–16 December 1999 disaster at Cervinara and San Martino Valle Caudina (Campania, southern Italy)* Natural Hazards and Earth System Sciences, 3: 457–468 DOI: 10.5194/nhess-3-457-2003

IRPI website *http://rainfallthresholds.irpi.cnr.it/references.htm*

Iverson R.M. (2000) *Landslide triggering by rain infiltration*, Water Resources Research, 36 (7): 1897-1910 DOI: 10.1029/2000WR900090

Iverson R.M., Reid M.E., Iverson N.R., LaHusen R.G., Logan M., Mann J.E., Brien D.L. (2000) *Acute sensitivity of landslide rates to initial soil porosity*, Science, 290: 513– 516 DOI: 10.1126/science.290.5491.513

Jacob M., Hungr O. (2005) *Introduction* In: Jacob M. & Hungr O. (eds.) Debris-flow Hazards and Related Phenomena: 1-7 ISBN: 978-3-540-20726-9

Jakob M, Weatherly H., (2003), *A hydroclimatic threshold for landslide initiation on the North Shore Mountains of Vancouver, British Columbia* Geomorphology, 54 , pp. 137–156

Jensen D.T., Hargreaves G.H., Temesgen B., Allen R.G. (1997) *Computation of ETo under nonideal conditions* Journal of Irrigation and Drainage Engineering, 123(5): 394-400 DOI: 10.1061/(ASCE)0733-9437(1997)123:5(394)

Johnson A.I. (1967) *Specific yield-compilation of specific yields for various materials* U.S. Geological Survey Water Supply Paper, 1662-D: 74pp.

Kanji M.A., Cruz P.T., Massad F. (2008) *Debris flow affecting the Cubatão Oil Refinery, Brazi*l Landslides, 5: 71-82 DOI: 10.1007/s10346-007-0110-3

Khazai B., Sitar N. (2000) *Assessment of seismic slope stability using GIS modeling* Geographic Information Sciences, 6(2): 121-128 DOI: 10.1080/10824000009480540

Kim D, I. S. (2010). *Predicting the rainfall-triggered landslides in a forested mountain region using TRIGRS model.* Journal of Mountain Science , 7, 83-91.

Krzeminska DM, Bogaard TA, Malet J-P, van Beek LPH. (2013) *A model of hydrological and mechanical feedbacks of preferential fissure flow in a slow-moving landslide.* Hydrol Earth Syst Sci;**17**:947-959.

Lentini F., Catalano S., Carbone S. (2000) *Note illustrative della carta geologica della Provincia di Messina* scala 1:50.000 S.EL.CA., Firenze 19 pp

Lionel E., Jackson Jr. (1979) A *catastrophic glacial outburst flood (jökulhlaup) mechanism for debris flow generation at the Spiral Tunnels, Kicking Horse River basin, British Columbia* Canadian Geotechnical Journal, 16 (4): 806-813 DOI: 10.1139/t79-087

Loheide II S.P., Butler Jr J.J., Gorelick S.M. (2005) *Estimation of groundwater consumption by phreatophytes using diurnal water table fluctuations: a saturated-unsaturated flow assessment* Water Resources Research, 41: W07030 DOI: 10.1029/2005WR003942

Longley P.A., Goodchild M.F., Maguire D.J., Rhind D.W. (2001). *Geographic Information Systems and Science* Wiley, Chichester, NY 454pp

Losi G. (2012) *Modellazione spazio temporale di fenomeni di soil slip: dalla scala di pendio alla scala territoriale.* Degree (PhD) Thesis, University of Parma (in Italian).

Lourenço S.D.N., Sassa K., Fukuoka H. (2006) *Failure process and hydrologic response of a two layer physical model: implications for rainfall-induced landslides* Geomorphology, 73: 115-130 DOI: 10.1016/j.geomorph.2005.06.004

Lu G.Y., Wong D.W. (2008), *An adaptive inverse-distance weighting spatial interpolation technique*. Comput. Geosci., 34, pp. 1044–1055

Lu N., Godt J.W. (2008) *Infinite-slope stability under steady unsaturated conditions* Water Resource Research, 44: W11404. DOI: 10.1029/2008WR006976

Lu N., Godt J.W., Wu D.T. (2010) *A closed-form equation for effective stress in unsaturated soil* Water Resources Research, 46(5): W05515 DOI: 10.1029/2009WR008646

Ly S., Charles C., Degré A. (2011) *Geostatistical interpolation of daily rainfall at catchment scale: the use of several variogram models in the Ourthe and Ambleve catchments,* Belgium Hydrology and Earth System Sciences, 15: 2259-2274 DOI: 10.5194/hess-15-2259-2011

Mair A., Fares A. (2011) *Comparison of rainfall interpolation methods in a mountainous region of a tropical island* Journal of Hydrologic Engineering, 16(4): 371-383 DOI: 10.1061/(ASCE)HE.1943-5584.0000330

Marchi L., Arattano M., Deganutti A.M. (2002) *Ten years of debris-flow monitoring in the Moscardo Torrent (Italian Alps)* Geomorphology, 46: 1-17 DOI:10.1016/S0169-555X(01)00162-3

Mari M. (2000) *Un metodo per la valutazione del grado di stabilità di pendii a rischio di scivolamenti superficiali* Degree (MSc) Thesis, University of Parma

May D.R., Julien P.Y. (1990) *Raingage network resolution with spatial statistics* In: Riggins R.E., Jones E.B., Singh R., Rechard P.A. (eds.) Watershed Planning and Analysis in Action: 38-47 ISBN: 0872627675 American Society of Civil Engineers, New York

McCoy S.W., Kean J.W., Coe J.A., Tucker G.E., Staley D.M., Wasklewicz T.A. (2012) *Sediment entrainment by debris flows: In situ measurements from the headwaters of a steep catchment* Journal of Geophysical Research, 117: F03016 DOI:10.1029/2011jf002278

Melfi D., Zauli F., Biron D., Vocino A., Sist M. (2012) *The impact of NEFODINA convective clouds identification in the rain rate retrieval of H-SAF* In: Proceedings of the 2012 EUMETSAT Meteorological Satellite Conference, Sopot, Poland, September 3rd – 7th, EUMETSAT P. 61: 7 pp.

Mergili M., Schneider D., Worni R., Schneider J.F. (2011) *Glacial lake outburst floods in the Pamir of Tajikistan: challenges in prediction and modeling* In: Genevois R., Hamilton D.L., Prestininzi A. (eds.) 5th International Conference on Debris-Flow Hazards Mitigation: Mechanics, Prediction and Assessment. Padua, June 14 - 17, 2011: 973-982 ISBN 978-88-95814-46-9 ISSN 1825-6635

Merritt W.S., Letcher R.A., Jakeman A.J. (2003) *A review of erosion and sediment transport models* Environmental Modelling & Software, 18(8-9): 761-799 DOI: 10.1016/S1364-8152(03)00078-1

Montgomery, D.R., Dietrich, W.E. (1994). *A physically based model for the topographic control of shallow landsliding.* Water Resour Res 30, 1153–1171.

Montrasio L. (2000) *Stability analysis of soil slip*. In: Brebbia CA, editor. Proc. of Int. Conf. Risk 2000. Southampton: Wit Press; . p. 357-366.

Montrasio L, Valentino R. (2007) *Experimental analysis and modelling of shallow landslides.* Landslides ;**4**:291-296.

Montrasio L, Valentino R. (2008) *A model for triggering mechanisms of shallow landslides*. Nat Hazards Earth Syst Sci ;**8**:1149-1159.

Montrasio L, Valentino R, Losi GL (2009). *Rainfall-induced shallow landslides: a model for the triggering mechanism of some case studies in Northern Italy*. Landslides ;**6**:241-251.

Montrasio L, Valentino R, Losi GL (2011). *Towards a real-time susceptibility assessment of rainfall-induced shallow landslides on a regional scale.* Nat Hazards Earth Syst Sci ;11:1927-1947.

Montrasio L, Valentino R, Losi GL. (2012) *Shallow landslides triggered by rainfalls: modeling of some case histories in the Reggiano Apennine (Emilia Romagna Region, Northern Italy*). Nat Hazards ;60(3):1231-1254.

Montrasio L, Valentino R, Losi GL, Corina A, Rossi L, Rudari R. (2013) *Space-time hazard assessment of rainfall-induced shallow landslides.* In: Margottini C, Canuti , Sassa K, editors. Landslide Science and Practice, Vol. 4: Global Environmental Change. Springer;. p. 283-294.

Montrasio L, Valentino R, Terrone A.(2014) *Application of the SLIP model*. Procedia Earth Planet Sci;

Morandi M. C., (2013) *Land use management in mountainous areas: combining ground-based and EO (Earth Observation) data to investigate the shallow landsliding susceptibility in the Duron valley (Trento, Italy)* Degree (PhD) Thesis, University of Bologna.

Morgenstern, N.R., and Sangrey, D.A., (1978), *Methods of stability analysis*, in Landslides: Analysis and Control: National Academy of Sciences, Washington, D.C., Special Report 176, p. 155-171.

Morgan RPC, Rickson RJ. (1995). *Slope Stabilization and Erosion Control* . E&FN Spon: London; 274.

Moser, M., Hohensinn, F. (1983). *Geotechnical aspects of soil slips in Alpine Regions.* Engineering Geology , 19, 185-211.

Mothes P., Hall M.L., Janda R.J. (1998) *The enormous Chillos Valley Lahar: an ash-flow-generated debris flow from Cotopaxi Volcano, Ecuador* Bulletin of Volcanology, 59: 233-244 DOI: 10.1007/s00445005018

Mugnai A., Casella D., Cattani E., Dietrich S., Laviola S., Levizzani V., Panegrossi G., Petracca M., Sanò P., Di Paola F., Biron D., De Leonibus L., Melfi D., Rosci P., Vocino A., Zauli F., Pagliara P., Puca S., Rinollo A., Milani L., Porcù F., Gattari F. (2013) *Precipitation products from the hydrology SAF* Natural Hazards and Earth System Sciences, 13: 1959-1981 DOI: 10.5194/nhess-13-1959-2013

Nalder I.A., Wein R.W (1998) *Spatial interpolation of climatic normals: test of a new method in the Canadian boreal forest* Agricultural and Forest Meteorology, 92(4): 211–225 DOI: 10.1016/S0168-1923(98)00102-6

Narama C., Duishonakunov M., Kääb A., Daiyrov M., Abdrakhmatov K. (2010) *The 24 July 2008 outburst flood at the western Zyndan glacier lake and recent regional changes in glacier lakes of the Teskey Ala-Too range, Tien Shan, Kyrgyzstan* Natural Hazards and Earth System Sciences, 10: 647-659 DOI: 10.5194/nhess-10-647-2010

Nimmo J.R. (2005) *Unsaturated zone flow processes* In: Anderson M.G. & Bear J. (eds.) Encyclopedia of Hydrological Sciences: part 13 Groundwater: 2299-2322 Wiley, Chichester, UK DOI: 10.1002/0470848944.hsa161

Olivares L, Damiano E. *Post-failure mechanics of landslides: laboratory investigation of flowslides in pyroclastic soils.* J Geotech Geoenviron Eng ASCE 2007;133(1):51–62.

Olivares L, Damiano E, Greco R, Zeni L, Picarelli L, Minardo A, Guida A, Bernini R. *An instrumented flume for investigation of the mechanics of rainfall-induced landslides in unsaturated granular soils*. ASTM Geotech Test J 2009;32(2):108-118.

O'Loughlin,E . M., (1986) *Prediction of surface saturation zones in natural catchments by topographic analysis*, Water Resour. Res., 22,794-804

Pack, R. T., D. G. Tarbotonand C. N. Goodwin, (1998). *The SINMAP Approach to Terrain Stability Mapping.* 8th Congress of the International Association of Engineering Geology, Vancouver, British Columbia, Canada 21-25 September 1998.

Pegram G. (2003) *Spatial interpolation and mapping of rainfall (SIMAR)* – Volume 3: Data merging for rainfall map production Water Resource Commission Report n. 1153/1/04 ISBN: 1-77005-159-7

Pelletier J.D., Rasmussen C. (2009) *Geomorphically based predictive mapping of soil thickness in upland watersheds* Water Resource Research, 45: W09417 DOI: 10.1029/2008WR007319

Penna D., Borga M., Aronica G.T., Brigandì G., Tarolli P. (2014) *The influence of grid resolution on the prediction of natural and road-related shallow landslides* Hydrology and Earth System Sciences, 18: 2127-2139 DOI: 10.5194/hess-18-2127-2014

Peres D.J., Cancelliere A. (2014) *Derivation and evaluation of landslide triggering thresholds by a Monte Carlo approach* Hydrology and Earth System Sciences Discussion, 11: 2759-2794 DOI: 10.5194/hessd-11-2759-2014

Pérez F.L. (2001) *Matrix granulometry of catastrophic debris flows (December 1999) in central coastal Venezuela* Catena, 45 (3): 163-183 DOI: 10.1016/S0341-8162(01)00149-7

Petley D.N. (2012) *Global patterns of loss of life from landslides* Geology, 40 (10): 927-930 DOI: 10.1130/G33217.1

Petrakov D.A., Krylenko I.V. (2007) *Debris flow hazard of glacial lakes in the Central Caucasus* In: Chen C.L., Major J.J. (eds.) Debris-Flow Hazards Mitigation: Mechanics, Prediction and Assessment: 703-714 ISBN: 9789059660595

Pierson T.C. (1985) *Initiation and flow behavior of the 1980 Pine Creek and Muddy River lahars, Mount St. Helens, Washington* Geological Society of America Bulletin, 96 (8): 1056-1069 DOI: 10.1130/0016-7606(1985)96<1056:IAFBOT>2.0.CO;2

Pierson T.C., Janda R.J., Thouret J.C., Borrero C.A. (1990) *Perturbation and melting of snow and ice by the 13 November 1985 eruption of Nevado del Ruiz, Colombia and consequent mobilization, flow, and deposition of lahars* Journal of Volcanology and Geothermal Research, 41 (1-4): 17-66 DOI: 10.1016/0377-0273(90)90082-Q

Prochaska A.B., Santi P.M., Higgins J.D., Cannon S.H. (2008) *A study of methods to estimate debris flow velocity* Landslides, 5:431-444 DOI: 10.1007/s10346-008-0137-0

Reder A, Rianna G, Pagano L. (2014) *Prediction of suction evolution of silty pyroclastic covers in flume tests and field monitoring*. Procedia Earth Planet Sci;

Revellino P., Hungr O., Guadagno F.M., Evans S.G. (2003) *Velocity and runout simulation of destructive debris flows and debris avalanches in pyroclastic deposits, Campania region, Italy* Environmental Geology, 45: 295-311 DOI: 10.1007/s00254-003-0885-z

Revellino P., Guadagno F.M., Hungr O. (2008) *Morphological methods and dynamic modelling in landslide hazard assessment of the Campania Apennine carbonate slope* Landslides, 5: 59–70 DOI: 10.1007/s10346-007-0103-2

Richards L.A. (1931) *Capillary conduction of liquids in porous mediums* Journal of Applied Physics, 1:318–333 DOI:10.1063/1.1745010

Rossetti, R. (1988). *Condizioni termo-pluviometriche del versante padano della fascia appenninica tra la valle del torrente Scrivia e quella del torrente Reno*. Il paesaggio fisico dell'alto Appennino emiliano, 19-24.

Salciarini D., Godt J.W., Savage W.Z., Conversini P., Baum R.L. (2006) *Modeling regional initiation of rainfall-induced shallow landslides in the eastern Umbria Region of central Italy* Landslides, 3 (3): 181-194 DOI: 10.1007/s10346-006-0037-0

Salciarini D., Godt J.W., Savage W.Z., Baum R.L., Conversini P. (2008) *Modeling landslide recurrence in Seattle, Washington, USA* Engineering Geology, 102: 227-237 DOI: 10.1016/j.enggeo.2008.03.013

Saulnier G.M., Beven K., Obled C. (1997) *Including spatially variable effective soil depths in TOPMODEL* Journal of Hydrology, 202 (1-4): 158–172 DOI: 10.1016/S0022-1694(97)00059-0

Savage W.Z., Godt J.W., Baum R.L. (2003) *A model for spatially and temporally distributed shallow landslide initiation by rainfall infiltration* In: Rickenmann D., Chen C.L. (eds.) Debris-

Flow Hazards Mitigation: Mechanics, Prediction and Assessment: 179-187 ISBN: 907701778X Millpress, Rotterdam

Savage W.Z., Godt J.W., Baum R.L. (2004) *Modelling time-dependent areal slope stability* In: Lacerda W.A., Erlich M., Fontoura S.A.B., Sayao A.S.F. (eds.) Landslides: Evaluation and Stabilisation, Proceedings of the 9th International Symposium on Landslides: 23-36 A.A. Balkema Publishers, London ISBN: 9780415356657

Schaap M.G., Leij F.J., van Genuchten M.T. (2001) *ROSETTA: a computer program for estimating soil hydraulic parameters with hierarchical pedotransfer functions* Journal of Hydrology, 251(3-4): 163-176 DOI: 10.1016/S0022-1694(01)00466-8

Schilirò L., (2015) *Evaluation of shallow landslide triggering scenarios by means of a multimethodological approach.* Ph.D Thesis

Schilirò L., De Blasio S.V., Esposito C., Scarasci Mugnozza G., (in press) *The October 1st 2009 destructive debris flow in Scaletta Zanclea (ME, North Eastern Sicily, Italy): Description, modeling and lessons learned. Submitted to Earth Surface Processes and Landforms*

Schuurmans J.M., Bierkens F.P. (2007) *Effect of spatial distribution of daily rainfall on interior catchment response of a distributed hydrological model* Hydrology and Earth System Sciences, 11: 677-693 DOI: 10.5194/hess-11-677-2007

Scott K.M., Pringle P.T., Vallance J.W. (1995) *Sedimentology, behavior, and hazards of debris flows at Mount Rainier,* WA U.S. Geological Survey Professional Paper, 1547: 56 pp

Sicily Region Precipitation Data website: http://www.osservatorioacque.it/

Sidle R.C., Chigira M. (2004) *Landslides and debris flows strike Kyushu, Japan* Eos, Transactions American Geophysical Union, 85 (15): 145-151 DOI: 10.1029/2004EO150001

Silva D. (2000) *Experimental analysis on the behaviour of slope layered soils*. Degree (MSc) Thesis, University of Parma (in Italian).

Šimůnek J., Huang M., Šejna M., van Genuchten M.Th. (1998) *The HYDRUS-1D software package for simulating the one-dimensional movement of water, heat, and multiple solutes in variably-saturated media.* Version 1.0 International Ground Water Modeling Center, Colorado School of Mines, Golden, Colorado: 186 pp

Sinclair S., Pegram G. (2005) *Combining radar and rain gauge rainfall estimates using conditional merging* Atmospheric Science Letters, 6: 19-22 DOI: 10.1002/asl.

Sorbino G., Sica C., Cascini L. (2010) *Susceptibility analysis of shallow landslides source areas using physically based models* Natural Hazards, 53 (2): 313-332 DOI: 10.1007/s11069-009-9431-y

Springman SM, Thielen A, Kienzler P, Friedel S. (2013) *A long-term field study for the investigation of rainfall-induced landslides*. Geotechnique; 63(14):1177-1193.

Srivastava R., Yeh T.C.J. (1991) *Analytical solutions for one dimensional, transient infiltration toward the water table in homogeneous and layered soils* Water Resources Research, 27(5): 753–762 DOI: 10.1029/90WR02772

Takahashi T. (2007) *Debris flow: mechanics, prediction and countermeasures* Taylor & Francis, London, UK: 448 pp ISBN 978-0-415-43552-9

Tang C., Rengers N., Van Asch T.W.J., Yang Y.H., Wang G.F. (2011) *Triggering conditions and depositional characteristics of a disastrous debris flow event in Zhouqu city, Gansu Province, northwestern China* Natural Hazards and Earth System Sciences, 11: 2903–2912 DOI: 10.5194/nhess-11-2903-2011

Tang C., Van Asch T.W.J., Chang M., Chen G.Q., Zhao X.H., Huang X.C. (2012) *Catastrophic debris flows on 13 August 2010 in the Qingping area, southwestern China: The combined effects of a strong earthquake and subsequent rainstorms* Geomorphology, 139-140: 559-576 DOI: 10.1016/j.geomorph.2011.12.021

Tarboton, D. G., (1997), *A New Method for the Determination of Flow Directions and Contributing Areas in Grid Digital Elevation Models*, Water Resources Research, 33(2): 309-319.

Tesfa T.K., Tarboton D.G., Chandler D.G., McNamara J.P. (2009) *Modeling soil depth from topographic and land cover attributes* Water Resource Research, 45: W10438 DOI: 10.1029/2008WR007474

Tortorici L. (1982) *Lineamenti geologico-strutturali dell'Arco Calabro-Peloritano* Rendiconti della Società Italiana di Mineralogia e Petrologia, 38: 927-940

Vallance J.W., Scott K.M. (1997) *The Osceola Mudflow from Mount Rainier: Sedimentology and hazard implications of a huge clay-rich debris flow* Geological Society of America Bulletin, 109 (2): 143-163 DOI: 10.1130/0016-7606(1997)109<0143:TOMFMR>2.3.CO;2

Vanapalli S.K., Fredlund D.G. (2000) *Comparison of different procedures to predict unsaturated soil shear strength* In: Shackelford C.D., Houston S.L., Chang N.Y. (eds.) Advances in Unsaturated Geotechnics American Society of Civil Engineers: 606 pp. DOI: 10.1061/9780784405109

van Genuchten M.T. (1980) *A closed-form equation for predicting the hydraulic conductivity of unsaturated soils* Soil Science Society of America Journal, 44(5): 892-898 DOI: 10.2136/sssaj1980.03615995004400050002x

Varnes D.J. (1978) *Slope movements types and processes* In: Schuster R.L. & Krizek L.J. (eds.) Landslides, analysis and control National Academy of Sciences, Transportation Research Board Special Report, 176:11-33

Velasco-Forero C.A., Sempere-Torres D., Cassiraga E.F., Gomez-Hernandez J.J. (2009) *A non-parametric automatic blending methodology to estimate rainfall fields from rain gauge and radar data* Advances in Water Resources, 32(7): 986-1002 DOI: 10.1016/j.advwatres.2008.10.004

Verworn A., Haberlandt U. (2011) *Spatial interpolation of hourly rainfall - effect of additional information, variogram inference and storm properties* Hydrology and Earth System Sciences, 15(2): 569-584 DOI: 10.5194/hess-15-569-2011

Villarraga C, Ruiz D, Vaunat J, Casini F. (2014) *Modelling landslides induced by rainfall: a coupled approach.* Procedia Earth Planet Sci;

Wang G., Sassa K. (2001) *Factors affecting rainfall-induced flowslides in laboratory flume tests* Géotechnique, 51(7): 587–599 DOI: 10.1680/geot.2001.51.7.587

Wang G., Sassa, K. (2003) *Pore-pressure generation and movement of rainfall-induced landslides: effects of grain size and fine-particle content* Engineering Geology, 69: 109–125 DOI: 10.1016/S0013-7952(02)00268-5

Wang C., Sassa K., Fukuoka H. (2003) *Downslope volume enlargement of a debris slide–debris flow in the 1999 Hiroshima, Japan, rainstorm* Engineering Geology, 69 (3-4): 309-330 DOI: 10.1016/S0013-7952(02)00289-2

Wang H.B., Sassa K. (2005) *Comparative evaluation of landslide susceptibility in Minamata area,* Japan Environmental Geology, 47: 956-966 DOI: 10.1007/s00254-005-1225-2

Wang C., Esaki T., Xie M., Qiu C. (2006) *Landslide and debris-flow hazard analysis and prediction using GIS in Minamata-Hougawachi area, Japan* Environmental Geology, 51 (1): 91-102 DOI: 10.1007/s00254-006-0307-0

Warrick A.W. (1995) *Correspondence of hydraulic functions for unsaturated soils* Soil Science Society of American Journal, 59(2): 292–299 DOI: 10.2136/sssaj1995.03615995005900020003x

Wieczorek G.F. (1987) *Effect of rainfall intensity and duration on debris flows in central Santa Cruz Mountains, California* In: Costa J.E., Wieczorek G.F. (eds.) Debris flows/avalanches: Process, Recognition and Mitigation: 23-104 ISBN: 978-0813741079

Wieczorek G.F., Morgan B.A., Campbell R.H. (2000) *Debris-Flow Hazards in the Blue Ridge of Central Virginia* Environmental & Engineering Geoscience, 6 (1): 3-23 DOI: 10.2113/gseegeosci.6.1.3

Wieczorek G.F., Mossa G.S., Morgan B.A. (2004) *Regional debris-flow distribution and preliminary risk assessment from severe storm events in the Appalachian Blue Ridge Province, USA* Landslides, 1: 53-59 DOI: 10.1007/s10346-003-0003-z

Yu HS. (1988) *CASM: A unified state parameter model for clay and sand*. International Journal of Numerical and Analytical Methods in *Geomechanics*; 22:621-653.

Zanchetta G., Sulpizio R., Pareschi M.T., Leoni F.M., Santacroce R. (2004) *Characteristics of May 5-6, 1998 volcaniclastic debris flows in the Sarno area (Campania, southern Italy): relationships to structural damage and hazard zonation.* Journal of Volcanology and Geothermal Research, 133: 377-393 DOI: 10.1016/S0377-0273(03)00409-8

Zhan TLT, Ng CWW, Fredlund DG. (2007) *Field study of rainfall infiltration into a grassed unsaturated expansive soil slope.* Can Geotech. J.;44:392-408.